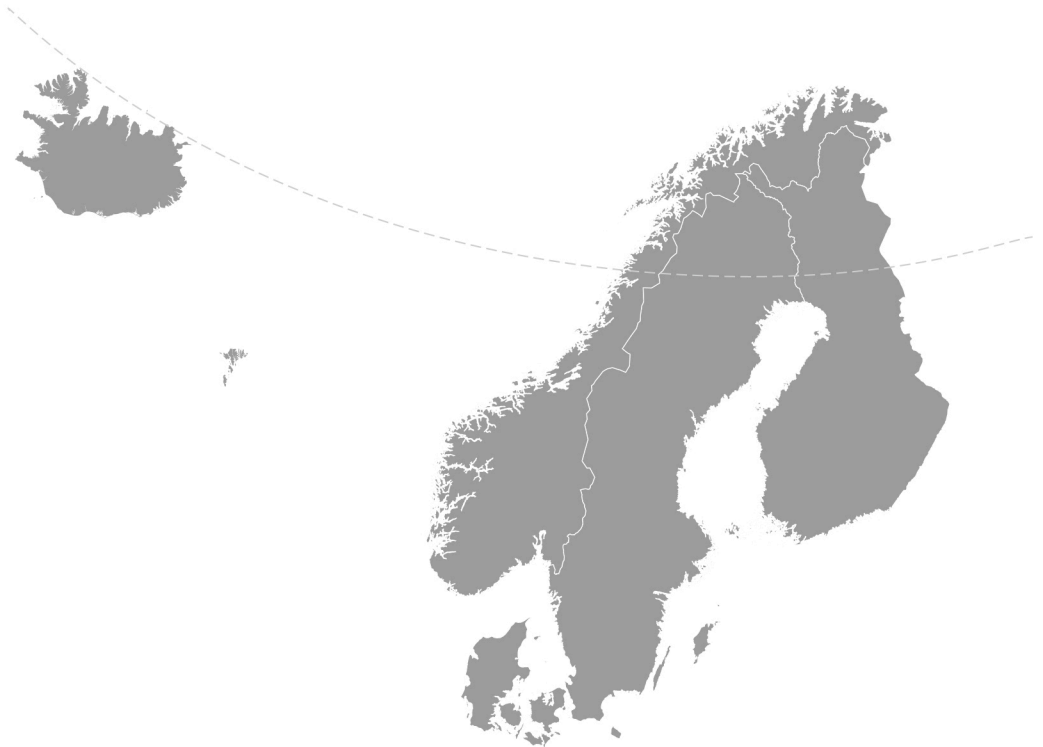


Nordic Concrete Research



Nordic
Concrete
Federation

PUBLICATION NO. 39 1/2009

NORDIC CONCRETE RESEARCH

**EDITED BY
THE NORDIC CONCRETE FEDERATION**

**CONCRETE ASSOCIATIONS OF: DENMARK
FINLAND
ICELAND
NORWAY
SWEDEN**

**PUBLISHER: NORSK BETONGFORENING
POSTBOKS 2312, SOLLI
N - 0201 OSLO
NORWAY**

AALBORG, JUNE 2009

CONTENTS

1.	Lauge Fuglsang Nielsen Self-Compacting Concrete - modelled as a Bingham Composite	1
2.	Irina Sæther & Bjørnar Sand FEM simulations of reinforced concrete beams attacked by corrosion	15
3.	Peter Simonsson & Mats Emborg Industrialized construction: Benefits using SCC in cast in situ construction	33
4.	Peter Simonsson & Mats Emborg Increasing productivity through utilization of new construction techniques and Lean Construction philosophies in civil engineering projects	53
5.	Hendrik Schlune, Mario Plos & Kent Gylltoft Non-linear Finite Element Analysis for Practical Application	75
6.	Peter Harryson Laboratory test and finite element analyses of a prototype bridge beam	89
	Instruction for Authors	105

Preface

Nordic Concrete Research is since 1982 the leading scientific journal concerning concrete research in the five Nordic countries, e.g., Denmark, Finland, Iceland, Norway and Sweden. The content of *Nordic Concrete Research* reflects the major trends in the concrete research.

Nordic Concrete Research is published by the Nordic Concrete Federation that beside the publication activity also organizes the Nordic Concrete Research Symposia that have constituted a continuous series since 1953 in Stockholm. The Symposium circulates between the five countries and takes place every third year. The next will be held in Finland at Hanasaari, the Swedish-Finnish Cultural Centre near Helsinki June 5 – 8, 2011.

The homepage of the Nordic Concrete Federation, www.nordicconcrete.org have now been revised. Missing items will be added shortly.

Papers presented in the journal are also published on the homepage. For the first half year only the abstracts are published there, thereafter the full paper.

Since 1982, 344 papers have been published in the journal. Since 1994 the abstracts and from 1998 both the abstracts and the full papers can be found on the homepage.

The layout of cover of the *Nordic Concrete Research* journal has been changed, and in the future no colour changes will be made from issue to issue.

Aalborg, June 2009

Dirch H. Bager

Editor, *Nordic Concrete Research*

Research Committee

Mr. Klaus Söderlund, Chairman for the Research Committee

Dr. Dirch H. Bager, Editor of Nordic Concrete Research

Denmark

Dr. Dirch H. Bager
DHB-Consult
Lavendelparken 5
DK - 9310 Vodskov
Tel: +45 98292412
Mobile: +45 2049 7324
Fax:
E-mail: dirch.bager@webspeed.dk

Mr. Claus Pade
Concrete Centre,
Danish Technological Institute
Gregersensvej
DK - 2630 Taastrup
Tel: + 45 7220 2183
Mobile: +45
Fax: + 45 7220 2373
E-mail: claus.pade@teknologisk.dk

Finland

Mr. Klaus Söderlund
Concrete Association of Finland
Unioninkatu 14 PL 11
FI - 00130 Helsinki
Tel: +358 9 6962 3620
Mobile: +358 40 900 3576
Fax: +358 965 1145
E-mail: klaus.soderlund@betoniyhdistys.fi

Lic.Sc.Tech. Klaus Juvas
Consolis Technology Oy Ab
Box 72
FI – 21291 Rusko
Tel: +358 205 77 5386
Mobile: +358 40 5160 316
Fax: +358 205 77 5377
E-mail: klaus.juvas@consolis.com

Iceland

Dr. Børge Johannes Wigum
Mannvit
Grensásvegur 1
IS - 108 Reykjavik
Tel: +354 422 3030
Mobile: +354 896-0756
Fax: +354 422 3001
E-mail: wigum@mannvit.is

Dr. Jón E. Wallevik
Innovation Center Iceland
IS - 112 Keldnaholti
Tel: +354 522 9362
Mobile: +354
Fax: +354 522 9111
E-mail: jon.w@nmi.is

Norway

Dr. Terje F. Rønning
Norcem, FoU Department
P.O.Box 38
N - 3991 Brevik
Tel.: +47 3557 2347
Mobile: +47 9157 6046
Fax: +47 3557 0400
E-mail: Terje.ronning@norcem.no

Mr. Hans Stemland
SINTEF
Concrete
N - 7465 Trondheim
Tel: +47 7359 4527
Fax: +47 7359 7136
E-mail: Hans.stemland@sintef.no

Sweden

Tekn.Dr, Docent Mikael Hallgren
Tyréns AB Byggprojektering
Peter Myndes Backe 16
SE - 118 86 Stockholm
Tel: +46 8566 411 33
Mobile: +46 70 661 05 33
Fax: +46 8566 410 50
E-mail: Mikael.Hallgren@tyrens.se

Tekn. Dr. Peter Utgenannt
CBI Swedish Cement and Concrete Research
Institute
P.O. Box 857
SE - 501 15 Borås
Tel: +46 105 165 107
Mobile:
Fax: +46 33 13 45 16
E-mail: peter.utgenannt@cbi.se

Publishing

Ms. Siri Fause
Norsk Betongforening
Postboks 2312 Solli
N - 0201 Oslo
Tel: +47 22 94 75 00
Mobile: +47
Fax: +47 2294 7501
E-mail: siri.fause@tekna.no

Tuesday, 21 April 2009

Self-Compacting Concrete - modelled as a Bingham Composite -



Lauge Fuglsang Nielsen
Department of Civil Engineering
Technical University of Denmark
DK-2800 Lyngby, Denmark
e-mail: lfn@byg.dtu.dk

Abstract: A method is developed by which the well-known Bingham description of flow in homogeneous liquids with yield strength is generalized to apply also for composite Bingham materials. In the present context such materials are defined as Bingham materials mixed with very stiff particles of known shape distributions. Two simple shape distributions are considered in details: A mixture of uni-shaped particles – and a mixture of double-shaped particles.

For practice the composite aspects of a generalised Bingham description is a major advantage. Only a few parameters are needed to describe the Bingham behaviour at any composition of the composite considered. Bingham methods normally used need experimental calibration for any new composition

In building materials technology a composite analysis is of relevance for the description of fresh self-compacting concretes (SCC). In a special section of the paper some potentials of the theory developed are demonstrated on some aspects of materials design of SCC.

Key words: Bingham, Composite Bingham, Shape distribution, Self-compacting concrete (SCC).

1. INTRODUCTION

The paper presents a method by which the well-known Bingham description of flow in homogeneous liquids with yield stress can be generalised to apply also for composite Bingham materials. In the present context such materials are defined as traditional Bingham materials, mixed with very stiff particles of known shape distributions. In practice the composite aspects of a generalised Bingham description is a major advantage. Only a few parameters are needed to describe the Bingham behaviour at any composition of the composite considered. Bingham methods normally used need experimental calibration for any new composition. Most composite analysis made in this paper is based on the author's own work (1,2,3) on composite properties as influenced by phase geometry.

2. BINGHAM MATERIAL

Equation 1, illustrated in Figure 1, describes the constitutive equation for a Bingham material (4,5).

It performs as a liquid with viscosity, $\hat{\eta}$, as soon as the shear stress subjected, τ , exceeds a yield stress of τ^0 . Before that it behaves as a rigid solid, which we may think of as an ideal stiff elastic-plastic material with a yield stress, τ^0 . The angle of deformation is denoted with γ . The rate of angle deformation is $d\gamma/dt$.

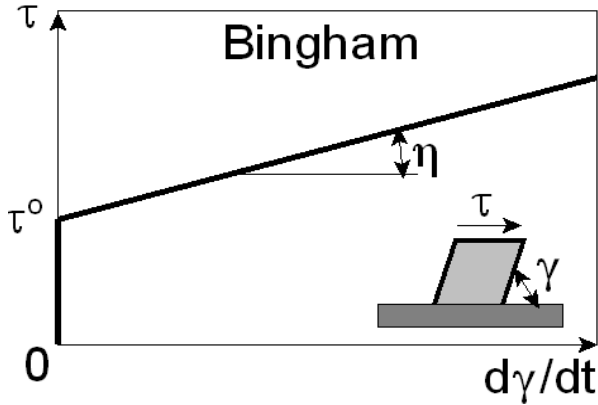


Figure 1. Behavior of a Bingham material. τ is shear stress. τ^0 is yield stress, and η is viscosity. γ is angle of deformation.

Experimentally the Bingham parameters can be determined in a number of ways (6). One of the most common methods is to deduce them from relations, obtained by the so-called coaxial cylinder rheometer, between torsional moment and rate of revolution, see (7).

$$\frac{d\gamma}{dt} = \frac{\tau - \tau^0}{\eta} \quad \text{Bingham material} \quad (1)$$

3. COMPOSITE BINGHAM MATERIAL

Figure 2 defines a composite Bingham material. It is a mixture of very stiff and strong, non-flexible particles (P) in a Bingham matrix (S). The volume concentration of particles is defined by Equation 2 where V denotes volume. In general subscripts P and S refer to particle phase and matrix phase S respectively. A complete list of symbols is presented at the end of this paper.

$$c = \frac{V_P}{V_P + V_S} \quad \text{Volume concentration of particles} \quad (2)$$

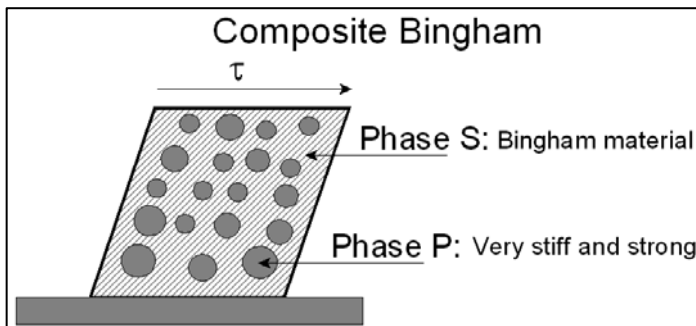


Figure 2. Composite Bingham material. The non-flexible particles need not be of spherical shapes.

The term 'non-flexible' particles mean invariable particle shapes. This is contrary to a general composite geometry, where phase geometries adapt to each other at any concentration without leaving voids.

3.1 Phase geometry and shape functions

According to (1) the geometry of a composite with non-flexible particles can be described as presented in Figure 3 with so-called shape functions μ_P and μ_S mathematically expressed by Equation 3. These functions are controlled by the shape factors, μ_P^o and μ_S^o , which consider the particle shapes at $c = 0$, and the critical concentration c_S , which considers the particles ability to pack in the composite. c_S is also that concentration above which no further increase in particles concentration can occur unless voids will appear. Only void-less composite Bingham materials are considered relevant in the present study. Thus, unless otherwise indicated, volume concentrations always mean $c \leq c_S$ in this work.

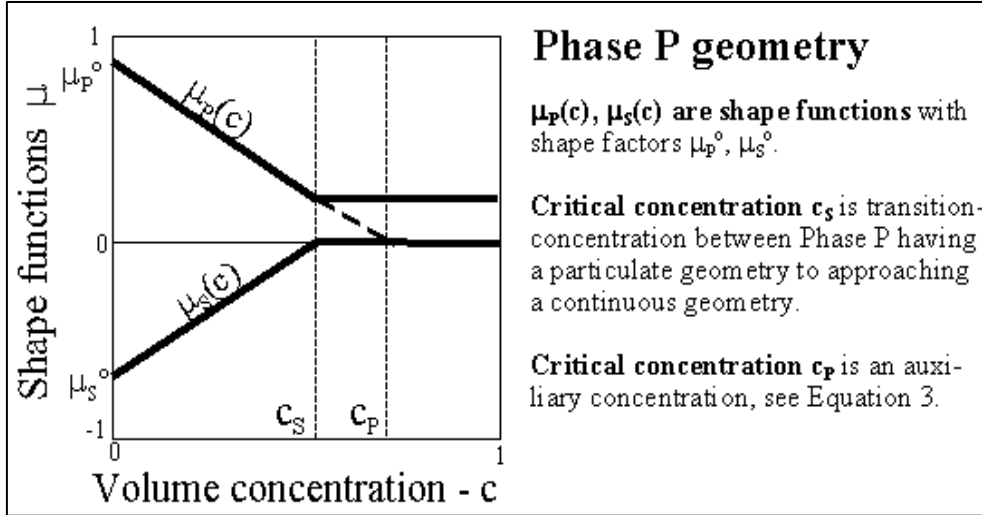


Figure 3. Composite geometry with non-flexible phase geometries

$$\mu_P = \mu_P^o \left(1 - \frac{c}{c_P} \right); \mu_S = \mu_S^o \left(1 - \frac{c}{c_S} \right) \quad ; \quad (c < c_S; c_P = -\frac{\mu_P^o}{\mu_S^o} c_S) \quad (3)$$

The shape factors in Equation 3 can be determined from Table B1 in Appendix B at the end of this paper. Examples are demonstrated in Figures 4 and 5 for mixtures of uni-shaped particles and double-shaped particles respectively¹⁾. More general shape distributions are considered in (2).

1. It is emphasized that the terms, uni- and double-shaped mixtures used mean mixtures of particles with equal shapes (aspect ratios) and mixtures of particles with two shapes respectively. They *do not refer to size* of particles.

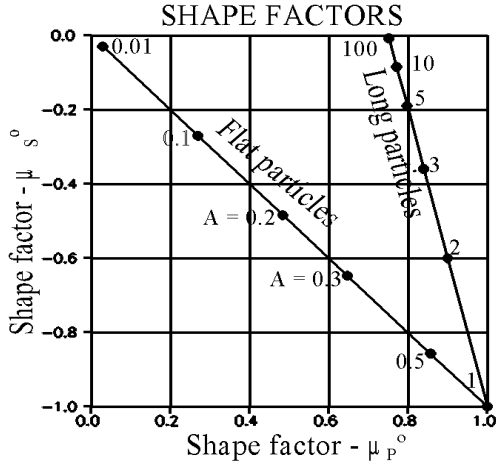


Figure 4. Shape factors for a uni-shaped mixture.

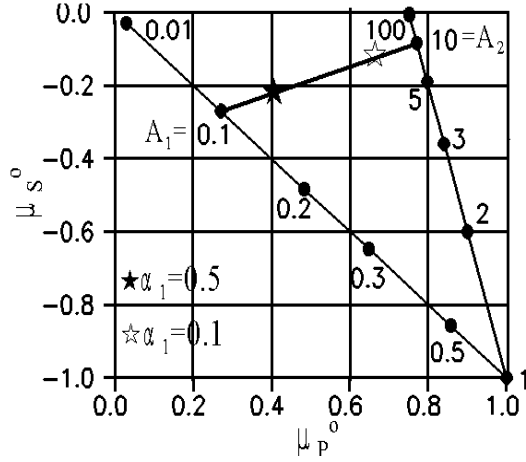


Figure 5. Shape factors for a double-shaped mixture. *Examples:* A mixture of volume fraction $\hat{\alpha}_1 = 0.5$ $A_1 = 0.1$ with $\hat{\alpha}_2 = 0.5$ $A_2 = 10$ is indicated by a closed star. A mixture of $\hat{\alpha}_1 = 0.1$ $A_1 = 0.1$ with $\hat{\alpha}_2 = 0.9$ $A_2 = 10$ is indicated by an open star.

4. COMPOSITE PROPERTIES

With known critical concentration (c_s) and shape factors (μ_p^0 , μ_s^0) shape functions for a composite Bingham can now be calculated from Equation 3.

4.1 Viscosity

Then composite viscosity can be determined as shown in Equation 4 reproduced from Equation A3 in Appendix A at the end of this paper.

Arbitrary concentration

$$\frac{\eta}{\eta_s} = \frac{1 + c\theta_{g^\infty}}{1 - c} \quad \text{with} \quad \theta_{g^\infty} = \frac{3\mu_p^0 + \mu_s^0 - 1}{2\mu_s^0}$$

Dilute composite (very small concentration)

$$\frac{\eta}{\eta_s} = 1 + c(1 + \vartheta_{g^\infty}) \quad \text{with} \quad \vartheta_{g^\infty} = \frac{3\mu_p^0 + \mu_s^0 - 1}{2\mu_s^0}$$

(4)

The relative viscosity predicted for dilute solutions by Equation 4 agrees with Equation 5, former expression, developed by Einstein (8) in his study of the viscosity of dilute sugar solutions. (Spheres have $A = 1 \Rightarrow (\mu_p^0, \mu_s^0) = (1, -1) \Rightarrow \vartheta_{g^\infty} = 1.5$).

The more general prediction of viscosity by Equation 4 agrees with data obtained from experiments on mixtures made of fluids with finite particle concentrations. Two empirical descriptions (Eilers and Brinkman) for such data are presented in Equation 5 reproduced from (9,10). In Figure 6 these results are compared graphically with the results obtained by the present theory (with $A = 1$ and $c_s = 0.78$ estimated from the Eilers expression for $\eta/\eta_s = \infty$).

$$\frac{\eta}{\eta_S} = \left. \begin{array}{l} \left(1 + 2.5c \right) \quad \text{Einstein (accurate dilute)} \\ \left(1 + \frac{1.25c}{1 - 1.28c} \right)^2 \quad \text{Eilers (empirical)} \\ (1 - c)^{3/2} \quad \text{Brinkman (empirical)} \end{array} \right\} \text{spherical particles} \quad (5)$$

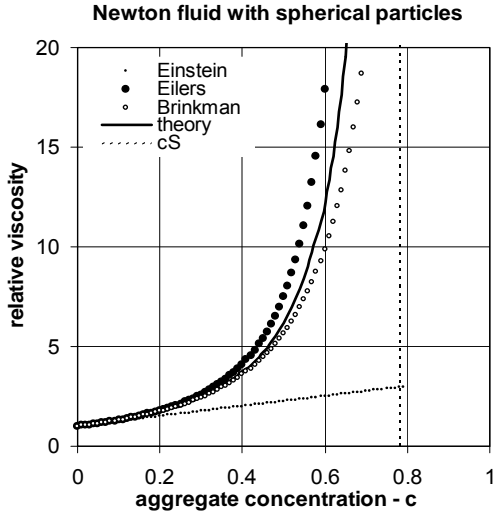


Figure 6. Spherical particles ($A = 1$) in a viscous matrix.

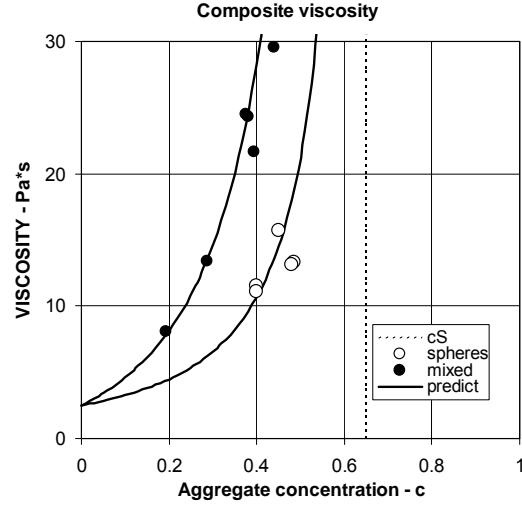


Figure 7. Viscosity of concrete as related to fraction of coarse aggregates

The experimental results shown in Figure 7 are from tests presented in (11,12). Concretes with various amounts of coarse aggregates were tested at an age of 15 minutes in a coaxial cylinder rheometer, see (7). Identical mortars were used in all concretes. Two coarse aggregate types were used: 1) Glass spheres and 2) a mix of 30% sea dredged and 70% crushed aggregates (typical Danish coarse aggregate). Both types of aggregates have a critical concentration of $c_s \approx 0.65$.

As before, spheres have an aspect ratio of $A = 1 \Rightarrow (\mu_p^0, \mu_s^0) = (1, -1)$. The average shape factors for the mixed aggregates are estimated to be $(\mu_p^0, \mu_s^0) = (0.40, -0.22)$ from assuming a 50-50% mixture of aggregates with aspect ratios of $A_1 = 0.1$ and $A_2 = 10$, see Figure 5. A mortar viscosity of $\eta_S = 2.5 \text{ Pa*s}$ has been estimated.

A complete investigation of aspect ratios was not made in (11,12). The few measurements/estimates made tell that any $A > 1$, which is very un-likely to fully characterize the geometry of natural aggregates. In the author's opinion some 'symmetry' around $A \approx 1$ must appear in shape-distributions for such particles. The very simple assumption (50-50%) made above reflects this idea – it does not, however, pretend to tell the truth. Various continuous shape distributions predict similar shape factors, see (2).

4.2 Yield stress

According to Equation A3 in Appendix A at the end of this paper the yield stress solution is expressed by Equation 6.

It is hereby assumed that the Bingham material behaves as an elastic matrix with extremely stiff particles until a matrix shear stress of τ_s^0 is obtained. In other words: The composite starts flowing when phase S starts flowing.

$$\frac{\tau^o}{\tau_S^o} = 1 + c\theta_{g\infty} \quad (6)$$

Pre-flow geometry

Equation 6 presumes particle phase geometry just as it is when the Bingham material is flowing according to Equation 4. For a number of reasons we cannot be sure that this assumption holds. More or less the ‘pre-flow’ geometry is influenced by effects which hold the materials structure in a stable state (here as an elastic solid). Special bounds (such as mechanical/physical/chemical) may have developed between matrix and particles, which have to be broken down before flow appears. Such effects add to the composite geometrical complexity.

It follows from (1) that increasing geometrical complexity of a composite is associated with lower (numerically) shape functions. We suggest that the ‘pre-flow’ geometry can be determined by modifying the ‘flow’ geometry as suggested in Equation 7, first expression. Then the yield stress becomes as expressed by the second expression,

$$\begin{aligned} \bar{\mu}_P &= \mu_P^o \left(\frac{\mu_P}{\mu_P^o} \right)^M & ; & & \bar{\mu}_S &= \mu_S^o \left(\frac{\mu_S}{\mu_S^o} \right)^M & \text{with interaction power } M \approx 3.5 & & (7) \\ \frac{\tau^o}{\tau_S^o} &= 1 + c\bar{\theta}_{g\infty} & \text{with} & & \bar{\theta}_{g\infty} &= \frac{3}{2} \frac{\bar{\mu}_P + \bar{\mu}_S - 1}{\bar{\mu}_S} \end{aligned}$$

It is anticipated that the interaction power M depends on both phases P and S – in a way which cannot, solely, be explained by normal shape functions. With identical phase S matrixes, the interaction power, M, probably will have to be calibrated to aggregate types (glass, granite, limestone, etc.). The interaction power indicated in Equation 7 has been determined by calibration to the concrete test results previously referred to (11,12).

It should be mentioned that the assumption of elasticity in the pre-flow state of a Bingham material can be disputed. An assumption of ideal stiff plasticity can also be stated. The present choice has been made in order to get a relatively simple method for determining the yield stress of Bingham composites.

Some support to the idea of the existence of an interaction power is presented in Figure 8: The test results in this figure are from the concrete tests previously referred to. A mortar yield stress of $\tau_S^o = 1.0$ Pa has been estimated. The predicted yield stresses in Figure 8 have been obtained by Equation 7 with an interaction power of $M = 3.5$, applying for both types of aggregates considered (glass and mixed).

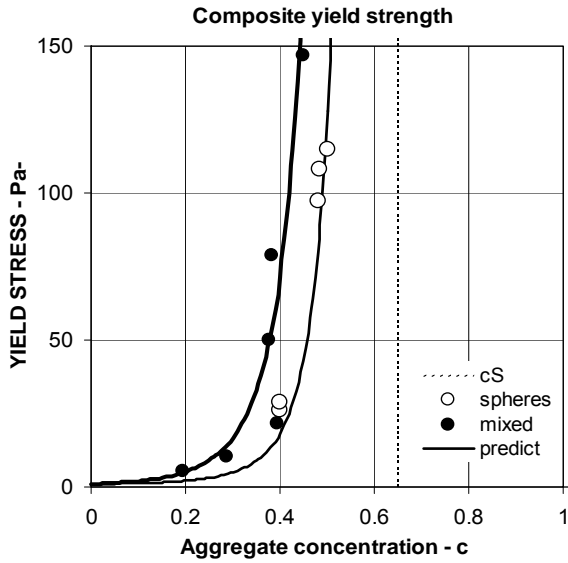


Figure 8. Yield strength of concrete as related to fraction of coarse aggregates. Further details are described in the main text.

5. APPLICATION

In this section we will demonstrate some potentials of the theory developed. Which mortar properties must be required in order to assure that the associated concrete becomes a SCC. The analysis made is based on material parameters deduced in this paper. For example, the pre-flow phase geometry is characterized by an interaction power of $M = 3.5$.

5.1 Fresh concrete (SCC) versus mortar

It is assumed that the concrete considered has a volume concentration, $c = 0.45$, of coarse aggregates similar to the mixed aggregates previously considered, meaning $(\mu_P^0, \mu_S^0) = (0.40, -0.22)$ and $c_S = 0.65$.

In order to work properly as self-compacting, a concrete must behave as a Bingham material with properties quantified inside the 'border lines' indicated in Figure 10 reproduced from recommendations presented in (13). For the target properties chosen in this example (dots in Figure 10) the theory presented in this paper (Equations 4 and 7) predicts qualified mortars to follow the Bingham properties indicated by dots in Figure 9.

Similar procedures can be applied to solve the problem, 'mortar versus paste', meaning: Which paste properties are required in order to develop mortars with prescribed Bingham parameters.

6. FINAL REMARKS

The well-known Bingham description of the rheology of homogeneous fluids with yield strength has been generalized in this paper also to include the rheological description of composite Bingham materials. For practice the advantage of such generalization is obvious: The Bingham behavior of composite Bingham materials can be described at any composition from knowing the Bingham properties of the matrix. The traditional composite Bingham descriptions need experimental calibration at any new composition.

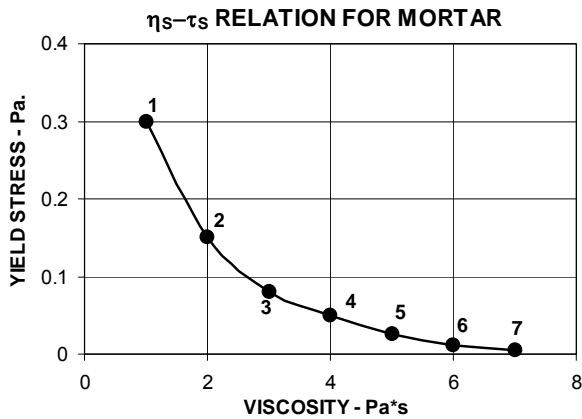


Figure 9. Mortars to be used in self compacting concretes with aggregate $c = 0.45$, see Figure 10.

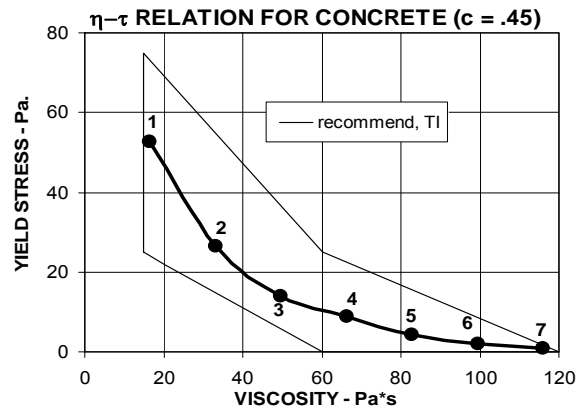


Figure 10. Concretes qualified as self-compacting concretes according to the T1-recommendations.

The geometry of the aggregate phase is considered in the theory by so-called shape functions with shape factors determined from shape distributions. Only two simple shape distributions are considered in this paper, namely a uni-shaped and a double-shaped distribution. References, however, are referred to where more general contributions are considered.

A hypothesis has been made that particle surfaces act differently (more efficiently) in the ‘pre-flow’ and in the ‘flow’ states of a composite Bingham material. A materials dependent interaction power, M , (to be experimentally determined) has been introduced to consider this effect.

Future research:

Two fields of future research are revealed: 1) The significance of the interaction power, M , has been explained in Section 4.2 (‘pre-flow geometry’). The hypothesis suggested has to be stronger justified. 2) The significance/importance of shape distributions has been identified (see Figures 4 and 5 and Table B1). Methods for practice have to be developed for measuring such distributions. Ideally, methods for measuring distributions, which consider both shapes and sizes of particles, have to be developed. Obviously, particles grading has a significant influence on the rheology of composite Bingham materials such as mortars (14). In the present paper this influence is clearly reflected by the critical concentration, c_s .

Curiosum:

The analysis made in this note on composite Bingham materials with stiff particles can easily be generalized to apply also for composite Bingham materials with soft particles (voids). Only a few obvious modifications have to be introduced (3). This feature might be useful when tailoring the viscosity of composite Bingham materials, for example by modifying the matrix (phase S) properties by air entrainment.

Application to fresh self-compacting concrete of the theory presented seems worthwhile. As such the theory may be considered as an alternative to other methods developed by other authors in the field of SCC - such as in (15,16,17,18,19,20,21).

7. NOTATIONS

Abbreviations and subscripts

V	Volume
P	Phase P
S	Phase S
g	Shear
No subscript	Composite material

Geo-parameters

$c = V_P / (V_P + V_S)$	Volume concentration of phase P
A	Aspect ratio, length/diameter of ellipsoidal particle
$\hat{\alpha}$	Volume fraction of joining aspect ratio (in a mixture of particles)
μ^0	Shape factor
μ	Shape function
c_S	Critical concentration
θ, ϑ	Geo-function
M	Interaction power

Stiffness and other properties (shear)

G	Stiffness (Shear modulus)
$n_g = G_P / G_S$	Stiffness ratio
η	Viscosity
Stress (shear)	
τ	Shear stress
τ^0	Yield stress

APPENDIX A: Composite properties

A.1 Elastic composite

Two elastic materials, phase P with shear modulus G_P , and phase S with shear modulus G_S , are mixed as explained in Section 3.1. How does the composite behave?

The elastic solution presently considered is the one where Poisson's ratios $\nu_P = \nu_S = 0.5$ apply, meaning that the phases are incompressible (such as in liquids). The composite solutions for shear modulus and phase stresses are the following deduced from (1) with shape functions (\cdot) introduced from Equation 3 of the main text.

$$\left. \begin{aligned} \frac{G}{G_S} &= \frac{n_g + \theta_g [1 + c(n_g - 1)]}{n_g + \theta_g - c(n_g - 1)} && \text{(Shear modulus)} \\ \frac{\tau_S}{\tau} &= \frac{n_g + \theta_g}{n_g + \theta_g [1 + c(n_g - 1)]} && \text{(Phase S stress)} \\ \frac{\tau_P}{\tau} &= \frac{n_g (1 + \theta_g)}{n_g + \theta_g [1 + c(n_g - 1)]} && \text{(Phase P stress)} \end{aligned} \right\} \begin{array}{l} \text{elastic composite in general} \\ \text{with stiffness ratio } n_g = G_P/G_S \end{array} \quad (A1)$$

with so-called geo-function $\theta_g = \frac{3}{4} \left[\mu_P + n_g \mu_S + \sqrt{(\mu_P + n_g \mu_S)^2 + 4n_g(1 - \mu_P - \mu_S)} \right]$

Extremely stiff phase P

When phase P is extremely stiff, meaning $n_g = \infty$, Equation A2 reduces as follows

$$\frac{G}{G_S} = \frac{1 + \theta_{g\infty} c}{1 - c} ; \quad \frac{\tau_S}{\tau} = \frac{1}{1 + c\theta_{g\infty}} ; \quad \frac{\tau_P}{\tau} = \frac{1 + \theta_{g\infty}}{1 + c\theta_{g\infty}} \quad \text{with geo-function } \theta_{g\infty} = \frac{3}{2} \frac{\mu_P + \mu_S^{-1}}{\mu_S} \quad (A2)$$

A.2 Viscous composite

According to the elastic-viscous analogy we can determine solutions to a liquid problem from the elastic counterpart solutions by replacing shear moduli with viscosities, deformations with deformation velocities, and considering stresses as shear stresses (τ) .

In the present context we will look at the Bingham liquid problem: Two liquids, phase S with viscosity $\hat{\eta}_S$, and phase P with viscosity $\hat{\eta}_P$, are mixed: How does the composite behave? For a very stiff phase P Equation A2 transforms as follows.

$$\left. \begin{aligned} \frac{\eta}{\eta_S} &= \frac{1 + \theta_{g\infty} c}{1 - c} && \text{Viscosity} \\ \frac{\tau_S}{\tau} &= \frac{1}{1 + c\theta_{g\infty}} && \text{Phase S stress} \end{aligned} \right\} \text{Liquid mixed with very stiff particles} \quad (A3)$$

We notice that the phase S stress solution applies for both elastic and a liquid composite. For the composite Bingham material, defined in Section 3, this means that this solution applies also in the 'pre-flow' state (see Section 4.2).

APPENDIX B: Shape factors

The shape factors needed for establishing the shape functions can be determined by the following Table B1 deduced from (1). Two simple shape distributions are considered in this table, Uni-shaped and Double shaped mixtures.

SHAPE FACTORS	
Uni shape mixture with A	
$\mu_P^0 = \begin{cases} \frac{3A}{A^2 + A + 1} & A < 1 \\ 3 \frac{A^2 - A + 1}{4A^2 - 5A + 4} & A > 1 \end{cases} ; \quad \mu_S^0 = \begin{cases} \mu_P^0 & A < 1 \\ 4\mu_P^0 - 3 & A > 1 \end{cases}$	
Double shape mixture with A₁ and A₂	
$\mu_P^0 = \langle m_0 \rangle; \quad \mu_S^0 = -\langle m_\infty \rangle \frac{1 - \langle m_0 \rangle}{1 - \langle m_\infty \rangle} \quad \text{with shape parameters } \langle m \rangle$	
$\frac{1}{\langle m_0 \rangle} = \frac{\alpha_1}{m_{0,1}} + \frac{\alpha_2}{m_{0,2}} ; \quad \frac{1}{\langle m_\infty \rangle} = \frac{\alpha_1}{m_{\infty,1}} + \frac{\alpha_2}{m_{\infty,2}}$ <p>α_1 and $\alpha_2 = (1 - \alpha_1)$ are volume fractions of aspect ratios A₁ and A₂ respectively</p>	
$m_{0,i} = \begin{cases} \frac{3A_i}{A_i^2 + A_i + 1} & (A_i \leq 1) \\ 3 \frac{A_i^2 - A_i + 1}{4A_i^2 - 5A_i + 4} & (A_i > 1) \end{cases} ; \quad m_{\infty,i} = \frac{3A_i}{A_i^2 + A_i + 1} \quad (\text{any } A_i) ; \quad (i = 1, 2)$	

Table B1. Determination of shape factors for a mixture of uni-shaped or double-shaped ellipsoidal particles. The aspect ratio is defined by $A = \text{length/diameter}$ of particles. Spheres (compacts) have $A = 1$, long particles have $A > 1$, and flat particles have $A < 1$. The auxiliary quantities 'm' are so-called shape parameters developed in (1).

REFERENCES

1. Nielsen, L. Fuglsang: "Composite Materials – Properties as Influenced by Phase Geometry", Springer Verlag, Berlin, Heidelberg, New York, 2005.
2. Idem: "A Bingham material mixed with stiff particles - some theoretical aspects", Report R-161 (2007), Department of Civil Engineering, Tech. Univ. of Denmark.
3. Idem: "Rheology of extreme composites", In "Papers in Structural Engineering and Materials - A Centenary Celebration", 179-187, Dept. of Struct. and Materials, Tech. Univ. Denmark, 2000.
4. Bingham, E.C.: "An investigation of the laws of plastic flow", Bur. of Standards Bull., 13(1916), 309. 'Colloid types', Fifth Coll. Symp. Monograph, 1(1928), 219.
5. Reiner, M.: "Lectures on theoretical rheology" (third edition), North-Holland Publishing Company, Amsterdam, 1960.
6. Ferraris, C.F.: "Test Methods to Measure the Rheological Properties of High-Performance Concrete: State of the Art report", J. Res. NIST, 104[5], 461-578 (1999).
7. Nielsen, L. Fuglsang: "Self-Compacting Concrete (SCC) - Quantifying and modelling the rheology of Fresh Concrete as a Bingham-material", Report R-58 (2003), Department of Civil Engineering, Tech. Univ. of Denmark.
8. Einstein, A.: "Eine neue Bestimmung der Moleküldimensionen", An. Physik, 19(1906), 289 and 34(1911), 104.
9. Holliday, L. (ed): "Composite materials", Elsevier Publishing Company, New York, 1966, (p. 34, Chapter on Inclusions in a Viscous Matrix).
10. Eirich, R.F. (ed): "Rheology, Theory and Applications", Academic Press Inc., New York, 1958, (p. 363, Chapter on Rheological Properties of Asphalt).
11. Geiker, M.R., Brandl, M., Thrane, L. Nyholm, and Nielsen, L. Fuglsang: "On the effect of coarse aggregate fraction and shape on the rheological properties of self-compacting concrete". ASTM, Cement, Concrete, and Aggregates, 24(2002), No.1.
12. Brandl, M. and Thrane, L. Nyholm: "Rheological properties of Self Compacting Concrete (SCC)", M.Sc. thesis, Department of Civil Engineering, Tech. Univ. Denmark, 2001.
13. Technological Institute, Denmark: "Knowledge about SCC" (Viden om SCC), Information sheet, updated 20.01.2007.
14. Bager, D.H., Geiker M.R., and Jensen, R.M.: "Rheology of self-compacting mortars, influence of particle grading", Nordic Concrete Research, 26(2001), 1-16.
15. Wallevik, O.H.: "The rheology of the fresh concrete and applications for concrete with and without silica fume", Dr.ing. thesis, The Norwegian Institute of Technology – NTH, Norway, 1990.
16. Ferraris, C.F. and de Larrard, F.: "Testing and modeling of fresh Concrete Rheology", National Institute of Standards and Technology, Washington DC, NIST Report 1094, 1998.
17. De Larrard, F.: "Concrete Mixtures Proportioning: A Scientific Approach", Modern Concrete Technology Series, E&FN SPON, London 1999.
18. Oh, S.G., Nogushi, T. and Tomosawa, F.: "Towards mix design for rheology of self-compacting concrete", in proc. of First International RILEM Symposium on Self-Compacting Concrete (eds. Skarendahl, Å. and Peterson, O.), Stockholm, September 13-14, 1999, Proc 7, S.A.R.L., Cachan, 1999, pp. 361-372.

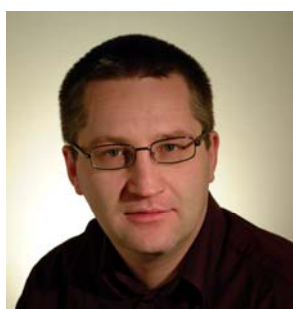
-
19. Wüstholtz, T.: “Experimentelle und theoretische Untersuchungen der Frischbetoneigenschaften von Selbstverdichtendem Beton”, Dr. thesis, Universität Stuttgart, Institut für Werkstoffe im Bauwesen, 2005.
 20. Idem: “A model approach to describe the fresh properties of self-compacting concrete (SCC)”, Otto-Graf-Journal, Vol. 16, 2005, pp. 79-93.
 21. Westerholm, M.: “Rheology of the Mortar Phase of Concrete with Crushed Aggregate”, Ph.D. thesis, Luleå Univ. of Technology, Dept. Chem. Eng. and Geosciences, Division of Mineral Processing, 2006.



FEM simulations of reinforced concrete beams attacked by corrosion



Irina Sæther
M.Sc., PhD student
Northern Research Institute Narvik (Norut Narvik)
PB 250, NO-8504 Narvik, Norway
E-mail: irina.saether@norut.no



Bjørnar Sand
Dr. ing., Research Scientist
Northern Research Institute Narvik (Norut Narvik)
PB 250, NO-8504 Narvik, Norway
E-mail: bjoernar.sand@norut.no

ABSTRACT

The present work is devoted to the application of finite element analysis to simulate the mechanical behaviour of reinforced concrete members with corroding steel bars using the finite element program DIANA. In the present approach only the effects of corrosion are taken into consideration. Accordingly, loss of steel bar section, and reduced bond between deteriorated concrete and corroded rebar are accounted for in the present work. The results of the simulations are validated against published results from laboratory tests on medium scale beams. The load-deflection behaviour obtained from the finite element simulations are in agreement with the test data.

Key words: Reinforced concrete, corrosion, load-carrying capacity, bond-slip behaviour.

1. INTRODUCTION

Deterioration and ageing of concrete structures and the increased traffic intensities and loads are some of the major problems facing civil engineers, industry and researchers today. Early deterioration of concrete due to aggressive environments and poor construction quality has occurred in many reinforced concrete structures. This may lead to a number of undesirable consequences such as loss of serviceability, loss of load carrying capacity and reduction in structural safety, or simply ugly appearance. Corrosion of steel reinforcement is the principal cause of deterioration of concrete structures [1], and corrosion affects the reinforcement, the concrete and the composite action between steel and concrete. Reduction in bar cross sectional area, cracking and spalling of concrete cover, reduction in bond strength and changes in bond-slip behaviour are known as the local effects of steel bar corrosion [2].

The most obvious consequence of reinforcement corrosion is the reduction in cross sectional area of the affected steel bars. While homogeneous attack penetration (uniform corrosion) occurs in carbonated concrete, chlorides usually produce localised attack known as pitting, which causes a significant decrease in cross section of the steel sometimes without visible signs of deterioration at the concrete surface [1, 3]. The uniform corrosion is associated with formation of 'brown rust' iron oxides. The oxides occupy a greater volume than the parent metal, and the expansion of the diameter of the bar as it corrodes generally leads to cracking and eventually spalling of concrete cover before an appreciable portion of the cross sectional area is lost. The corrosion products formed during local corrosion do not exhibit the same degree of volumetric expansion as brown rust [1]. Consequently, the tendency of splitting the concrete cover along the corroding bar is less with local corrosion. Bond between reinforcement and concrete is an important condition for the bar end anchorage and the composite interaction between steel and concrete at intermediate parts of the bar. However, corrosion reduces bond due to the weakening of the bar confinement produced by both the concrete cracking and the stirrup corrosion. Consequently, anchorage failure and loss of composite interaction may occur [3].

Bond stress is commonly regarded as pure shear stress acting on the surface of a bar. The relative displacement between the steel bar and the surrounding concrete, in the direction of the bar, is denoted slip. When slip occurs, frictional forces develop between bar and concrete. Corrosion affects bond between a steel bar and concrete in several ways. In the initial stage, the corrosion products accumulate on the surface of the bar and the associated increase in bar diameter causes an increase in radial stresses between the bar and concrete, thereby increasing the frictional component of bond [2]. At a later stage, longitudinal cracking reduces the effective confinement of the bar and also the bond strength. Corrosion products are mechanically weaker than the original steel and this contributes to reduced bond strength. Further reduction in bond strength can be anticipated at more advanced stages of corrosion where the height of the ribs of the deformed bar is being reduced.

The continuous degradation of the concrete infrastructure has thus lead to a need for reliable methods to predict residual service life of deteriorated structures. Design Codes and Standards are intended primarily for new construction, and may not contain the information required for assessment of deteriorated structures [1]. Review of available results from experimental and numerical studies carried out in international projects are presented in reports and other publications by several authors, and some general approaches and recommendations have been developed and presented to predict the behaviour of corroded concrete structures, for example [3, 4 and 5] .

The main objective of this work is to get an opportunity to assess available test data for nonlinear element analysis to obtain realistic prediction of behaviour of corroded concrete beams using the commercially available finite element program DIANA [6]. Further, the developed procedure is going to be used for numerical simulations of the experimental study of deterioration, retrofitting and strengthening of concrete beams carried out by Bergström [7].

2. PREVIOUS FINITE ELEMENT SIMULATIONS

During the recent years several research projects have been carried out to develop models which are suitable to investigate the effect of corrosion on bond strength between the corroded reinforcement and the surrounding concrete by the finite element method. The finite element

method is proved to be a convenient tool to assess the global flexural behaviour of corroded reinforced concrete structures. The relationships between the corrosion degree and the load capacity, deflection at service and failure loads, and the stiffness of the structure were investigated by several researches using their own finite element codes or different commercial finite element programs. Unfortunately, some few experimental investigations could be found in the literature, which are suitable for validation and verification of the finite element models. Some of numerical investigations which were carried out during the last ten years will be mentioned here.

Modelling of the effect of corrosion on bond deterioration for different confinement levels given by the transverse steel reinforcement have been carried out by Berra et al. [8] using the commercially available finite element code ABAQUS. Three-dimensional axi-symmetric elements were chosen to model one single bar with ribs of annular shape and the surrounding concrete. An approach was developed to model the corrosion product expansion causing concrete-cover cracking. The numerical analyses reproduced the experimental results of the bond tests. A parametric study represented the effect of the varying transverse steel percentage on the residual bond strength and the influence of different arrangements of confinement bars.

Three-dimensional finite element analysis with solid elements for concrete and reinforcement were performed by Lundgren [9, 10 and 11]. The finite element program DIANA was used for numerical analysis of corrosion cracking tests and pullout tests with corroded reinforcement. The interface elements were applied at the surface between reinforcement bar and the surrounding concrete to describe a relation between traction and relative displacement. The interface elements included both a frictional bond model and corrosion model. The frictional bond model is equivalent to the Coulomb friction model, complemented with a yield function describing the upper limit. The mechanical behaviour and the volume of the corrosion products were given as input for a corrosion layer. This layer was used, together with a model developed for the bond mechanism, in the finite element analysis of the tests with corroded reinforcement. As results of the finite element simulations the bond-slip behaviour of corroded concrete specimens for variable corrosion levels with different failure modes could be obtained. Reasonably good agreement between experimental test results and analyses was presented. The suggested model can be used for both ribbed and smooth bars.

Castellani and Coronelli [12] have been investigating the structural effects of bar corrosion in reinforced concrete beams by means of finite element analysis. The concrete was modelled using plane elements with thickness equal to the beam width. The truss elements, which represented the bar, were coupled to the concrete elements by bond link elements. The bond-slip law for uncorroded bars was specified using the CEB-FIP Model Code 1990, and a bond-slip model for corroded bars was proposed. The presented procedure considered the bond deterioration, bar cross section reduction, concrete cracking and covers spalling, and it proved to be efficient in reproducing the experimental behaviour of reinforced concrete beams. Some years later Coronelli and Gambarova [4] presented this procedure with some improvements in constitutive modelling. References were made to several tests on corroded beams, performed by other authors, in order to clarify the major consequences that corrosion has on the structural behaviour in service and limit states.

A finite element study of the flexural behaviour of corroded concrete beams in which the influence of the percentage of corrosion on the load–deflection curve was studied, was presented by Dekoster et al. [13]. CASTEM 2000 computation software was used and the output compared with two experimental studies, the first on uniformly corroded beams, and the second

based on a long-term experimental program inducing heterogeneously localised corrosion of beams. For the computation special “rust” elements were used to represent the interface between steel and concrete. A sensitivity analysis was carried out using different sizes of rust elements, in order to study their influence on the analysis accuracy. Comparison of the results showed good correlation between the finite element computation and the experimental studies, and highlighted the efficiency of the rust elements for the flexural behaviour study. In particular, the ultimate load and the deterioration of the stiffness with corrosion were accurately modelled.

Horrigmoe and Hansen [14] presented results of numerical simulation of corroded reinforced beams with only tensile reinforcement. The failure of the corroded beams was governed by bond failure. The finite element program ANSYS was used to carry out these numerical simulations with the bond-slip law specified by the Tørle and Horrigmoe [15]. Only reduction in the cross section area due to uniform corrosion of reinforcement and reduction of the bond strength between the corroded reinforcement and concrete were implemented into the model to estimate the residual load capacity of the beams. According to the authors excellent agreement between test data and the nonlinear finite element analysis was achieved.

The finite element program ANSYS was also used by Sand [16] to simulate the entire service life cycle of a reinforced concrete beam with tensile reinforcement attacked by uniform and pitting corrosion and with spliced tensile reinforcement attacked by only uniform corrosion. The concrete beam with a free span of 8.0 m was subjected to a sequence of phases with loading to serviceability load, corrosion, partial unloading, repair and loading until failure. In addition, the exposed length of the tensile reinforcement was varied as well as the degree of corrosion attack. The results of the numerical simulations showed that nonlinear finite element analysis can be effectively utilized to obtain realistic predictions of failure loads of repaired reinforced concrete beams.

3. PREVIOUS FINITE ELEMENT SIMULATIONS

3.1 Laboratory study by Rodriguez et al.

The laboratory study on the effect of steel bar corrosion on the serviceability and load carrying capacity of concrete beams carried out by Rodriguez et al. [17, 18] was chosen to be analysed in the present project. This experimental work included 31 beams tested with objective to study different variables such as levels of corrosion, detailing of reinforcement (ratio of tensile reinforcement, ratio of compressive reinforcement, shear reinforcement, anchorage of tensile reinforcement) and interaction between corrosion and loading [17, 18]. The geometry of the simply supported beams is shown in Figure 1. These beams had both tensile and compressive longitudinal reinforcement as well as stirrups. The beams selected for numerical simulations in the present study were the reference beams (no. 111 and 112) and a beam with corroded reinforcement (no. 115). In these beams the tensile, compressive and transverse reinforcement were bars of 10 mm, 8 mm and 6 mm diameter, respectively.

The concrete in the reference beams had uniaxial compressive strengths at the date of testing in the interval 48-52 MPa. In the concrete used for the corrosion damaged beams, calcium chloride (3 percent by weight of cement) was added to the mixing water in order to accelerate the corrosion process. For this concrete the uniaxial compressive strength ranged from 31 to 37 MPa. The beams were cured for 28 days in wet conditions. Then an accelerated corrosion procedure was initiated, in order to achieve the required level of corrosion in a time period

ranging from 100 to 200 days, approximately. The reinforcement was subjected to a constant current density of about 0.1 mA/cm².

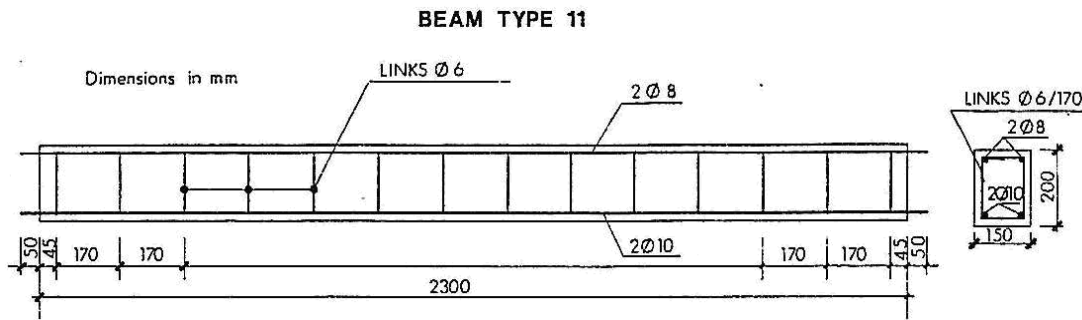


Figure 1 – Beam specimens tested by Rodriguez et al. [17, 18].

It is important to note that the corrosion attack penetration varies for tensile bars, compressive bars and stirrups in a single beam, for a given corrosion period. Moreover, due to the presence of stirrups the corrosion was not uniform along the longitudinal reinforcement. After the accelerated corrosion process was completed, the beams were subjected to a four-point bending test. The two reference beams (111 and 112) exhibit typical ductile flexural failure governed by yielding of the tensile reinforcement. As the level of corrosion is increasing, the load carrying capacity is reduced and the behaviour becomes less ductile. Corroded beams of this category failed by failure of the tensile bars at pits. Loading cracks perpendicular to the beam axis were also measured; the crack widths were typically 0.2 to 0.3 mm.

3.2 Numerical simulations

The numerical simulations carried out in the present study are based on the commercial finite element code DIANA (Release 9.1) [6]. Due to symmetry, only one half of the beam was modelled using eight-node quadrilateral CQ16M plane stress elements for concrete with a regular 14 x 48 mesh, see Figure 2. The main steel reinforcement and links was represented by discrete truss CL6TR elements with three nodal points located along the mesh of the concrete elements. Bond stress-slip relations are implemented for intact as well as corroded bars using interface elements IP33 CL12I.

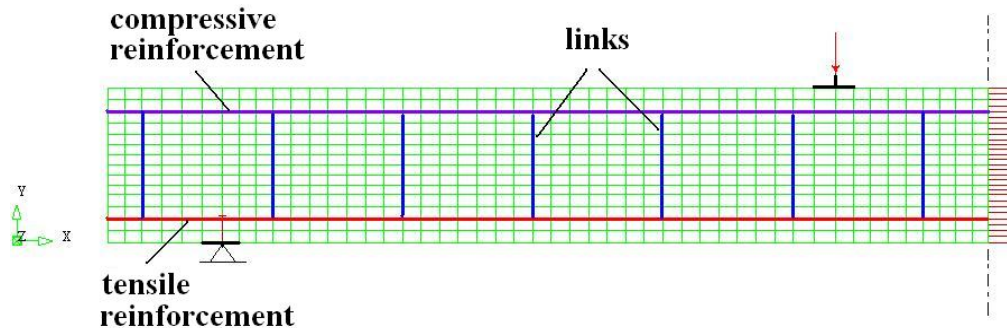


Figure 2 – Finite element model of one half of the beam.

The concrete is modelled with a smeared crack model. The total strain fixed crack model and the rotating crack model were employed in the present finite element analyses in order to investigate the effects of the type of crack model on the structural response. The best fits to the test data

were obtained with the rotating crack model. Time depended effects such as creep and shrinkage of concrete, and effect on strength of sustained load were not included in the present numerical analysis. Description of the different crack models available in the finite element program DIANA could be found in [19, 20].

The compressive behaviour of concrete was represented by two different stress-strain curves [19]. The first of these was the simple, elastic-ideally plastic relationship illustrated in Figure 3a. The second model utilized a more realistic representation of the compressive stress-strain curve for concrete (parabolic), see Figure 3b. The tensile behaviour of concrete was represented by a bilinear approximation (Figure 3a and 3b), where the tensile stress increases linearly up to the uniaxial tensile strength f_{ct} followed by linear softening behaviour. The same modulus of elasticity in tension and in compression was used in the numerical simulations. The crack bandwidth h was calculated as the root of the total area of a finite element for the higher order two-dimensional elements [6]. The fracture energy G_f in tension was used from Table 3.1.1 in CEB-FIP Model Code 1990 [21]. The area under the tensile stress-strain curve in Figure 3 is equal to G_f/h . The compressive fracture energy G_c was estimated as the area under the compressive parabolic stress-strain curve based on CEB-FIP Model Code 1990 [21].

The stress-strain curve of reinforcing steel [22] was taken as for an elasto-plastic material with linear strain hardening, see Figure 3b. The tangent modulus E_{ST} in the plastic regime was set equal to $E_s/250$.

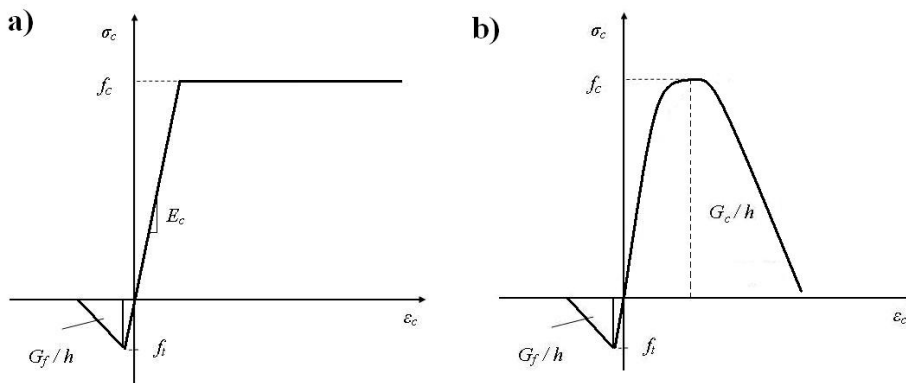


Figure 3 – Stress-strain curves for concrete [22].

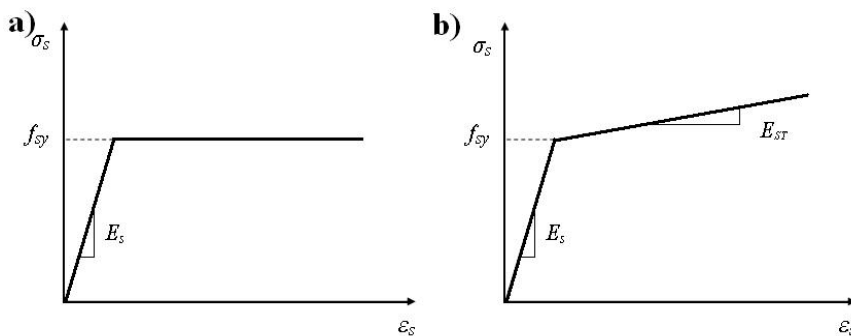


Figure 4 – Stress-strain curves for steel reinforcement: a) Standard elastic-ideally plastic material [22]; b) Elasto-plastic material with linear strain hardening.

The uniform corrosion model [3] is used in the present numerical analysis. Consider a reinforcing bar with initial (nominal) diameter ϕ_0 . As a result of corrosion, the bar diameter is reduced. The residual cross section area of the tensile reinforcement attacked by uniform corrosion may be evaluated as (Figure 5a):

$$A_{res} = \frac{\pi \cdot \phi_R^2}{4} = \frac{\pi \cdot (\phi_0 - \alpha x)^2}{4} \quad (1)$$

where ϕ_R is the residual bar diameter, α is coefficient depending on the type of attack and x is corrosion penetration.

When uniform corrosion occurs, α is equal to 2 [3]. In the case of localized pitting attack, the cross sectional area becomes irregular and the net loss of area may be significantly greater than for uniform corrosion. Eq. (1) can be used to estimate loss of bar section due to pitting by introducing an equivalent circular cross section with diameter ϕ_R , as shown in Figure 5b. In the case of pitting the value of α may be in the range between 4 and 8 [23].

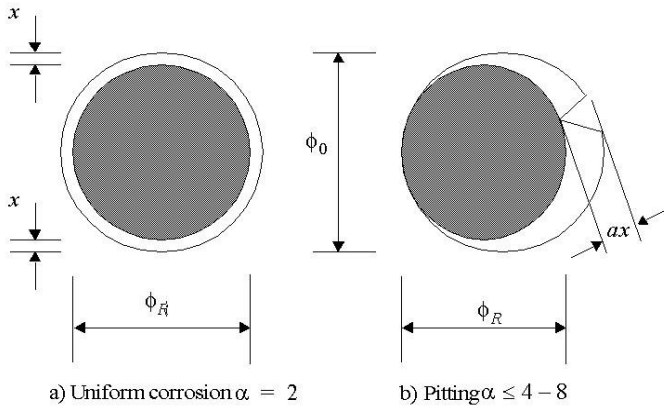


Figure 5 – Residual steel bar cross section [3].

Bond between steel bars and the surrounding concrete may play a crucial role in the mechanical response of structures attacked by corrosion. For steel bars embedded in well confined concrete the mode of failure is by pullout. The corresponding bond stress-slip relationship for uncorroded steel bars from CEB-FIP Model Code 1990 [21] is adopted in the present analysis. According to this model bond stress τ between the concrete and the reinforcing bar can be calculated as a function of the relative displacement (slip) s as follows (Eqs.2 - 5):

$$\tau = \tau_{\max} (s/s_1)^\alpha \quad \text{for } 0 \leq s \leq s_1 \quad (2)$$

$$\tau = \tau_{\max} \quad \text{for } s_1 \leq s_2 \quad (3)$$

$$\tau = \tau_{\max} - (\tau_{\max} - \tau_f) \left(\frac{s - s_2}{s_3 - s_2} \right) \quad \text{for } s_2 < s \leq s_3 \quad (4)$$

$$\tau = \tau_f \quad \text{for } s_3 < s \quad (5)$$

where τ_{\max} is the maximum bond strength and τ_f is the residual bond strength. The parameters used in these equations are defined in Figure 6. CEB-FIP Model Code 1990 suggests the following values for the bond strength τ_{\max} and the residual bond capacity τ_f for unconfined concrete and all other bond conditions (Eqs. 6 - 7):

$$\tau_{\max} = 1.0 \sqrt{f_{ck}} \quad (6)$$

and

$$\tau_f = 0.15 \tau_{\max} \quad (7)$$

where f_{ck} is the characteristic value of the uniaxial compressive strength of concrete measured on cylindrical specimens.

All parameters for defining the bond-slip relationship according to the equations above could be found in table in CEB-FIP Model Code 1990 [21].

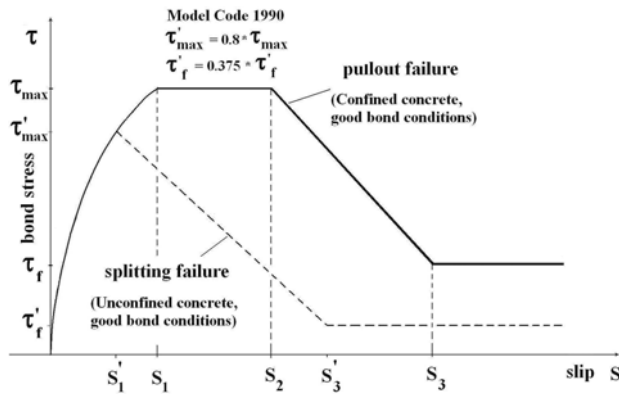


Figure 6 – Bond - slip diagram for monotonic loading. CEB-FIP Model Code 1990 [21].

The bond strength τ_{\max} of a steel bar attacked by corrosion depends on the depth of corrosion attack x as

$$\tau_{\max}^c = \tau_{\max}(x) \quad (8)$$

Bond deterioration in the post-cracking regime may be estimated using the empirical formulas by Rodriguez [24]. The bond stress-slip diagram adopted in the CEB-FIP Model Code 1990 was taken as a basic for development of some models of corroded bars used for numerical simulations.

Tørlien and Horrigmo [15] proposed a model (Figure 7a) which was obtained by scaling of both axes of the bond stress – slip diagram for uncorroded reinforcement. In the simple application of this method only the bond stress values may be reduced, while the slip values remained unchanged. The scaling factor may be obtained as a ratio between the residual τ_{\max}^c and maximum bond strength τ_{\max} or a ratio between the value of slip s_1 at maximum bond strength and value of slip corresponding to the residual bond strength s_1^c . The residual bond strength τ_{\max}^c may be calculated from the empirical formula by Rodriguez or based on experimental data.

The residual bond τ_f^c is suggested to be taken as a fraction of this value or set equal to zero. In the numerical simulations by Tørle and Horrigmoe [15] the maximum bond strength was reduced by 50 % for corroded reinforcement and was assumed to be unchanged along the deteriorated region.

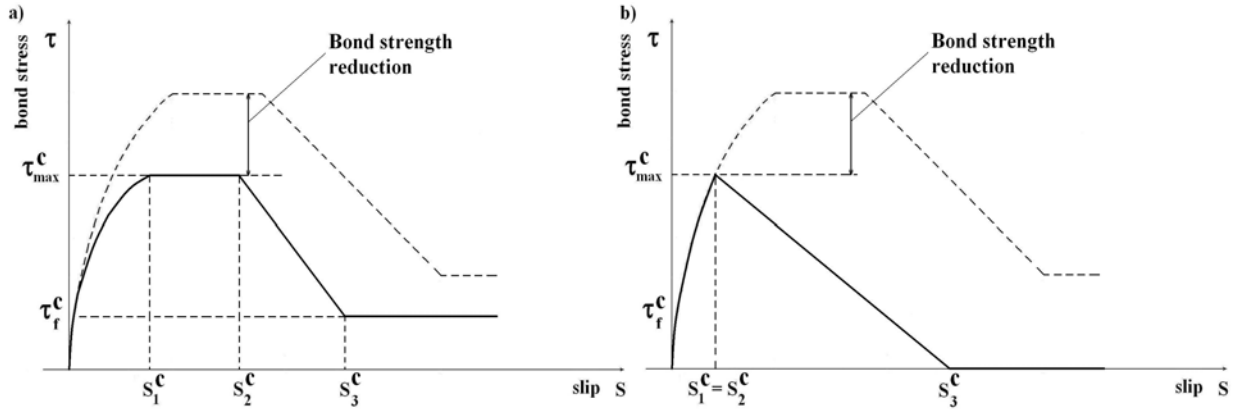


Figure 7 – Bond-slip model for corroded reinforcement: a) Tørle and Horrigmoe [15]; b) Castellani and Coronelli [12].

Castellani and Corronelli [12] modified also the bond-slip model of CEB-FIP Model Code 1990 to account for several corrosion effects (Figure 7b). The stiffness of the increasing branch of the bond-slip curve up to the maximum bond stress is possible to describe by determining the value slip s_1^c . To represent a ductile pull-out failure, the slip s_1^c and s_2^c can be assigned in order to determine a flat portion of the curve at maximum stress, followed by a gradual decrease down to the end of the descending branch. To model the splitting failure mode, s_2^c must be taken close to s_1^c and the descending branch must be sharp, reducing the value of s_3^c , and considering $\tau_f^c = 0$. The maximum bond strength in the bond-slip relation may be evaluated using the empirical formula proposed by Rodriguez et al. [24] as for Tørle and Horrigmoe's bond-slip model for corroded bars [15].

Bond-slip relationship for the reference beams

No experimental data on bond is available in [17, 18]. The bond strength and slip parameters for the reference beam (no corrosion) adopted in the present finite element simulations are chosen based on CEB-FIP Model Code 1990: $\tau_{\max} = 7.0$ MPa; $\tau_f = 1.05$ MPa; $s_1 = s_2 = 0.6$ mm; $s_3 = 2.5$ mm; $\alpha = 0.4$. Trial calculations with varying bond properties documented that the response of the beam is insensitive to the choice of bond strength and slip values for the case with elastic-ideally plastic representation of the compressive stress-strain curve (Figure 3).

Bond-slip relationship for the corroded beams

In the absence of test data it was assumed that the bond strength of corroded bars of beam no. 115 was reduced to 65 % or alternatively 80 % of the bond strength used for the reference beam, hence $\tau'_{\max} = 4.55$ MPa or $\tau'_{\max} = 5.6$ MPa. Furthermore the entire bond stress-slip relationship was scaled by the same factors 0.65 or 0.8 (both axes). For the corroded compressive

reinforcement the original bond stress-slip curve was left unchanged, simply because the bond stresses here are so low that bond failure is excluded.

Material parameters

The concrete compressive cylindrical strengths for the various series of beam specimens are specified by Rodriguez et al. [17, 18]. It should be noted that the compressive strength of the corroded beams were only about 70 % of the strength of the reference beams. Hence, the two sets of beams were made of different materials and this must be accounted for in the selection of material parameters. Rodriguez et al. [17, 18] specify only the basic strengths of concrete and reinforcing steel. The remaining material parameters required for the finite element simulations had to be calculated using Norwegian Code for Design of Concrete Structures NS 3473 [24, CEB-FIP Model Code 1990 [21] or assessed based on previous experience see Table 1.

Table 1 – Material parameters

Parameter	Symbol	Value		Remark
		Reference beam	Corroded beams, no.115	
Uniaxial compressive strength, cylinder (cube)	f_{cc}	50 MPa (61MPa)	31.4 MPa (40.8 MPa)	Ref.18, calculated NS 3473
Uniaxial tensile strength	f_{ct}	3.5 MPa	2.8 MPa	Calculated NS 3473
Modulus of elasticity, concrete	E_c	32 200 MPa	28300 MPa	Model Code 1990
Fracture energy (tension)	G_f	0.116 Nmm·mm ⁻²	0.091 Nmm·mm ⁻²	CEB-FIP Model Code 1990 (dmax = 16 mm)
Crack bandwidth	h	17 mm	17 mm	Predefined in DIANA
Fracture energy (compression)	G_c	0.15 Nmm·mm ⁻²	0.132 Nmm·mm ⁻²	Assumed based on CEB-FIP Model Code 1990
Uniaxial yield strength/ Uniaxial ultimate strength for steel	φ_{10}	575/655 MPa	575/655 MPa	Ref. 17
	φ_8	615/673 MPa	615/673 MPa	Ref. 17
	φ_6	626/760MPa	626/760MPa	Ref. 17
Modulus of elasticity, steel	E_s	206 GPa	206 GPa	Ref. 17
Elasto-plastic tangent modulus, steel	E_{ST}	824 MPa	824 MPa	Assumed

3.3 Verification against the experimental data

Finite element analysis was first carried out for the reference beams, which were not subjected to corrosion. During the laboratory testing, two reference beams (no. 111 and no. 112) were tested and the measured load-deflection response of these two beams is illustrated in Figure 8. The small differences between the two experimental results are of acceptable magnitude. Also the results obtained from the finite element simulations using the bilinear and parabolic representation of the compressive stress-strain curve of concrete in compression are shown in this diagram. The agreement between the numerical solution and the test data is good, particularly with regard to beam no. 111. The reference beams had a low ratio of tensile reinforcement and exhibited flexural failure with yielding of the tensile reinforcement in the laboratory tests. The same type of behaviour was obtained in the finite element simulations and is characterized by the long horizontal plateau of the load-deflection diagram in Figure 8.

Further, in the numerical analysis, increasing deflections will eventually lead to crushing of the concrete compressive cover. Unfortunately, the high cracking load is observed in the analyses compared to measurements in the laboratory. The choice of the values of the material parameters used in the numerical simulations will influence the behaviour of concrete beam before cracking.

Accurate simulation of the behaviour of beams with corroded reinforcement is complicated due to the fact that corrosion varied along the longitudinal bars due to the presence of stirrups. Also, for a given beam, the average corrosion level differed for the tensile, compressive and transverse reinforcement. After the laboratory testing had been carried out the total weight loss of each bar was measured, so that the average loss of bar section could be calculated. In addition, the maximum corrosion penetration at the pits was obtained by geometrical measurements. To simplify the problem somewhat, it was decided to simulate the behaviour of beam no. 115, for which the average levels of corrosion of tensile and compressive reinforcement were similar, 13.9 % for the tensile reinforcement and 12.6 % for the compressive reinforcement. In Figure 9 the load-deflection diagrams of the reference beam (no. 111) and the corroded beam no. 115 are compared. Firstly, only area reduction of reinforcement is used to describe the corrosion for the corroded beams. It is seen that both beams behave in ductile fashion. While the failure load of the reference beam was recorded at 42.5 kN, the failure load of the corroded beam was only 32.9 kN in the case of bilinear representation of the compressive stress-strain, or 77 % of the reference beam. Results of the finite element simulations using both constitutive models for the compressive behaviour of concrete are illustrated in Figure 9.

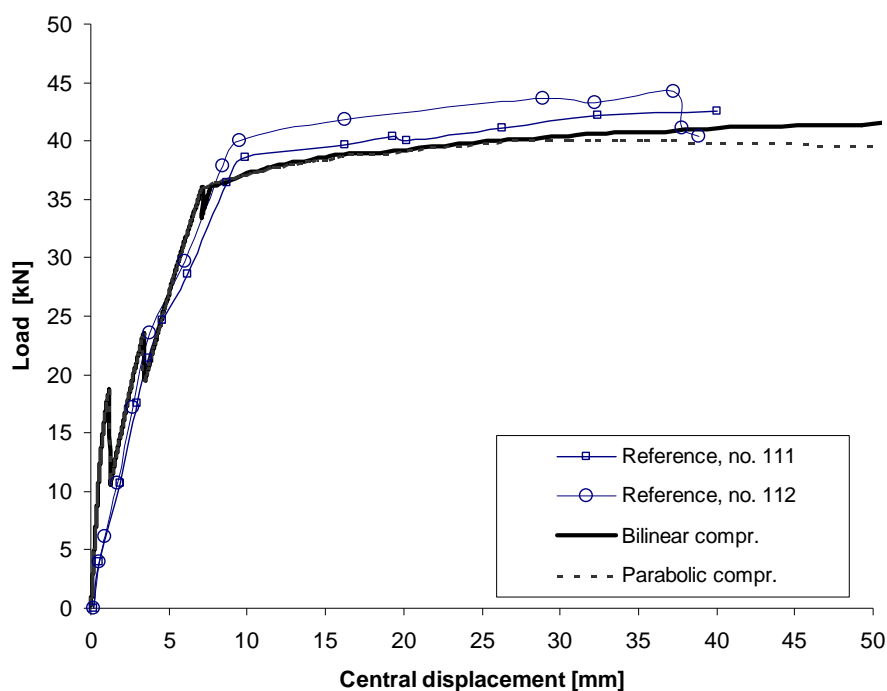


Figure 8 – Load versus central deflection for the reference beams (no. 111 and no. 112); bilinear and parabolic stress-strain curve in compression.

It is seen that the two numerical solutions are very close and the behaviour resembles the experimental behaviour of both the reference and the corroded beams. Accordingly, the results obtained with the bilinear model are used subsequently. The finite element analysis produced a

load-deflection behaviour which deviates slightly from the experimental curve. The calculated failure load was 34.2 kN, which is 3.9 % larger than the test failure load.

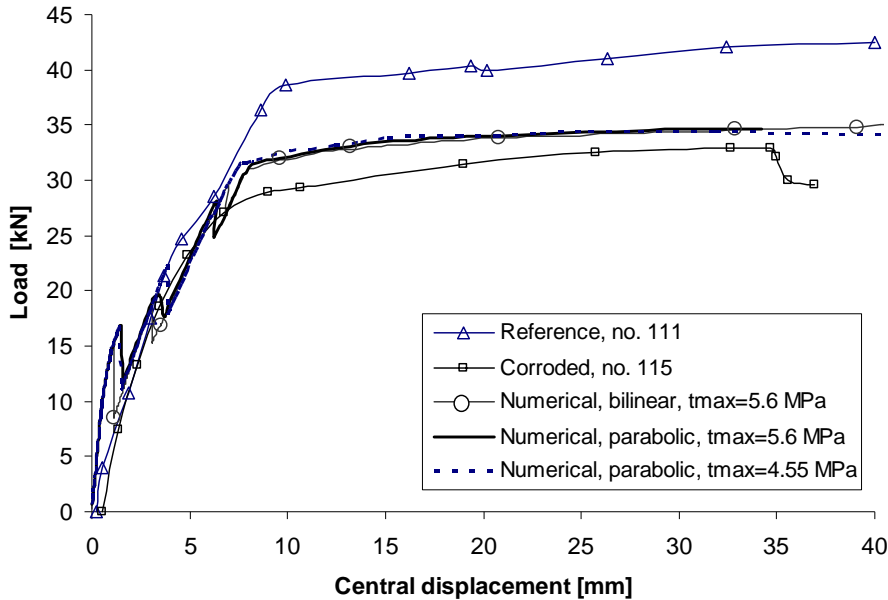


Figure 9 – Load versus central deflection for the corroded beam (no. 115): bilinear and parabolic stress-strain curve in compression with reduction in bond strength.

An attempt to simulate the behaviour of the corroded beam with reduced bond strength is also presented in Figure 9. No significant influence of the bond reduction on the behaviour and failure load of corroded beam is registered in the case of bilinear and parabolic representation of the compressive stress-strain curve. It can be concluded that in these tests the area reduction is the main parameter of the strength reduction in the corroded beams.

Calculated distributions of bond stress along the tensile and compressive reinforcement for the reference and corroded beams are depicted in Figure 10. The slip and bond stress distribution show that the higher slip and bond stress values are reached in the reference beam. The maximum bond stress in the tensile zone for reference and corroded beams are approximately 5.2 MPa and 4.5 MPa, respectively, which is less than the assumed bond strength (7.0 MPa and 5.6 MPa). Along the compressive reinforcement, the bond stress does not exceed 3.7 MPa for reference beam and 2.9 MPa for corroded beam. The reference and corroded beams exhibited flexural failure (yielding of the tensile reinforcement) where cracking occurred in the portion of the beam with maximum bending moment, see Figure 11a. Similar failure was also observed in the finite element simulations as evidenced by the long horizontal plateau of the load-deflection curve in Figure 8 and Figure 9. The localized tensile strains occurring along a vertical section close to the mid section of the beams are representative of a large, flexural crack at this location (Figures 11c and 11e). The calculated crack pattern is further illustrated in Figure 11b and Figure 11d from which the major bending cracks are presented. The location of these cracks corresponds to the oscillations in the bond stress distributions in Figure 10.

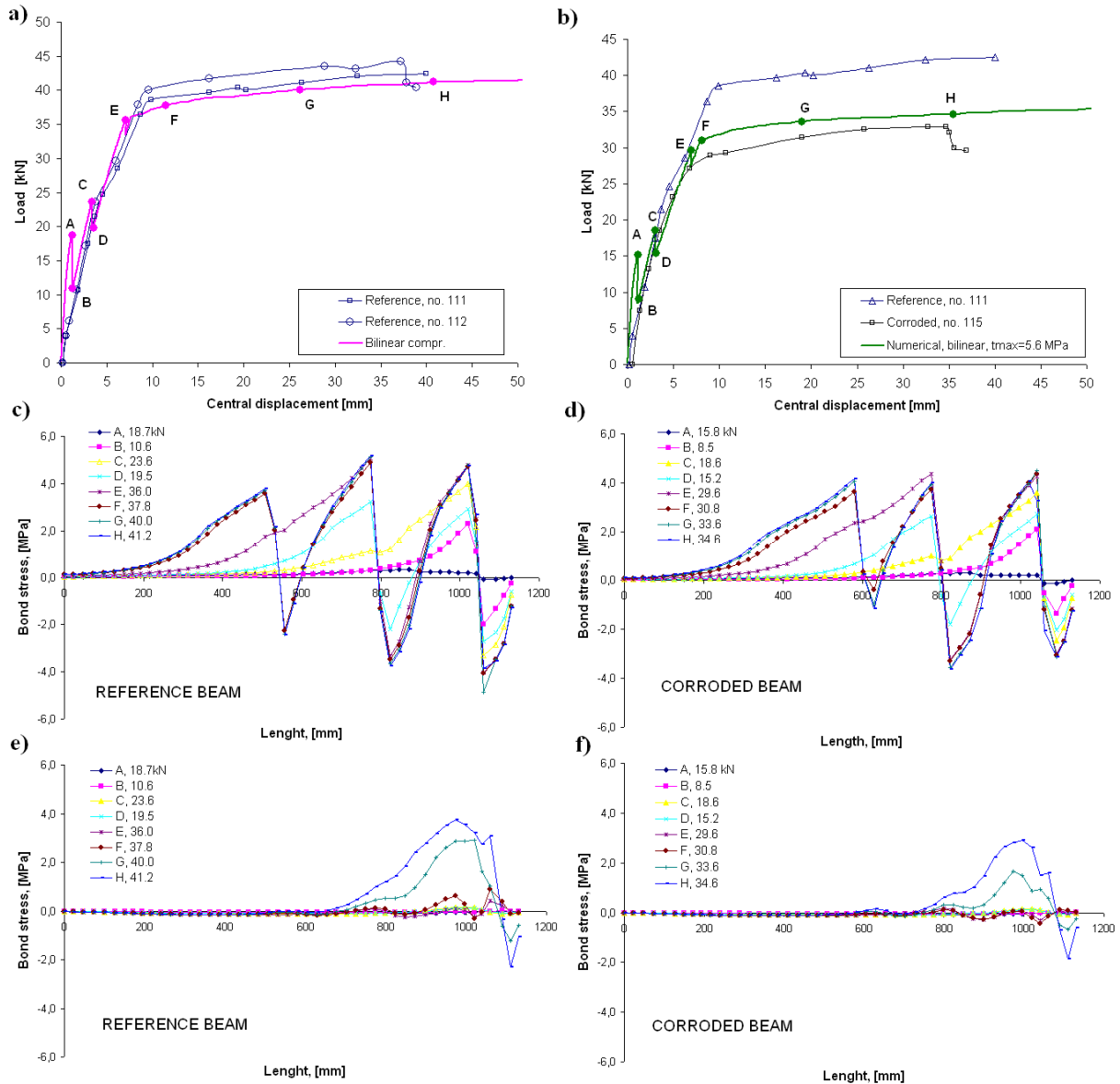


Figure 10 – Results of numerical simulations: a) Load-deflection curves for the reference beam; b) Load-deflection curves for the corroded beam compared to the load-deflection curve for the reference beam; c) Distribution of bond stress along tensile reinforcement (reference beam); d) Distribution of bond stress along tensile reinforcement (corroded beam); e) Distribution of bond stress along compressive reinforcement (reference beam); f) Distribution of bond stress along compressive reinforcement (corroded beam).

In the analyses presented above the corrosion was assumed to be uniformly distributed along the bars and the degree of corrosion was set equal to the average value given for beam no. 115 by Rodriguez et al. [17, 18]. However, the corrosion attack varies along the reinforcing bars. The average (and maximum) attack penetration for beam no. 115 for tension bars, compression bars, and links are 0.36 (1.0) mm, 0.26 (-) mm and 0.37 (3.0) mm, respectively. It is seen that the maximum penetration for the tensile bars (pitting) is about three times the average penetration. The maximum attack penetration for the compressive steel bars is not specified in [17, 18]. As it was mentioned before, the load carrying capacity of corroded beams was reduced and the behaviour becomes less ductile with increasing of the corrosion level. Corroded beams failed by

failure of the tensile bars at pits. However, no data about the distribution of maximum penetration or pitting along a tension bar was presented in the experimental study.

A simplified investigation of varying corrosion levels was carried out by assuming that one of the two tensile bars had a uniformly reduced cross sectional area corresponding to the maximum corrosion level while the corrosion level of the other bar was kept at the average value. All the other parameters remained unchanged. The resulting load-deflection diagram is shown in Figure 12 together with the corresponding curve based on average corrosion level.

The use of the maximum corrosion level for one bar leads to a drastic reduction in failure load and underestimates the load-carrying capacity of the beam. This analysis should be considered as an illustration only of the capabilities of finite element simulations to assess the effect of varying corrosion levels along the reinforcement [26]. The present method also allows for a more accurate representation of local corrosion by assuming that a single steel element has reduced cross section.

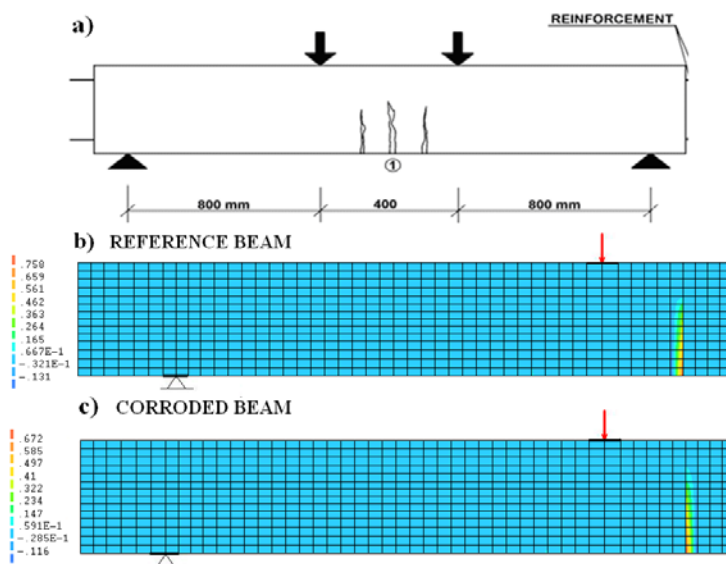


Figure 11 – Crack pattern and longitudinal strain in concrete at failure: a) Type of failure of beam from the experimental study (Rodriguez et al. [17, 18]); b) Longitudinal strain for the reference beam (point H); c) Longitudinal strain for the corroded beam (point H).

4. CONCLUDING REMARKS

The present work has been devoted to the use of nonlinear finite element analysis to simulate the mechanical response of reinforced concrete structures with corroding steel reinforcement using the commercially available finite element program DIANA.

Steel bar corrosion, with the associated loss of bar cross section, longitudinal cracking and bond strength reduction leads to complex distributions of strains and stresses and highly nonlinear, path-dependent behaviour. Simple section analysis, as used in the design of new concrete structures, is therefore of limited value for the assessment of serviceability or ultimate capacity of severely deteriorated concrete structures.

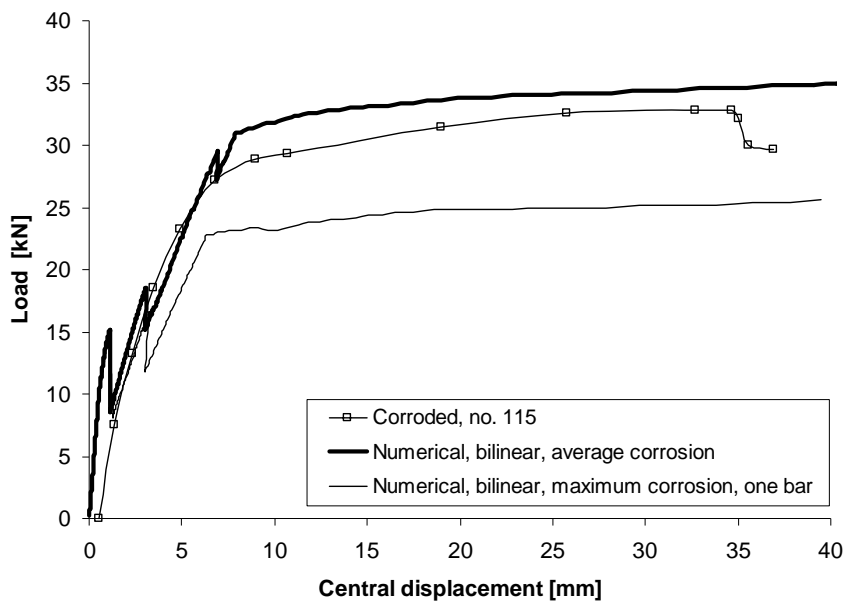


Figure 12 – Load versus central deflection for corroded beam (no. 115); different levels of corrosion.

On the other hand, this class of problems is well suited for computerized discretization procedures such as the powerful finite element method [26]. The validation of the presented simulations was limited to the study of medium scale beams and based only on the results of previously published laboratory investigations. The results from finite element simulation were validated against published test data. The failure loads of the beams from the finite element simulations seem to be in good agreement with the experimental values. Further, the presented numerical approach is going to be used for numerical simulations of the service life cycle of reinforced concrete structures.

ACKNOWLEDGEMENTS

The research work has been carried out in Northern Research Institute Narvik (Norut Narvik) through the European founded research project “Sustainable bridges”. A part of the presented work was financed by the Norwegian Research Council through the project “RECON – Renewal of Concrete Infrastructure” at Northern Research Institute Narvik (Norut Narvik), Norway.

REFERENCES

1. “Bond of Reinforcement in Concrete”, State-of-the art report, fib Bulletin No. 10, 2000.
2. Cairns, J., “Consequences of reinforcement corrosion for residual strength of deteriorating concrete structures”, Proceedings of the First International Conference on Behaviour of Damaged Structures, Rio de Janeiro, May 1998.
3. “CONTECVET A validated Users Manual for assessing the residual service life of concrete structures”, Manual for assessing corrosion-affected concrete structures, GEOCISA and Toroja Institute, 2004.

4. Coronelli, D. and Gambarova, P., "Structural assessment of corroded reinforced concrete beams: Modeling guidelines", *Journal of Structural Engineering - ASCE* 130 (8), 2004, pp. 214-1224.
5. Zandi Hanjari, K., "Load-Carrying Capacity of Damaged Concrete Structures", Lic. Thesis, Department of Civil and Environmental Engineering, Chalmers University of Technology, Gothenburg, 23 pp.
6. DIANA - User's Manual, Release 9.1, TNO DIANA BV, Delft, The Netherlands, 2005.
7. Bergström, M., "Life cycle simulation of concrete beams – Laboratory experiment and probabilistic evaluation", Licentiate thesis 2006:59, Luleå University of Technology, Luleå, Sweden, ISBN 978-91-85685-05-9, 153 p.
8. Berra, M., Castellani, A., Coronelli, D., Zanni, S. and Zhang, G., "Steel-concrete bond deterioration due to corrosion: finite-element analysis for different confinement levels", *Magazine of Concrete Research*, Vol. 55 (2003), No. 3, pp. 237-247.
9. Lundgren, K., "Bond between ribbed bars and concrete. Part 1: Modified model", *Magazine of Concrete Research*, 57 (7), 2005, pp. 371-382.
10. Lundgren, K., "Bond between ribbed bars and concrete. Part 2: The effect of corrosion", *Magazine of Concrete Research*, 57 (7), 2005, pp. 383-396.
11. Lundgren, K., "Effect of corrosion on the bond between steel and concrete: an overview", *Magazine of Concrete Research*, 59 (6), 2007, pp. 447-461.
12. Castellani, A. and Coronelli, D., "Beams with corroded reinforcement: Evaluation of the effects of cross-section losses and bond deterioration by finite element analysis". *Structural Faults and Repair -99*, London, U.K., July 1999.
13. Dekoster, M., Buyle-Bodin, F., Maurel, O. and Delmas, Y., "Modelling of the flexural behaviour of RC beams subjected to localised and uniform corrosion", *Engineering Structures*, 25 (2003), pp. 1333-1341.
14. Horrigmoe, G. and Hansen, T., "Assessment of the performance of structures attacked by reinforcement corrosion", *International RILEM Symposium on Advances in concrete Through Science and Engineering*, Northwestern University, Evanston, Illinois, March 22-24, 2004.
15. Tørten, A. and Horrigmoe, G., "Modelling of bond between reinforcement and concrete for deteriorated and repaired beams", Report No. NTAS A98034, NORUT Technology, 1998, Narvik, Norway. (in Norwegian).
16. Sand, B., "Nonlinear finite element analysis of deteriorated and repaired RC beams", Report No. NTAS F2000-30, 2001, NORUT Technology, Narvik, Norway. (in Norwegian).
17. Rodriguez, J., Ortega, L.M. and Casal, J., "Load carrying capacity of concrete structures with corroded reinforcement", *Proceedings of the International Conference on Structural Faults and Repair*, Vol. 2, London, 1995, pp. 189-198.
18. Rodriguez, J., Ortega, L.M., Casal, J. and Diez, J.M., "Assessing structural conditions of concrete structures with corroded reinforcement", *Concrete Repair, Rehabilitation and Protection* (Edited by R. K. Dhir and M. R. Jones), E & FN Spon, London, 1996, pp. 65-78.
19. Rots, J.G., "Computational modelling of concrete fracture", Delft University of Technology, Delft, 1988.
20. de Borst, R., "Computational methods in non-linear solid mechanics, part 1 and part 2", Delft University of Technology, Delft., 1991.
21. Comité Euro-International du Béton, CEB-FIP Model Code 1990, Design Code, Thomas Telford, London 1993.
22. Chen, W.F., "Plasticity in Reinforced Concrete", McGraw-Hill, New York, 1982.

23. Gonzalez, J.A., Andrade, C., Alonso, C., Feliu, S., “Comparison of rates of general corrosion and maximum pitting penetration on concrete embedded steel reinforcement”, *Cement and Concrete Research*, 25(2), 1995, 257-264.
24. Rodriguez, J., Ortega, L. and Casal, J., “Corrosion of reinforcing bars and service life of reinforced concrete structures: corrosion and bond deterioration”, International Conference on Concrete Across Borders, Odense, Denmark, 1994, Vol. 2, pp. 315-326.
25. Norwegian Code NS 3473: Design of Concrete Structures (in Norwegian), Fifth edition, Norges Byggstandardiseringsråd (NBR), Oslo, November 1998.
26. Horrigmoe, G., Sæther, I., Antonsen, R. and Arntsen, B., “Laboratory investigations of steel bar corrosion in concrete”, Sustainable Bridges WP3 D3.10 (Norut Technology, Norway, 2007).

Industrialized construction: Benefits using SCC in cast in-situ construction



Peter Simonsson
Ph.D. Student
Luleå University of Technology (LTU), Luleå
971 87 Luleå, Sweden
E-mail: Peter.Simonsson@ltu.se

Mats Emborg
Professor LTU / Head R&D Betongindustri AB
LTU, 971 87 Luleå, Sweden
Betongindustri AB 100 74 Stockholm, Sweden
E-mail: Mats.Emborg@Betongindustri.se
Mats.Emborg@ltu.se

ABSTRACT



As known the product SCC comprises many advantages compared with traditional concrete but yet it has not changed the market of cast-in-situ concrete as expected. This may be related to some robustness problems of the concrete and to a general opinion that the product is considered to be expensive. However, SCC has become more robust over the last few years and manufacturers have improved their quality vastly.

To increase the use of SCC, the actors of the building trade need to be informed how to benefit from all the advantages of SCC (i.e. the working environment the health and safety of the workers, the productivity etc).

The paper deals with full-scale examples on the use and the realization of SCC obtaining several benefits during the whole project time. Specially, the economics and the working environment - are treated.

Key words: SCC, benefits, economy, productivity, working environment, robustness

1. INTRODUCTION

Self-compacting concrete (SCC) is an important element in the development of the industrialization process of civil engineering projects as it can, if managed properly, decrease the number of workers needed during casting and become economically profitable as well.

What happened with the expected development of SCC? In the late 1990's many specialists argued that they expected SCC to have more than 50 % of the total concrete market within a five year period. Today, ten years later however, the market shares of SCC in EU nations are clearly below 10 % with large variations from country to country. For instance Cussigh [1] reports that only about 3 % of all ready mixed concrete in France is SCC while in Denmark the SCC market

share is as high as 25 %. In Sweden, the SCC market share is about 10 % with very large local variations. However, the definition of SCC varies from country to country.

According to recent international findings, SCC is on the cutting edge of scientific and technological developments, [1], [2] and it is essential to introduce the technique in a broader manner in cast-in-situ concrete construction. However, still, the utilization of SCC is very low and one important reason is, according the authors above, the economy. The need for high quality constituents of materials results in a more expensive product that not compensates for the possible economical benefits.

Thus, it is essential to clearly document all the direct and indirect benefits using SCC. This article is a contribution to this topic dealing with economic questions, working environment, and industrialization possibilities in projects where SCC has been used.

2. OBJECTIVE OF THE PH D PROJECT

The research project “Industrialized civil engineering with cast-in-situ concrete” at Luleå University of Technology aims to evaluate methods to increase the degree of industrialization in bridge construction. One of the objectives is to investigate possible productivity benefits using SCC at cast-in-situ construction sites. Other objectives are to examine the economic potential of the product and the impact on the working environment.

3. ROBUSTNESS AND TARGET VALUES OF SCC

3.1 Benefits and obstacles with SCC

Among the positive effects of SCC are: improved working environment and reduced noise level, easiness of placing, productivity enhancements, higher strength, faster construction, and less man hours needed for production, can be especially mentioned.

Regarding civil engineering projects, there are certain parts where SCC is superior to traditional vibrated concrete, i.e.: high walls, columns or plate structures [3]. Most often, when casting these structures with traditional vibrated concrete, concrete workers have to climb down inside the form to be able to carry out the compaction of the concrete properly resulting in low productivity and poor working environment.

However, according to Shah et al. [2] there are some issues hindering the introduction of SCC on a broader front; questions regarding the development of formwork pressure, problems related to static and dynamic segregation resistance, rapid loss of slump flow and doubtful robustness. Cussigh [1] has other explanations for the low adoption of SCC in Europe; a need for high quality materials which in turn results in SCC materials costs clearly exceeding the traditional concrete, an insufficient accuracy of concrete production equipment, as well as a lack of quality control requirements and standards.

Another factor hindering the introduction of SCC is that it is important to establish a quality assurance system for difficult concrete works, especially when the structural section is narrow or the reinforcement is very dense as in most bridges today [4]. However, this is seldom done in praxis.

3.2 Robustness

Two reasons why SCC is not being used more frequently are the relatively large quality variations and the difficulty in keeping SCC robust. Though, concrete manufacturers in recent time have improved the quality and hence the robustness of SCC, these negative effects are still present, with the result that the contractor calculates the risk of using SCC to be too high. Therefore, the contractors simply do not use the product even though both costs and time can be saved.

According to Taguchi [5], robustness generally is defined as insensitive against disturbance. For SCC the disturbance can occur in the form of fluctuations of properties of the concrete constituents, mixing procedure and transport conditions. Thus, an important feature of SCC is the ability to maintain its fresh properties and structure during transport and casting of a single batch or multiple batches, [6] and [7]. According to the European guidelines for SCC [8] a well designed and robust SCC can typically tolerate a variation of 5-10 liters/m³ in mix water content which in practice is about 3-6 % of the total water content.

3.3 Target values

Different target values are preferred for different structural parts in a construction. For civil engineering applications this implies that for a slab compared with a column or foundation, the concrete have different properties. Figure 1 show possible target values and allowed variations of the filling ability expressed by slump flow and T50. The slump flow for bridge foundations, columns or walls should be greater than for a bridge slab where a slightly less fluid concrete is preferred creating opportunities for a proper form filling.

Another example of target values has been suggested by Walraven [9], Figure 2, stating nine consistency classes for SCC regarding slump flow, T50, V-funnel time, segregation and passing ability. As seen the consistency class is dependent on the construction type (e.g. ramps, walls, floors). Walraven [9] concludes that SCC can be tailor-made for any kind of construction including fairly steep inclination (up to 30°).

It is thus evident that it is important to design and modify the concrete for a specific project and also for specific structural parts within the same project.

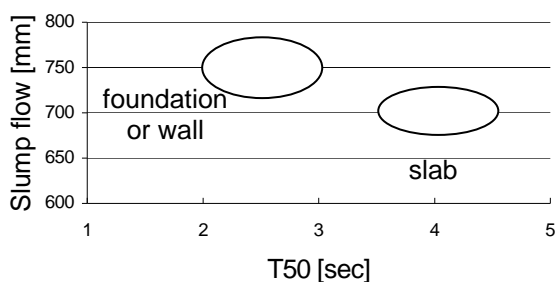


Figure 1. A) Examples of criteria for SCC for wall and slab in a workability diagram (slump flow vs. T50), where the ellipse represents target value and tolerance.

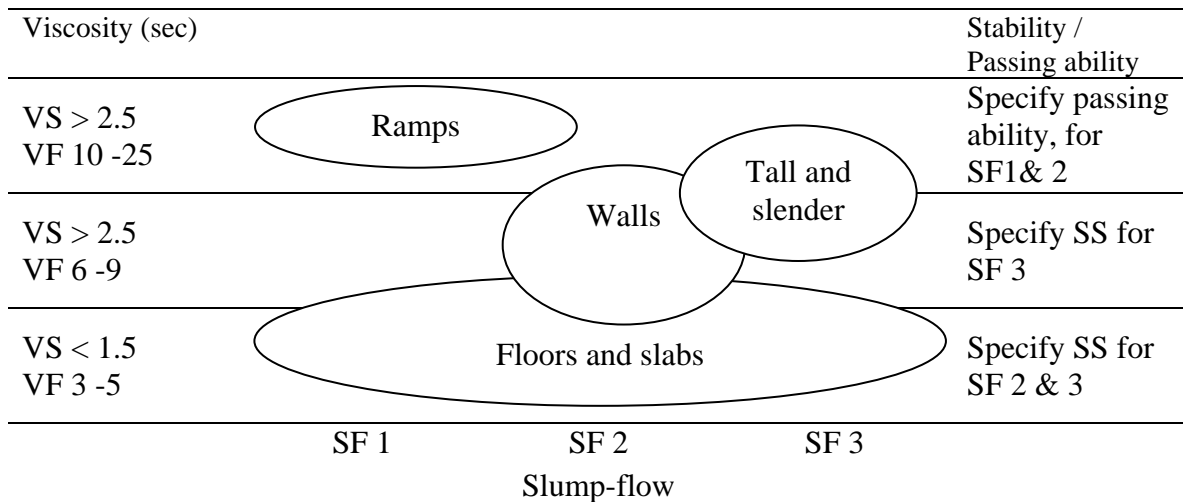


Figure 2. Properties of SCC for various types of application [8], [9].

4. INDUSTRIALIZATION AND SCC

4.1 Possibilities for an increased concrete construction

Experience has shown that SCC not alone automatically implies a clear step into industrialization. Therefore, within the research project at LTU, feasibility studies were carried out to grade various measures for industrialization of bridge construction. Ten already constructed concrete bridges were followed up regarding unit times and costs for reinforcement, formwork, and concrete. Areas of major improvement were identified. Figure 3 shows estimated effect on man power requirements if industrial methods regarding formwork, concrete, and reinforcement theoretically were applied to these bridges.

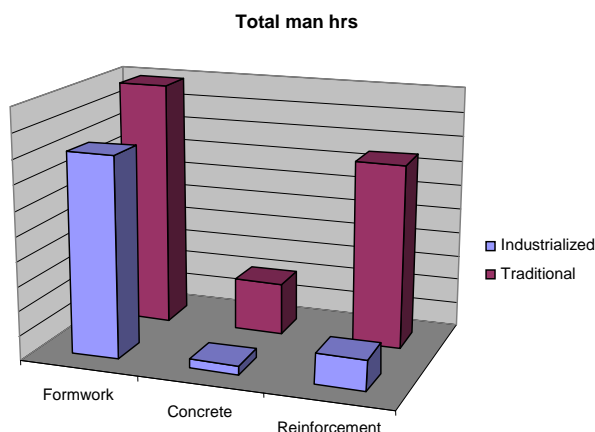


Figure 3. Possible reduction of man power requirements if industrial methods are applied to concrete bridge construction. Theoretical estimations based on follow ups of ten Swedish concrete bridge objects 2003 – 2005 (i.e. “traditional” in the figure).

A large man power reduction was achieved with a more effective handling of reinforcement – which is well known. Different solutions for effective reinforcement fixing can thus be applied at various parts of bridges. At e.g. geometrically more complicated parts, reinforcement can be

traditionally placed piece by piece in the formwork. For major parts of the structures the reinforcement can be prefabricated into cages in a controlled environment in a factory or at a manufacturing location at the production site and lifted directly into the form. Reinforcement can also be prefabricated into rebar carpets and rolled out at site (Figure 4), preferably in superstructures of the bridges, see e. g. [10].



Figure 4: a) and b) Manufacturing of carpet reinforcement in a controlled factory environment. c) Placing of carpet reinforcement on the superstructure.

The formwork can be designed to be a permanent part of the structure which often is the case in house production. This method of production can be applied for foundations, columns and/or plate structures, while an extensive use of permanent formwork for bridges is not realistic.

Considering the potential for SCC, apart from a significant reduction of man hours, as shown in Figure 3, it also increases the casting rate, and improves the working environment, see e.g. Skarendahl [11].

4.2 Productivity according to Lean Construction

Another important component in industrialization is the organisation at the site and the attitude of the personnel. Philosophies of Lean Construction can thus be a useful tool. In Lean Construction waste (in Japanese: *muda*) plays a central role, whose definition is any human activity that absorbs resources without creating any value [12]. Two types of *muda* are defined: Type one *muda* creates no value but is necessary with current technologies while the type two *muda* creates no value at all and is immediately avoidable. Increased productivity is dependent on how much the *muda* can be eliminated.

Considering the concrete from this point of view, vibrating is not waste when casting traditional concrete, but on the other hand not very productive either. Therefore, the compaction of concrete can be graded as type one *muda* according to the definition above. On the other hand, in case of SCC, the vibrating should be regarded as type two *muda*.

When using SCC, concrete workers are being released from their traditional assignment of vibrating the concrete and free to perform other tasks during the form filling. For example, the workers can fix reinforcement and prepare form for next section to be cast i.e. a leap in productivity is near at hand.

Regarding the reinforcement a similar reasoning can be made. When traditional reinforcement is mounted for the bridge foundation for instance, the worker fetches and fixes each reinforcement bar at the correct location piece by piece. Traditional placing of reinforcement involves a lot of movement and carrying of reinforcement which can be considered as type one *muda*, since it is

necessary with this technology but does not create any value. Using prefabricated reinforcement cages or rebar carpets, the element of movement/walking is reduced to a minimum or completely eliminated on site. If this is still done, the reinforcement handling ends up as a type two muda.

The productivity could consequently be improved simply by choosing the correct components, materials or prefabrication level to work with. Another method of improving the productivity is to increase standardisation, making structural parts more similar. It can be as simple as limiting the types of distance blocks for keeping the correct concrete cover layer, or to design identical foundations, columns or superstructures similarly in larger project to make them repeatable.

4.3 Working environment ergonomic analysis through ErgoSAM

According to a study at the Danish Technological University [13] some 26 % of a workers average day consists of concrete casting and reinforcement fixing (approximately 10 % and 16 % respectively). If this is translated into time, it will be just over 2 hours per working day, or 57 full working days a year. This work is often done in awkward positions with heavy equipment such as the poker vibrators for the traditional concrete or with heavy material when placing the reinforcement piece by piece.

According to Nielsen [14], construction workers is one of the most exposed groups of employees when it comes to noise, heavy lifts, poor ergonomics and varying weather conditions in society today. It is concluded that a chance of improving the working environment often is denied, because the contractor considers the short term prize for material and man power only, and not the total long term cost reduction from an improved working environment.

The difference in working environment between traditional casting of concrete and casting SCC has been debated recently; see e.g. Geel et al. [15], Nielsen et al. [16], Lecrux et. al. [17] to name but a few, who all, debate the importance of introducing SCC for the workers point of view. However, there are few researchers presenting numbers which actually show the environment when casting traditional concrete as compared to SCC.

To be able to perform the comparison between different working methods a model is needed. The ErgoSAM model together with the Cube Model is such a tool. The ErgoSAM is based on the Cube Model that has been used on site observations to acquire the risk of Work-related Muscular Skeletal Disorders (WMSDs) combine the variables; work posture, force and repetition. For every work task and for each variable separately, demand levels may be defined as low, medium, or high. The demand criterion is chosen so as to discriminate between good or poor work ergonomics, and assigned weight factors 1, 2, and 3 respectively. The combined value, representing the load level or exposure level, is obtained by multiplying the result of the three variables illustrated in Figure 5. The product determines the acceptability of the task [18].

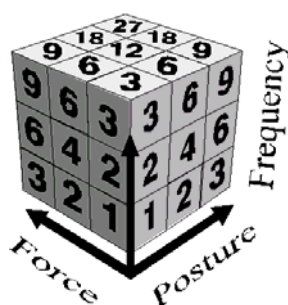


Figure 5. The Cube model combining the variables; work posture, force and frequency [18].

Combinations of these demands will largely decide whether a work situation involves risks of strain injuries or musculoskeletal disorders [19]. The ErgoSAM model has been used by different Swedish companies within the manufacturing industry. For instance, studies have been carried out at Volvo Cars in Gothenburg [20]. At the full scale project, the observations were done as a construction site-walkthrough, video filming identified steel reinforcement and/or concrete casting activity work cycles and interviews with the workers. These observations were the basis for a further assessment with ErgoSAM.

4.4 Economy

One of the drawbacks with SCC is that it is considered to be more expensive to manufacture than traditional concrete, a cost that is difficult to meet by a higher prize [1]. Hence, to be able to make SCC profitable also the casting phase needs to be included. Therefore, the productivity when casting SCC should be high which means that the production system needs to be adapted to the “new” concrete. The difference between the manufacturing cost for the original concrete and the SCC cannot be too large if SCC is to become profitable [21].

There are factors reducing the cost for SCC; reduced energy consumption due to the absence of vibration, lower future maintenance cost, reduced illness of construction workers, as mentioned above [9], as well as lower over-head costs for projects due to decreased rental costs for various types of equipment and shorter construction time.

However, the probably most important factor when considering the economy of SCC is to have the whole life span of the project in mind when choosing material. SCC has often an increased strength and durability which should be utilized when considering the reduction of maintenance needed for a project during its life span. This could also be utilised for the possible reduction of shear force reinforcement as well as minimization of the structures cross sections. This of course applies for any high strength concrete. These factors together with faster casting and less labour needed will result in considerable reduction in costs and risks, and it will also reduce the traffic disruption during construction.

5. LABORATORY STUDIES

5.1 General

As mentioned earlier, to be able to produce a robust SCC product the focus should be on keeping the fluctuations of the different constituents as low as possible and to design a robust concrete mix. Among possible fluctuations e.g. the quality of the coarse aggregate, cement or additives are important, whereas, the moisture content in the coarse aggregate might be the factor causing the most common and largest variations. Therefore, the recipes of the SCC used in the two full scale projects (Chapter 7), were tested in the laboratory regarding sensitivity to fluctuation in water content. This corresponded to a moisture content variation of $\pm 0,5\%$ and $\pm 1,0\%$ with no compensation in the mix design. Two test series were performed for mix proportions, according to Table 1. Variations in filler content were performed by adjusting the aggregate content. The fine and coarse grained aggregate curves featured $\pm 14\%$ deviations from the original curve at the fractions 1 mm. Figure 6 and 7 show documentations of workability (slump flow, T50 and V-funnel) and rheology (shear stress and viscosity) for the mixes.

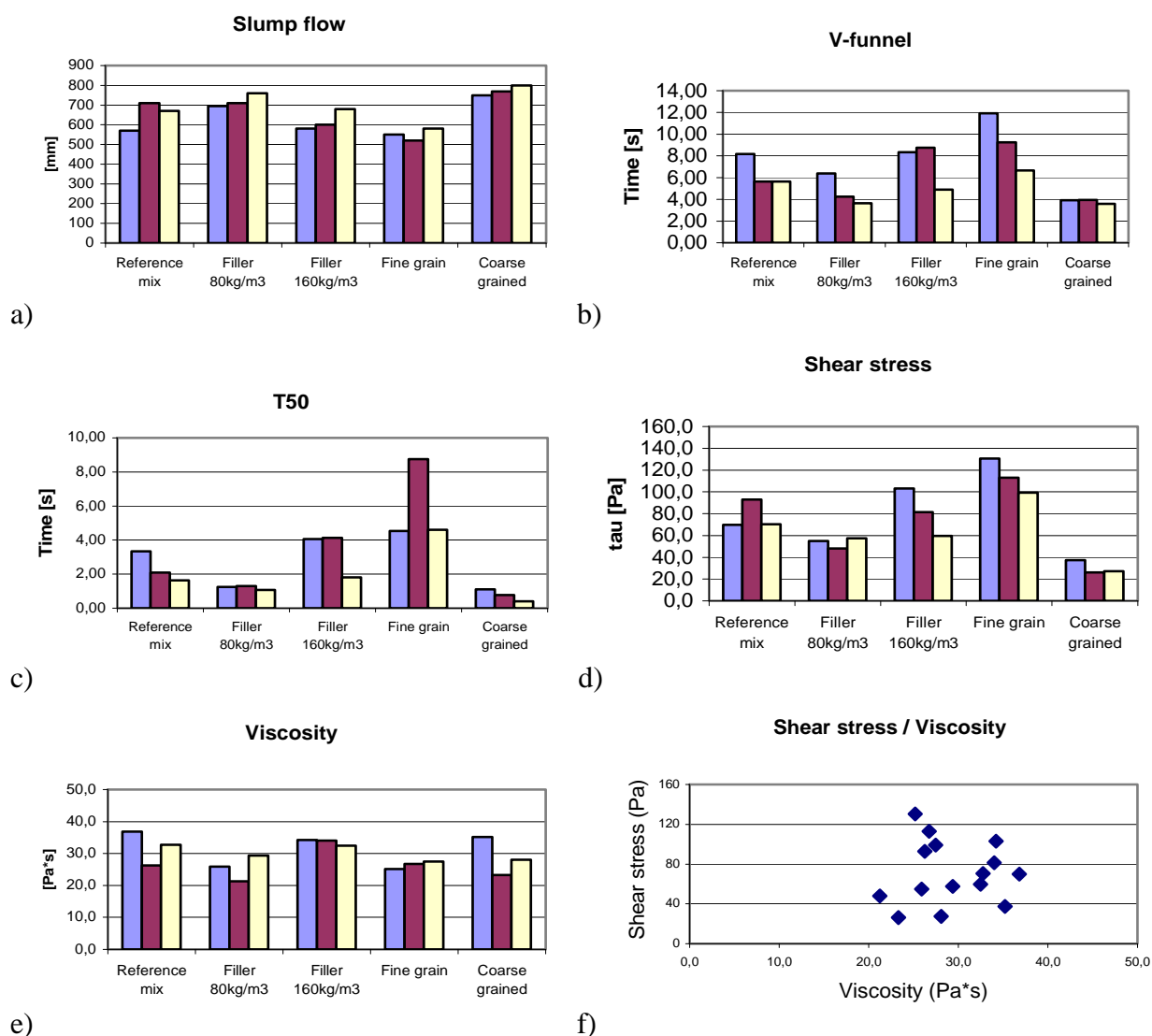
Table 1. Concrete mix proportions at laboratory tests for two recipes. SCC 1 is the mix used in study no 1 and SCC 2 is a mix used at study no 2 however, here, with the same aggregate as SCC 1.

Materials (kg/m ³)	SCC 1	SCC 2
0-8 mm	1012	899
8-16 mm	545	651
Cem	450	430
Limestone filler	122	130
Water	175	172
Superplastcizer	0,8	0,6
Water / Cement ratio	0,39	0,40

5.2 Results

The first studies were carried out on SCC 1. The variations in moisture content varied between $\pm 1,0\%$ for this recipe, with one exception. In the mix with a filler content of 80 kg/m^3 only $\pm 0,5\%$ water was added due to considerable separation when $+ 1,0\%$ water was added.

Regarding the slump flow of SCC 1, it was observed that the concrete is not particularly sensitive to the moisture change of the aggregate. However, when studying the V-funnel test results, it can be seen that the flow time is noticeably longer for the drier mix than for the wetter and, hence, the moisture content clearly affects the concrete for this type of test. It is also observed that, the concrete gets less fluid when the filler content increases. Moreover, the concrete with the fine sieve curve is rather sensitive to moisture, as compared to the insensitiveness of the concrete with the coarse grained aggregate.



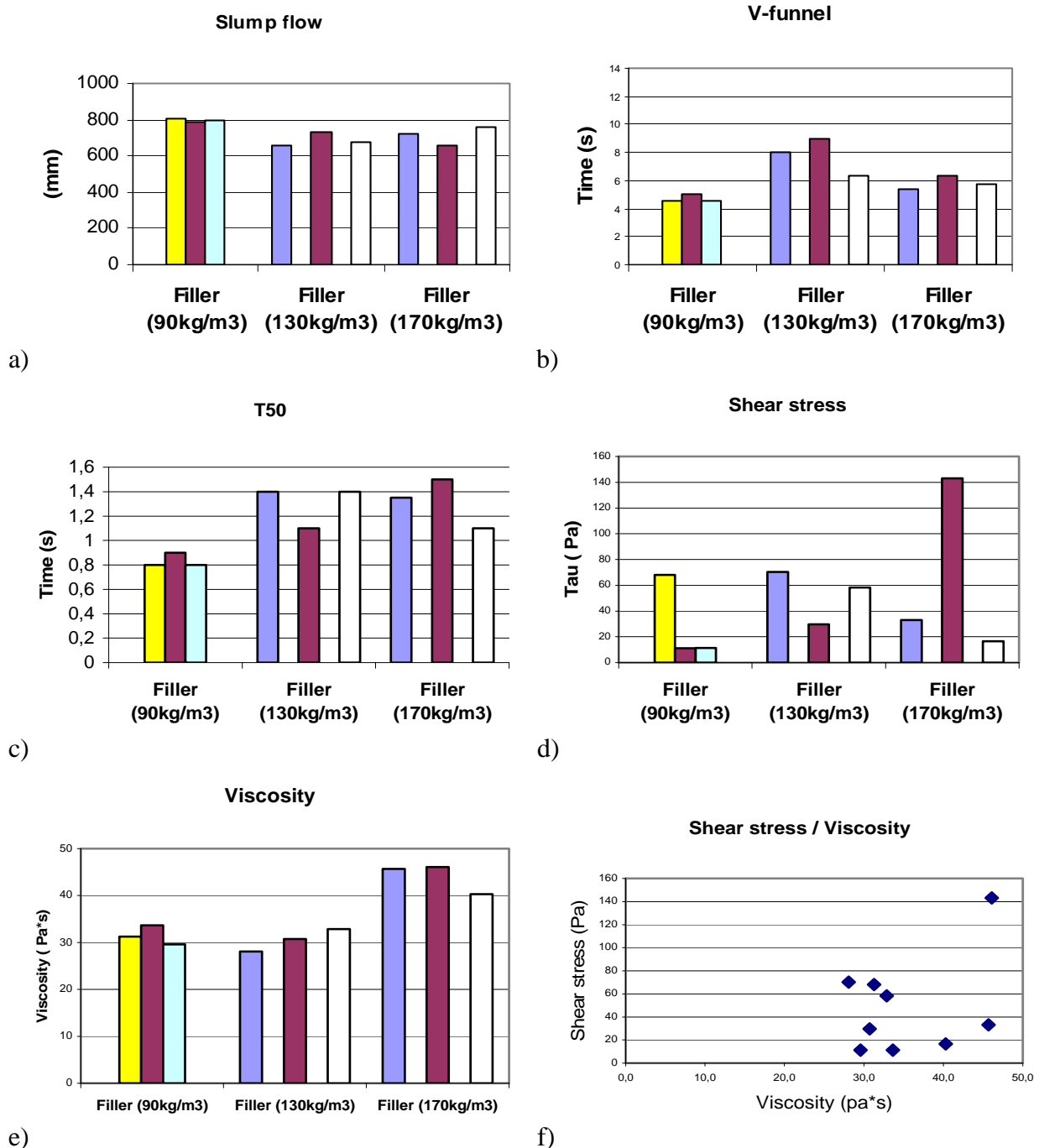
a) f) *Figures 6 a to f. Workability and rheology tests on SCC 1: slump flow, V-funnel, T-50, shear stress, viscosity and shear stress / viscosity. Variations of moisture content in 0-8 mm; -1% (left column) and +1% (right column) from reference mix (middle column) (80 kg/m³ filler: ± 5 % variation).*

Considering the T50-time, it can be seen that the moisture content has a small effect, since the test time is significantly shorter for the wet mix compared with the dry mix. Regarding the fine grain mix and T50, the test with reference moisture content was affected by the laboratory equipment, and the value is therefore not relevant.

According to the shear stress values of Figure 6 d), there is an obvious difference between the fine grain and coarse grained results. The fine grained material is more sensitive to water content than the coarse grained aggregate.

The test results in Figure 6 e) (viscosity) and 6 f) (viscosity versus yield stress) do not show any apparent differences and no specific conclusions can be drawn. However, there is a difference in the filler content; the viscosity is larger with a higher amount of filler. Also, it can be observed that the drier mixes have higher viscosity values.

In the tests with SCC 2, the slump flow and V-funnel, Figures 7 a) and 7 b), were rather insensitive to the water content in the concrete. The slump flow for the mix with reference water content, declines with increasing filler content. On the other hand, regarding the v-funnel test, the reference filler content gives a long flow time while both high and low filler content lead to shorter flow times.



Figures 7 a to f. Workability and rheology tests on SCC 2 for filler variations: slump flow, V-funnel, T-50, shear stress, viscosity and shear stress / viscosity. Variations of moisture content in 0-8 mm; -1% (left) and +1% (right) for filler content 130kg/m³ and 170 kg/m³ from reference mix (middle). Variations of moisture content for 90 kg/m³ -0,5% (left) and +0,5% (right) from reference mix (middle).

Considering the viscosity test results, there is probably a break point between filler content 130 kg/m³ and 170 kg/m³, since there is a clear difference between these two test values. The T50 test results are very low and can be said to be within the margin of error and no clear conclusions can be drawn.

Generally, from the laboratory tests it is observed that both SCC mixes are relatively insensitive to the moisture variations studied even though the filler content was both increased and decreased from the reference mix. However, SCC 1 is somewhat more sensitive than SCC 2 to the changes of moisture content.

Furthermore, some relation between slump flow and shear stress is present as well as between T50-time, V-funnel time and viscosity as similar observations can be observed for the rheology tests as for the workability tests when varying the mix.

6. FULL SCALE PROJECTS

6.1 General

Two full scale projects have been studied with two concrete suppliers that had different experience with the SCC product. The first supplier had never delivered SCC to a civil engineering project before and had accordingly little experience and no recipe while the second supplier had more experience and several SCC mixes available as commercial products.

Study No 1: The Kalix bridge

Near the village Kalix, approximately 100 km NE of Luleå, the most comprehensive studies were carried out. The bridge “*the industrial concrete bridge*” featured a span of 10 m and a width of 15 m. The full scale project comprised “new” reinforcement solutions such as reinforcement cages for the foundations and rebar carpets for the superstructure. Prefabrication was also chosen for some of the very dense shear reinforcement. SCC was used for all parts of the bridge. To facilitate the introduction of these new working methods, the design and production planning of the bridge were carried out according to Lean Construction philosophy [22].

In total, the bridge consisted of approximately 280 m³ SCC cast at four stages: foundation, plate structures, end walls and superstructure. The superstructure comprised 16 tons reinforcement of which 13 tons were placed using rebar carpets. The reinforcement for the foundation was prefabricated in two sections, one for each foundation plate, each weighing 2.7 tons. The cages were mounted in single pieces directly from the delivery truck into each of the foundation formwork, ready to be cast as soon as the connecting reinforcement had been installed.

Study No 2: The Nynäsvägen bridge

The project at Nynäsvägen (50 km SE of Stockholm) consisted of two identical bridges next to each other (bridge spans of 18 m and widths of 9 m). The total amount of concrete for the foundations, columns and superstructures for both bridges was approximately 550 m³. Each bridge was cast at five stages and the largest single casting was approximately 210 m³ for the superstructures. SCC was used for the entire structure.

At these bridges the reinforcement were placed traditionally except some 1.8 ton of the superstructure where rebar carpets were used. The low degree of prefabrication was due to the late introduction of use of rebar carpets, and accordingly little time for proper redesign.

6.2 Documentation of concrete properties

The concrete properties, slump flow and T50, were recorded after the pump at the building site for all delivered batches in study no 1, see Figure 8. In study no 2, slump flow and air content were recorded on nearly half of the batches prior to the pump, Figure 9.

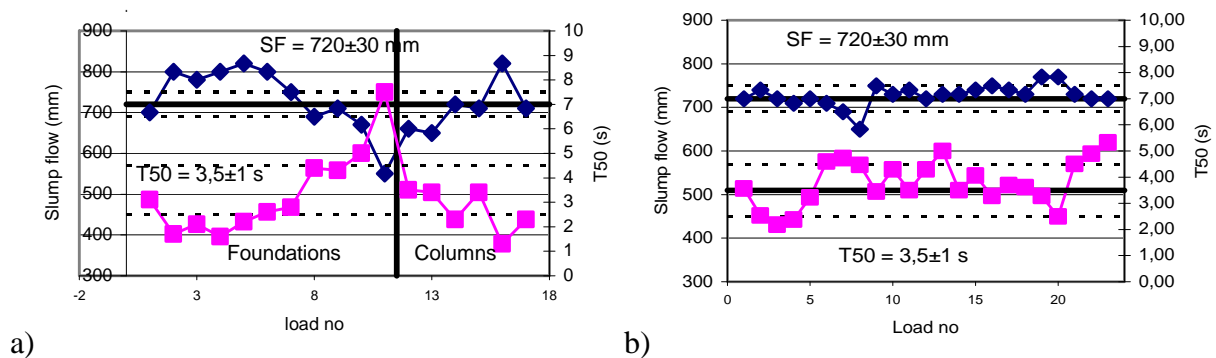


Figure 8 Slump flow and T50 documentation at study no 1. Castings of foundations and columns at two occasions (a). Casting of end walls and superstructure at one occasion (b).

When casting the substructures of the study no 1 some difficulties occurred in delivering the concrete with constant properties see Figure 8. This is probably depending on the inexperience of the concrete supplier and the relative small separate volumes. On the other hand, casting of the bridge superstructure was performed with a constant and high concrete quality, Figure 8 b. Only some batches out of 24 had properties outside the criteria e.g. 720 ± 30 mm for slump flow and 3.5 ± 1 s for T50. For two high values above the interval, the measuring can have been affected by disturbance, and these two values are neglected in the context.

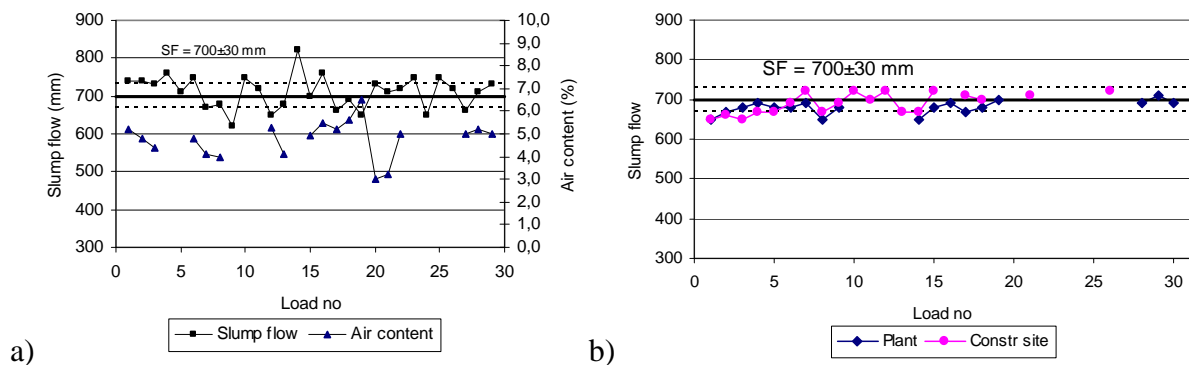


Figure 9. a) Slump flow and air content measured on casting of foundations and columns at study no 2, cast in five stages. b) Slump flow at concrete plant and at building site, casting of superstructure at study no 2.

In the second study, the conditions for the slump flow were changed and the criteria were set to 700 ± 30 mm, T50 was not measured at all in this study. In Figure 9 a, there are five different

castings for the substructure, i.e. foundation and columns, accumulated. Almost 30 % of all delivered concrete batches were measured outside of the set conditions for slump flow (Figure 9 a). Nevertheless, there was only one recorded batch of separated concrete.

The air content is fluctuating during the castings with an average value of 4.8 %. There were never any specific values set for the air content in this project. The air content for a civil engineering project is generally accepted within a span of 4-8 %.

Casting the superstructure at study No 2 on Nynäsvägen, Figure 9 b, the slump flow was measured both at the concrete plant and at the construction site. During the delivery from concrete plant to construction site the slump flow has increased in most cases. This probably indicates that the super plasticizer needs to be more thoroughly mixed into the concrete at the concrete plant. Furthermore, the first deliveries had less slump flow than the latter; this can be due to the fact that the drums of the trucks were dry in the beginning.

It is also noted that very few batches showed slump flow values outside the criteria, and they were accepted by the client.

6.3 Economy of SCC

Study No 1: Kalix project

As the Kalix project was a local pioneer full scale project, neither workers nor management had experience in working with SCC. Therefore, at the first two cast occasions (foundation and plate structures) the number of workers was too large, see Table 2 showing man power and costs of the full scale project. Also, some concrete delivery problems occurred, implying about 50 % longer casting times than expected. This had however, nothing to do with the SCC mix i.e. these problems would have occurred even if traditional concrete had been used. Thus, the comparison between traditional concrete and the outcome of SCC for these two castings is not representative.

When casting the superstructure at two different occasions, the delivery problems were eliminated, and the workers had also become more experienced with SCC. Therefore, the castings went well and the outcome was almost as planned using SCC, see Table 2. Approximately € 1200 was saved at these castings as compared with conventional concrete. However, the concrete was more expensive (about € 15 per m³) resulting in a material cost increase of €2000 and hence the total cost became approximately €800 higher in total.

On the other hand, the price difference of €15 per m³ SCC is rather high, and if the difference had been the same as in the project at study no 2 (€ 8) the result would have come out differently. The increase in material cost would have become roughly €1100, with the decrease in placing cost of €1200 mentioned above resulting in minor savings of about €100.

Table 2. Expected time (h) and costs (€) for casting with traditional concrete, the actual outcome of using SCC at site and theoretical expectations of SCC castings when fully exploited at the study no 1. Superstructure – left, bridge deck – right.

Traditional casting					Traditional casting (planned work)						
	m3	No of workers	proj time	work time	cost €		m3	No of workers	proj time	work time	cost €
	64	4	5	20	800		47	4	4,5	18	720
	36	4	3	12	480		90	4	6	24	960
Total	100		8	32	1 280	Total	137			42	1 680

Outcome of SCC					Outcome of SCC						
	m3	No of workers	proj time	work time	cost €		m3	No of workers	proj time	work time	cost €
	64	4	7	28	1120		47	1	4,5	4,5	180
	36	2	5	10	400		90	1	4	4	160
Total	100		12	38	1 520	Total	137			8,5	340

SCC Theoretical					SCC Theoretical						
	m3	No of workers	proj time	work time	cost €		m3	No of workers	proj time	work time	cost €
	64	1	3	3	120		47	1	3	3	120
	36	1	2	2	80		90	1	4	4	160
Total	100		5	5	200	Total	137			7	280

Study No 2: Nynäsvägen

At the Nynäsvägen project the casting of the foundations and columns included a total of approximately 140 m³ of SCC. While the traditionally planned casting involved approximately 38 working hours for casting the concrete, the theoretical casting of SCC would contain approximately 8 hours for casting, see Table 3. The actual outcome of the project ended up on a sum of 26 hours for the casting, i.e. a saving of 12 working hours from the planned work schedule could be made. However if the full potential of SCC would have been utilized (SCC theoretical) approximately 30 working hours or 80 % of the planned work time could have been saved. With an assumed construction worker cost of €40 per hour, the saving in form filling costs is approximately €500 for the outcome and €1200 for the theoretical SCC.

For the superstructure the traditional casting was planned to be performed by 9 workers during 15 hours of production, ending up on 270 hours for the two bridges. A theoretical calculation using SCC shows that the actual time for casting can be considerably reduced. Savings of approximately 170 working hours can be achieved. With €40 per hour the saving of man power is roughly €6800.

The actual outcome for the superstructure ended up in 90 work hour's reduction due to faster casting and some € 3600 in cost savings. However, the material costs increased by approximately €8 per m³ for SCC compared with traditional concrete, which resulted in a more expensive concrete for the superstructure of almost €3400.

Table 3. Expected time (h) and costs (€) for casting traditional concrete, the actual outcome of using SCC at site and theoretical expectations of SCC when fully exploited for study no 2. Superstructure- left, bridge deck – right

Traditional casting (planned work)				
m3	No of workers	proj time	work time	cost €
25	3	2	6	240
30	3	2	6	240
35,5	3	3,75	11,25	450
36	3	3,25	9,75	390
10	3	1	3	120
5	2	1	2	80
141,5		13	38	1520

Traditional casting (planned work)				
m3	No of workers	proj time	work time	cost €
206,8	9	15	135	5400
206,8	9	15	135	5400
413,6			270	10800

Outcome of SCC				
m3	No of workers	proj time	work time	cost €
25	2	2	4	160
30	2	2	4	160
35,5	2	3,75	7,5	300
36	2	3,25	6,5	260
10	2	1	2	80
5	2	1	2	80
141,5		13	26	1040

Outcome of SCC				
m3	No of workers	proj time	work time	cost €
206,8	9	10,5	94,5	3780
206,8	9	9,5	85,5	3420
413,6			180	7200

SCC Theoretical				
m3	No of workers	proj time	work time	cost €
25	1	1,25	1,25	50
30	1	1,5	1,5	60
35,5	1	2	2	80
36	1	2	2	80
10	1	0,5	0,5	20
5	1	0,5	0,5	20
141,5		7,75	7,75	310

SCC Theoretical				
Two teams	No of workers	proj time	work time	cost €
7-14,30	3	7,5	22,5	900
10-16,30	4	6,5	26,0	1040
7-14,30	3	7,5	22,5	900
10-16,30	4	6,5	26,0	1040
			97,0	3880

Nevertheless, the overall result for the superstructure was positive as compared to a traditional concrete solution even though SCC's potential was not fully utilized, and the total costs were reduced with roughly €200. Hence, if SCC had been fully utilized as the theoretical calculation in Table 3 suggests the possible savings would become €3400 for the superstructure.

6.4 Working environment

Probably the largest benefit with SCC is, as mentioned earlier, the improvement in working environment. The improvement in our documentation is threefold in comparison with traditional concrete casting, Figures 10 and 11. The work cycle mean value is computed to 18.2 in our project if traditional vibrated concrete had been used at study no 1, while the actual outcome was 5.7 for SCC [23]. This when comparing relatively small and easy to produce plate structures. Considering, for instance, the case with a 10 meter high plate structure with dense reinforcement, the improvement is possibly even larger due to fact that the worker has to climb down inside the construction carrying the vibrating equipment. This result in exceptionally poor working environment, and also in a probable loss of productivity, due to much lower unit time for casting traditional vibrated concrete.

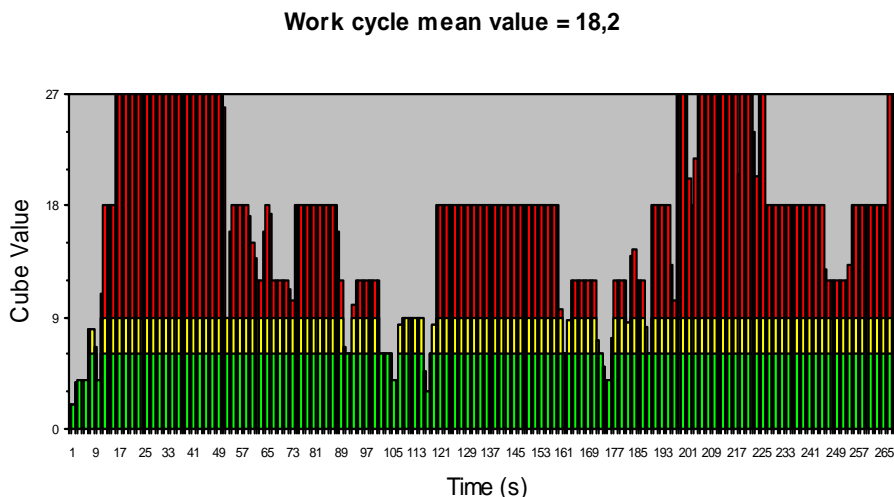


Figure 10: ErgoSAM analysis of concrete worker's short work cycle during casting of traditional vibrated concrete. Below 6 is acceptable, 6 to 9 is conditionally acceptable and 9 and above is unacceptable.

When the value in the Cube model reaches 27 in Figure 10, the worker lifts the heavy poker vibrator (Force = 3) repeatedly (repetition = 3) in awkward positions (Work posture = 3) resulting in the top value which is unacceptable. When the value reaches 18, the worker has the value three for two of the variables and the value two for the third variable. These individual values can vary during a work cycle.

The top value of 9 for SCC in Figure 11 is achieved when the worker pushes the pump hose from one place to another, resulting in the value three for force and working position, and the value one for repetition.

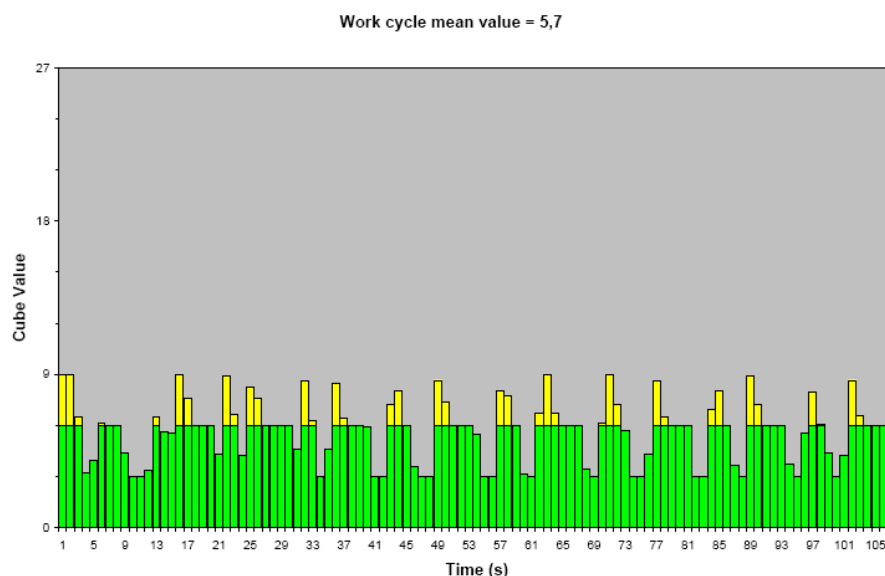


Figure 11: ErgoSAM analysis of concrete worker's short work cycle during SCC casting. The average value for the work cycle is 5.7 which is below 6 and hence acceptable.

Injury cost estimations according to the Swedish Social Insurance Agency [24], show that the single largest cause for sick leaves in general is back pain which accounts for 15 % of all sick

leaves among men and 12 % among women. The average of the total back pain illness compensation per case for men (focusing on men which constitutes 92 % of the construction industry's workforce) is about 4 600 €, this cost denotes 45 € per sick leave day. Considering only the construction industry, Samuelsson and Lundholm [25] reported that out of all 1582 cases of sick leaves caused by occupational illnesses reported for 2004, 1342 cases of sick leaves were caused by ergonomic risk factors (including vibration and noise).

For concrete workers 279 cases of WMSDs were reported, and their sick leave compensations is estimated up to 1 280 000 € for the taxpayers [26]. There are of course other direct and indirect costs such as productivity loss and hiring substitute workers that are not often included in such calculations.

Improved working environment also implies an increase in productivity given that the workers are at the site performing work tasks and there are no vacancies or unskilled substitute workers at the production sites.

7. CONCLUSIONS

The largest economic benefit from introducing SCC to a contractor in civil engineering projects is probably on the superstructure of a bridge, since a large number of workers are needed during casting of traditional vibrated concrete, and it is therefore associated with large casting costs. Hence, the number of workers needed for casting can be markedly reduced if SCC is introduced and proper planning has been carried out before casting.

However, controversially it is often easier to introduce SCC for foundations, columns or plate structures since these structural parts are less dominant in the construction and the "risk" related to using SCC is small. However, for these smaller less people demanding castings it is more difficult to achieve economical benefits in using SCC.

The overall risk using SCC is that the product it is not robust enough, which might result in the concrete does not enclose the reinforcement satisfactory and rework is needed. Also, after casting, it can be visual lines (inward bends) in the finished construction which is not acceptable. Therefore, most often, contractors calculates the risk enclosed in using SCC to be too high, especially for the more important superstructure and simply does not use the product even though both costs and time evidently can be saved.

The SCC delivered to the superstructures on both projects was robust and was of desired quality. The "risk" involved using this SCC was minimal and the contractors were satisfied with both the delivered product and the order of in which the casting was performed. Hence, the castings of the superstructures on both projects were carried out in shorter time and could have been carried out using fewer personnel than planned with traditional concrete. The SCC delivered to the substructures at both projects was not entirely acceptable, however, the SCC at the two projects differed and the quality was better at study 2.

Probably the largest benefit with using SCC is, as mentioned earlier, the improvement in working environment. Therefore, the economy of the Swedish construction industry and society can benefit significantly from using the right kind of working method during construction. As mentioned earlier, 1342 sick leaves were reported for 2004 due to ergonomic risk factors. If these sick leaves costs as much as expected above e.g. €4600 per sick case, it suggests that the

total costs ends up on roughly €6 170 000 annually! This is according to Lean Construction a great deal of muda!

To be able to utilize the redundant personnel during casting of SCC, projects need to be planned and managed properly. Hence, the organisation at the worksite needs to be optimized during the whole project. Clear work instructions need to be formulated for all workers involved and for all work tasks to be performed. Also, a list of buffer work needs to be logged so that workers can be temporarily occupied with other productive work tasks during casting but still within reach if needed during casting, Ballard [27].

REFERENCES

1. Cussigh F, SCC in practice: opportunities and bottlenecks. 5th international RILEM symposium on SCC 3-5 sept 2007, Ghent. PP 21-27.
2. Shah S P, Ferron R P, Ferrara L, Tregger N, Kwon S, Research on SCC: some emerging themes. 5th international RILEM symposium on SCC 3-5 sept 2007, Ghent. PP 3-14.
3. Nielsen, C 2007, Does SCC really improve the working environment? 5th international RILEM symposium on SCC 3-5 sept 2007, Ghent. PP 967-974.
4. Swedish Concrete Association, 2002. Självkompakterande betong, rekommendationer för användning. Betongrapport nr 10 (in Swedish) ISBN 91-973445-3-2.
5. Taguchi Genichi, Robust engineering, Subir Chowdhury, Shin Taguchi ISBN 0-07-134782-8 , 2000
6. Emborg M, Simonsson P, Carlswärd J, Nilsson M, Industrial casting of bridges combining new production methods and materials, like a robust SCC, utilizing lean construction principles. 5th international RILEM symposium on SCC 3-5 sept 2007, Ghent. PP 485-490.
7. Bonen D, Deshpande Y, Olek J, Shen L, Struble L, Lange D, Khayat K, Robustness of self-consolidating concrete. 5th international RILEM symposium on SCC 3-5 sept 2007, Ghent. PP 33-42.
8. The European Guidelines for Self Compacting Concrete, specification, production and use, BIBM, CEMBUREA, EFCA, ERNARC, ERMCO, 2005, 68 pp.
9. Walraven J, Structural aspects of self compacting concrete. Proceedings of the 3rd international RILEM Symposium on SCC 2003, pp 15-22.
10. Ålander C, Advanced systems for rational slab reinforcement. ERMCO Heading for concrete solutions Helsinki 2004. ISBN 952-5075-64-8.
11. Skarendahl Å, Market acceptance of self-compacting concrete, the Swedish experience. Proceedings of the Second International Symposium on Self-Compacting Concrete Tokyo 2001, Kochi: COMS Engineering Corporation, pp1-12.
12. Womack J P and Jones D T (2003), Lean Thinking-Banish waste and create wealth in your organization. ISBN 0-7432-3164-3.
13. Nielsen C, New results regarding SCC and working environment, The Nordic SCC Network Workshop, SCC, Vision and Reality 19th June 2006, Copenhagen, Danish Technological University, 1981.
14. Nielsen C, Does SCC really improve the working environment? 5th international RILEM symposium on SCC 3-5 sept 2007, Ghent. PP 967-974.
15. Geel A, Beushausen H, Alexander M G, SCC in South Africa – the challenge to introduce a new technology to the construction industry. 5th international RILEM symposium on SCC 3-5 sept 2007, Ghent. PP 1035-1040.

16. Nielsen C V, Glavind M, Gredsted L, Hansen C N, SCC – a technical breakthrough and a success for the Danish concrete industry. 5th international RILEM symposium on SCC 3-5 sept 2007, Ghent. PP 993-999.
17. Lecreux S, Cussigh F, Guerin M, French specifications for SCC: conclusions of the French national SCC project (PN B@P). 5th international RILEM symposium on SCC 3-5 sept 2007, Ghent. PP 1049-1054.
18. Sperling L, Dahlman S, Kilbom Å, and Kadefors R, A Cube Model for the classification of work with hand tools and the formulation of functional requirements. *Applied Ergonomics* (1993), 24, 212-220
19. Christmansson M, Falk A-C, Amprazis J, Forsman M, Rasmusson L, and Kadefors R, Modified method time measurements for ergonomic planning of production systems in the manufacturing industry, *Int. J. Prod. Res.*, Vol. 38 (2000), No. 17, 4051-4059.
20. Wikström B-O and Hägg G, International seminar on Corporate Initiatives in Ergonomics. Stockholm 19-20 mars 1999. ISBN 91-7045-521-X.
21. Grauers M, Self compacting concrete – the way to cost effective production of buildings. Proceedings of the Second International Symposium on Self-Compacting Concrete Tokyo 2001, Kochi: COMS Engineering Corporation, pp723-728.
22. Simonsson P, and Emborg M, Industrialization in Swedish bridge engineering: a case study of Lean construction. International Group for Lean Construction, IGLC, 15th Annual conference on Lean Construction, East Lansing, Michigan USA, July 2007.
23. Simonsson P, and Rwamamara R, Consequences of industrialized construction methods on the working environment. International Group for Lean Construction, IGLC, 15th Annual conference on Lean Construction, East Lansing, Michigan USA, 2007.
24. Swedish Social Insurance Agency (Riksförsäkringsverket) (2004) (in Swedish), Vad kostar sjukdomarna för kvinnor och män? Sjukpenningkostnaderna fördelade efter kön och sjukskrivningsdiagnos. Rapport 2004:5.
25. Samuelsson B, and Lundholm L, (2006), (in Swedish), Arbetsskador inom byggindustrin 2005. Bygg- och anläggning. Privat sector. BCA 2006:2.
26. Lundholm L, and Swartz H, (2006), musculoskeletal ergonomics in the construction industry. Facts & figures in brief No. 5.2006. Swedish Work Environment Authority. http://www.av.se/dokument/inenglish/statistics/Sf_2006_05_en.pdf.
27. Ballard G, (2000), The last planner system of production control, PhD thesis, School of Civil Engineering. Faculty of Engineering, The University of Birmingham.

Increasing productivity through utilization of new construction techniques and Lean Construction philosophies in civil engineering projects



Peter Simonsson
Ph.D. student
Luleå University of Technology (LTU)
971 87 Luleå, Sweden
E-mail: Peter.Simonsson@ltu.se

Mats Emborg
Professor LTU / Head R&D Betongindustri AB
LTU, 971 87 Luleå, Sweden
Betongindustri AB, 100 74 Stockholm
E-mail: Mats.Emborg@betongindustri.se
Mats.Emborg@ltu.se

ABSTRACT



The implementation of Self Compacting Concrete (SCC) together with two types of reinforcement and form techniques makes it possible to increase the degree of industrialization at construction sites markedly. To be able to realize this, Lean Construction principles prove to be important utensils during the planning and design phase. Also, the working environment is improved vastly when using SCC and different prefabricated reinforcement solutions. At the construction of the first full scale project “The Industrialized Concrete Bridge”, which was built during 2006 in Sweden, the new techniques were applied. It was concluded that the working environment was improved by three fold, production time at site could be reduced with up to 20 % and that the number of workers could be reduced by virtually 25 %.

Key words: Industrialization, Lean Construction, Productivity, SCC, Prefabrication, Reinforcement

1. INTRODUCTION

1.1 General

Building bridges with in-situ cast concrete today suffers, to some extent from inefficiency and less developed production methods. The construction work is time consuming, expensive and often includes poor working environment. According to Byfors and Jäderholm [1], the productivity increase in the Swedish construction industry in general has been approximately 3% during the period 1995-2005, which should be compared with an almost 90% productivity increase for the manufacturing industries during the same time period. Since the productivity increase is that low, a comprehensive view is needed for technical development and different production planning methods together with new material and construction solutions. This is seldom realized resulting in that today’s production methods are not as productive as they most certainly can be. However, many larger companies in Sweden develop alternative methods

primary used for houses. The system of NCC Komplet was an interesting example where elements were totally pre-manufactured indoors and assembled in a protecting tent.

Industrialization is often mentioned as the measure to be taken to increase the productivity, and its definition is frequently debated in literature. Nevertheless, it is agreed that to achieve a more industrialized process, focus cannot only be on the production apparatus, i.e. the whole process needs to be managed from a project idea to completed structure. Other important issues that must be addressed at an industrialization level are logistics, collaboration between partners, standardized concepts, prefabrication of highly processed components, information technology and Lean Construction philosophies, [2] and [3].

1.2 Objective of the research project

The objective of the Ph.D research project “Industrial Concrete Bridge Construction” at Luleå University of Technology is to try to adapt Lean Construction to concrete construction and combine them with modern construction methods to develop a more industrialized process.

Lean Construction originates from Lean Production philosophies and theories that have offered lots of benefits to the manufacturing industry e.g. [4] and [5]. An interesting example of Lean Production use is the Toyota motor company, and one question is now if and how this way of thinking can be introduced into the construction industry.

By adopting and translating the principles and fundamentals of Lean Production into Lean Construction there is a possibility that the construction industry can make a leap in productivity, minimize costs for erection of buildings and bridges, and increase the health and safety of workers. The former can thus be defined as the long term objective of the research and the latter as the short term objectives.

2. THINKING LEAN

The platform for Lean Production is simple: to deliver what the customer wants when the customer needs it in the required quantity. A key issue is the focus on the well known waste or “*muda*”, i.e. any human activity that absorbs resources without creating any value [6]. Muda includes: 1) overproduction, 2) waiting, 3) unnecessary transports, 4) erroneous processes, 5) unnecessary inventory, 6) unnecessary movement, 7) goods with errors and 8) to not meet customer needs.

2.1 Origin

Toyota Motor Company was formed in 1937, and in the beginning of the 1950’s they had produced 2685 cars during thirteen years of production which should be compared with Fords Rouge plant that was manufacturing 7000 cars per day [5]! Something had to be done so Toyota sent over Eiji Toyoda on a study trip to Detroit for three months. Together with Taiichi Ohno they concluded that Toyota could not convert Fords production methods into the Japanese culture. Instead they lay the foundation for the Toyota Production System (TPS).

Toyota in the early 1950's had a small budget for its manufacturing as Japan was a poor country after the Second World War. This constrained Toyota in investing in different machines such as the stamping press that Ford for instance had hundreds of. Toyotas budget allowed them to use just a few stamping presses for a complete car model when Ford often could dedicate one press line for a specific part for months or even years without having to change the equipment. Using only a few press lines was impossible for Ford due to long lead times when changing dies. For Toyota the issue was to develop a way to minimize lead time for the equipment changes from hours or even days to minutes.

2.2 Key concepts

In Lean Production there are five key concepts; 1) to specify customer *value*, 2) to identify the *value stream*, 3) to make the value *flow* without any interruptions, 4) to make the customer *pull* the value out of the manufacturing and 5) to strive for *perfection*. Womack and Jones [6] suggest that customer value is the critical starting point for Lean Production. Value can only be specified by the end customer and it is only meaningful when expressed in a certain product, goods and/or service which meet customer demands to a specific price at a certain time. Value is created by the manufacturer but can be difficult for the manufacturer to specify.

After specifying customer value the value stream should be identified. The value stream is the action needed to convey a specific product, goods or service through three critical management steps which exist in all businesses; *problem solving* from concept to detailed design and production planning, *information handling* from order acceptance to detailed planning of delivery and-, *transformation* of raw material to produced product or goods to customer.

When the customer value is defined and the value stream is identified and optimized, the next step in Lean Production is flow. The product, goods and/or service should flow through the value adding activities. This often demands that all earlier production experience is set aside at the company and the company's management. It is important to manufacture in small batches because large quantities often mean long lead times at different operations for the product to pass during manufacturing. All unnecessary stops, waiting times or stock is to be excluded from the production sequence.

When flow has been dealt with the next step is pull. Mass production has a way of pushing products through the different parts of manufacturing from production to delivery. This means that production is set to produce upon prognosis and not on what the customer actually requests. Lean uses a different course of action, namely pull which means that no products are produced unless there is an end customer ordering the product. More thoroughly this means that even the internal customers does not get provided with products until they ask for it.

Pursue perfection in all parts of the manufacturing is the last step in line. By using pull instead of push the company will automatically discover new procedures for minimizing work efforts, space and costs, mistakes will decrease and the fact that the company will always be able to offer what the customer desires when he wants it will be open for new solutions. One of the largest obstacles to overcome with perfection is that manufacturing includes inappropriate working methods. Another difficulty is problems with the design. It is thus important to form a vision for perfection and to choose a few different parts to put focus on [6].

2.3 Toyota Production System (TPS)

Within the Toyota Production System (TPS) there are three concepts that are connected; *muda*, *muri* and *mura*. *Muda* is as explained above any human activity that absorbs resources without creating any value. *Muri* is to overload people and/or equipment and *mura* is unevenness that depends on lack of production planning or brake down of machinery, late deliveries, defects on parts etcetera.

Moreover, according to Liker [4], there are 14 principles of production in the TPS. These are subdivided into four different categories: Philosophy, Process, People and Partners, and Problem Solving, Figure 1. These are also called Toyotas four P's of production.

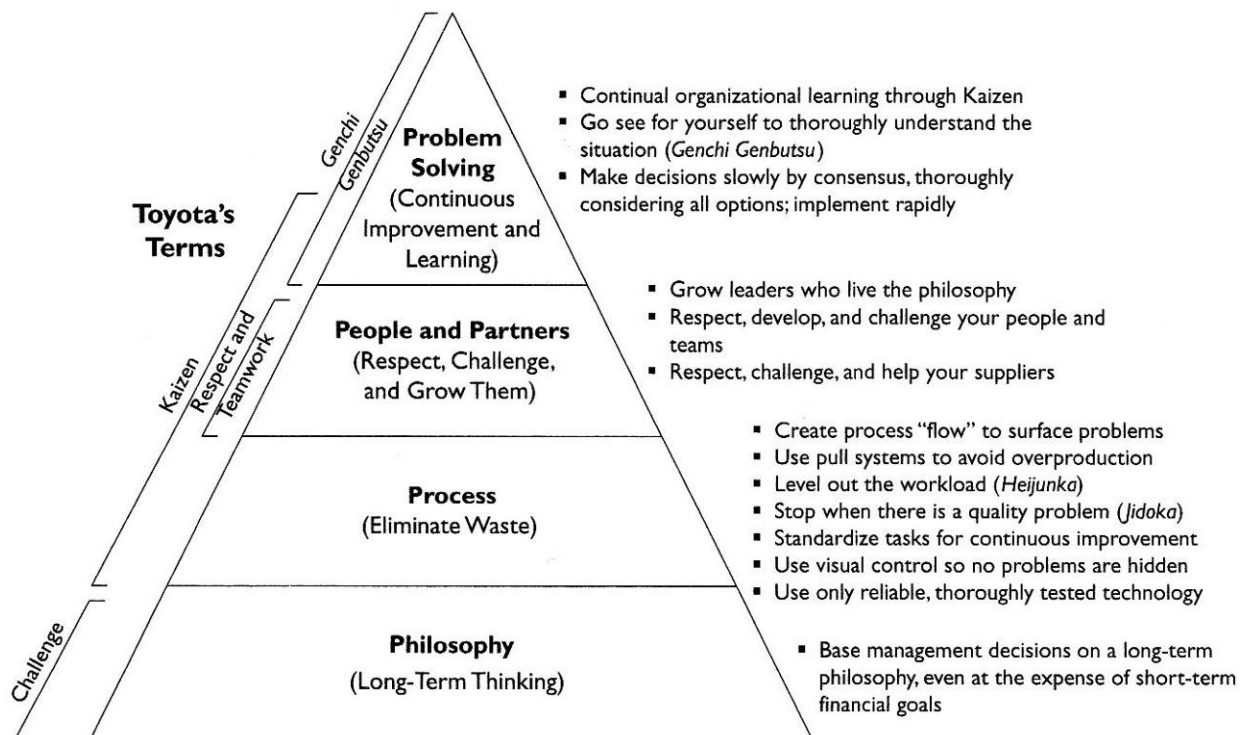


Figure 1 – Toyotas four P:s (middle) and 14 principles (right) of production, Liker (2004).

2.4 TPS tools

The term *Kaizen* in Figure 1 stands for continuous improvements and it teaches individuals skills and methods for working effectively in small groups, solving problems, documenting and improving processes, collecting data and self-managing them. *Kaizen* also allows decision making to be done by the workers in the different groups. Continuous improvements also mean improvement of products processes or services over time, with the goal of reducing waste to improve workplace functionality, customer services or product performance [4].

Kaizen is a term that involves different methods for continuous improvements. One of these methods is the five whys, which means that when a defect part or unit comes up in production the immediate reaction within the personnel is to try to understand why this has happened and how it can be prevented in the future by finding the source of the problem. This preventing work

is done by asking why five times. Another important term in this subject is value stream mapping, which helps focusing the Kaizen work, and prioritizing the customer value during the continuous improvement.

3 LEAN CONSTRUCTION IN CIVIL ENGINEERING

For the construction industry, it is of significant interest to convert the ideas of Lean Production into Lean Construction for the improvement of productivity, economy and working environment. This has been dealt with by many authors at conferences, for example organized by the International Group of Lean Construction, IGLC [7].

Toyota's first principle (and first P) in Figure 1 is "Base management decisions on long term philosophy, even at the expense of short term financial goals". It is evident that in the construction business most clients, contractors, designers, sub contractors do not apply this principle. They usually realize their short term financial goals in first hand because they do not see any long term relationship after the specific project. Instead, in traditional civil engineering projects in Sweden, most often clients do not contemplate anything but the bidding sum. Considering the fact that the client for such projects usually represents the community the prospects for changing their behavior are little. However, there are a few things the client can consider apart from the bidding sum, e.g. the working environment to promote health and safety for the construction workers and a reduction of the overall project time.

Another dilemma of the construction business is that contractors usually consider every project as an individual project. The local manager gets a project budget which he/she has to keep and manage the project with. There is seldom any room for errors or for that matter new thinking in the form of new material and/or production solutions that possibly could contribute to a profit in the next project. Because changes are nearly never profitable at first attempt this situation hinders the development of the construction industry. Also, contractors usually purchase their designers on quantities of steel reinforcement for instance and the designer that offers the slimmest solution together with a low bidding sum most often wins the purchase instead of purchasing designers on solutions for practical on-site build-ability.

There are a few exceptions, for instance, most often material suppliers see a continuance beyond a single project and they therefore do not maximize the profit for one single project.

Toyota's 13 *other principles* and their *three P's* of production, Figure 1, can be transformed into the construction business. The first P, "Problem solving", is an activity that the construction industry and contractors is very good at. However, the contractors and construction industry in general doesn't perform it the way Toyota intended. *Most often* the contractors solve upcoming problems but do not concern about learning from or finding the root cause of the problems. The learning process of continuous improvement philosophy (Kaizen) is not adopted in a broad manner within the construction industry. By implementing routines for problem solving in the contractor's day to day work, the Kaizen work can be improved rapidly and easily. What is needed is an understanding of the relative profits that can be achieved for a construction company if problems only occur once.

The second P of Figure 1 dealing with People and partners, implying that companies should develop leaders who live the philosophy of the company and that mutual respect is applied between suppliers and "main company" as well as management and workers.

The third P is dedicated to the Process flow. When production starts flowing in the right direction problems are going to surface and have to be dealt with. This is where the different concepts of the TPS are most visible and benefits the most. For instance the pull system produces only when the demand is there, it levels out the workload, and see to that the workers have an even production rate. When quality problems arise production stops and they can be taken care of. Also, it is of importance to make sure that all involved workers understand the problem and why it surfaced to make sure it doesn't happen again. Moreover, to further improve flow it is important to standardize work tasks, so that it is easy for workers to understand other work tasks and switch work tasks within the work group which eases and makes the continuous improvement work becomes more reliable.

3.1 Lean bridge design

To be able to increase productivity and make a specific production site more lean, the project must be designed and planned properly. To achieve a proper design and planning it is fundamental to establish a design team meeting the criteria. To be able to think lean in a project it is essential to start at the end, at the finished product, to see what is expected as an outcome. Then it is important to “walk backwards” in the process all the way to the start to locate bottlenecks and detect possible variance of construction, which are of importance and can cause problems to the production flow if not handled properly. It is also important to listen to the workers and their experience and to, in as many cases as possible, implement their suggestions for improvements.

A central point in forming the team is to include all areas of interest for the project from the beginning. Therefore, knowledge from production, design, management, future maintenance, suppliers and 3D and 4D modeling (3D plus time) should actively be implemented in the design phase together with a close relation to the customer, i.e. the client [8]. Furthermore, it is known that the earlier industrialization ideas can be introduced in the design and execution phase of a project, the greater the influence will be, see Figure 2 illustrating a traditional Swedish National Road Administration – Production department (SNRA-Production) project schedule (which of course can be valid for other contractor's project schedules).

To get the actors working together from the beginning make them understand each others difficulties and can act upon them to solve problems before they appear. This is in line with one important principle in Lean Construction that downstream actors are involved upstream in decisions and vice versa. Creating this lean design team also ensures that products and processes are designed in collaboration between partners, which in turn means that the contractor and sub-contractor can form and design solutions in the most favorable way in terms of construction.

Traditional SNRA Project schedule

1. Preliminary study
2. Feasibility study
3. Design plan
4. Purchasing
5. Building documents
6. Execution

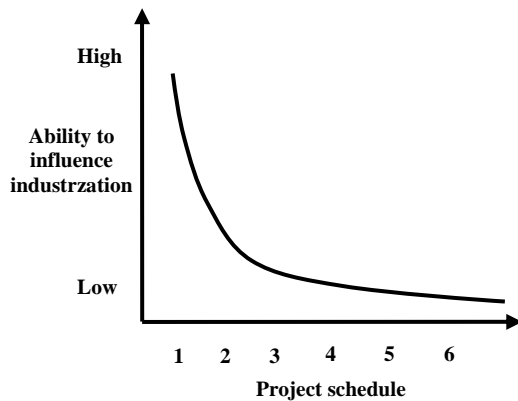


Figure 2. Project schedule of a traditional Swedish National Road Administration (SNRA) project and its industrialization possibilities. The earlier the efforts for industrialization the greater impact they have.

Several tools and methods are also available for planning, for instance applying Concurrent Engineering (CE) where resources are used effectively in cooperation between design, construction and production in cross functional working teams that are a part of the optimization of the planning process [2].

For the industrialization of construction with in-situ cast concrete focus should preferably be on the following six components [9]:

- Improved concrete qualities and optimal construction, e.g. self compacting concrete.
- Minimized reinforcement activities on site.
- Permanent and /or optimized formwork minimizing site logistics.
- Optimized concrete transport on site from the truck to form, e.g. pumping techniques.
- Weather independent construction processes, e.g. climate protective tent.
- IT and Lean construction tools, where multi-disciplinary decisions are made at design, production planning, and construction, e.g. reducing muda.

3.2 Responsibilities

To be able to introduce a Lean Design Team as described above it is essential that all actors take their responsibility. Therefore, a new way of thinking is probably necessary when starting the bidding process. It is thus important to develop long-term relationships between all partners. According to Toyotas 11th principle “respect your extended network of partners and suppliers by challenging them and helping them to improve” one should treat its partners and suppliers as an extension of the own business. This is one of the central cores of Toyotas reputation among their suppliers; they work together towards mutual goals. Toyota would never change supplier only because another one is a few percent cheaper. Changing partners because of price is however common in the construction industry, and here, the industry needs to implement another approach.

4 PROCESS FLOW IN CONSTRUCTION

A traditional view of looking at any kind of production is to see input become output, which is called a transformation process. In this case it is relatively easy to record productivity simply by

looking at the relationship between output and input during a given time. On the other hand, the process of input becoming output (in the construction process) usually involves different sub processes which makes it more complicated to record the productivity of different workstations in relation to total productivity, see Figure 3 [10].

Value stream is one of five key concepts mentioned in Section 2.2 for Lean Production and also Lean Construction. The definition of the term value stream is all the activities that are performed when refining a product, both those who add value and those that do not add value [4]. In the traditional manufacturing industry, companies make value stream mapping continuously but on a traditional construction site it is not that common at all. The reason for this is probably the constant change in production and the relatively little repetitive work that is performed at a construction site. Nevertheless, it is important for the construction industry to survey the value stream of the building sites. This is done to be able to map the different muda (Section 2.2) appearing during the various stages of production.

Mapping the value stream will support the company not only to eliminate waste but also to identify causes for wasteful activities. The value stream mapping visualizes the whole manufacturing process in a comprehensive and understandable form and demonstrates the connections between information and material flow.

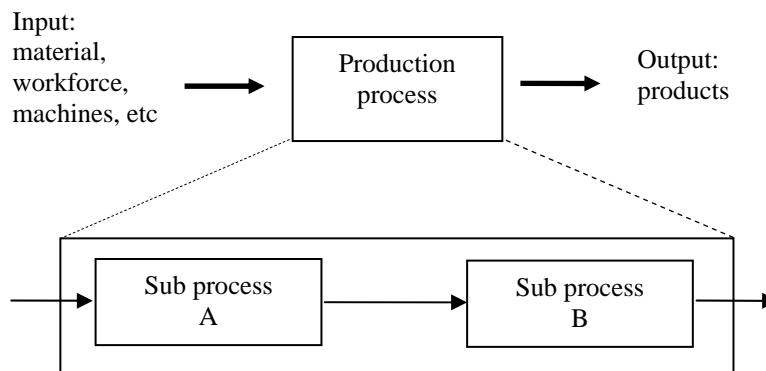


Figure 3. The transformation process of input becoming output according to Koskela [10].

Figure 4 visualizes the process with traditional handling of reinforcement, i.e. when reinforcement is placed piece by piece. The colored squares are non value adding steps or “activities” for the reinforcement, i.e. muda when the reinforcement is lying in a pile and not being used waiting for mounting. The waiting time can be anything from a few days to a week or several months depending on the project size and management. The waste for this “activity” is in the form of space occupancy and tied up funds etc. Different actors are affected in the various colored squares. For instance early in the stream it is the contractor, and later on it can be the purchaser or the society.

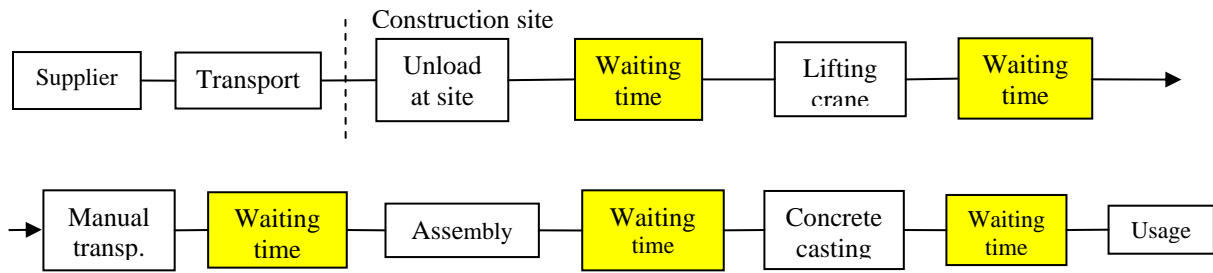


Figure 4. Value stream of traditional handling of single piece reinforcement on a construction site.

The pursuit here is to minimize the number of colored squares, i.e. the waiting time, and to minimize the time spent for the reinforcement in each of these squares. As can be seen in Figures 5 and 6 using prefabricated reinforcement, the number of colored squares has been reduced as compared to the traditional handling Figure 4. This implies that the mounting of prefabricated reinforcement, as known, goes faster than the traditional mounting.



Figure 5. Value stream when handling the prefabricated reinforcement sections for the foundation of the first full scale bridge project.

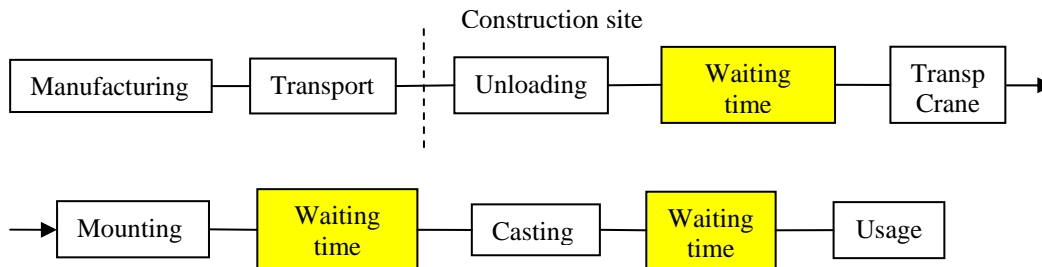


Figure 6. Value stream when handling the rebar carpet reinforcement used at the first bridge project.

Some waiting time is however necessary or somewhat unavoidable with current construction methods. For instance the waiting time between finished reinforcement assembly and casting the concrete is unavoidable but it can most definitely be reduced. Also, the waiting time after casting of the concrete and before usage of the bridge is to some extent unavoidable with current construction methods.

5 THEORETICAL PILOT STUDIES

Initially, one focus of the research was to examine which parts of a bridge that can be prefabricated conveniently and which parts that must be manufactured traditionally on site. Another focus was to evaluate where most man hours at the production site are spent and how the distribution of production costs is. Therefore, the project was initiated by interviewing

experienced representatives of SNRA-Production. The positions of the persons interviewed varied from site-managers and contract engineers to supervisors. The interviews considered some already constructed in-situ cast concrete bridges, in order to identify areas where major advancements in production can be achieved. The interviews included the main contractors own assignments and thus did not include work tasks assigned to sub-contractors such as asphaltting, railing etc.

According to the interview results, when constructing the superstructure, the formwork is the most time consuming activity for the main contractor, and the largest costs are connected to the reinforcement and concrete, see Table 1. For the foundation, the most time and cost consuming activity is the reinforcement work. The results indicate that the reinforcement work could possibly be suitable for prefabrication.

Table 1. Distribution of time and costs at construction of in-situ cast concrete bridges. Summaries of answers from interviews conducted with personnel from SNRA- Production.

	Foundation		Superstructure		Average	
	time	cost	time	cost	time	cost
Formwork	25%	20%	50%	30%	37%	25%
Reinforcement	45%	40%	35%	35%	40%	38%
Concrete	30%	40%	15%	35%	23%	37%

A follow up of already constructed bridges (a number of ten medium size highway bridges) made by the researchers at LTU based upon information from the bidding phases showed that reinforcement, formwork and in-situ casting of concrete typically make up for approximately 50 % of the total construction costs with relative ratios of approximately 1/3 each [11], Figure 7 a). The other 50 % of the costs is related to general establishment at the building site, foundation, pile driving, asphaltting, railing etc and mostly performed by sub-contractors.

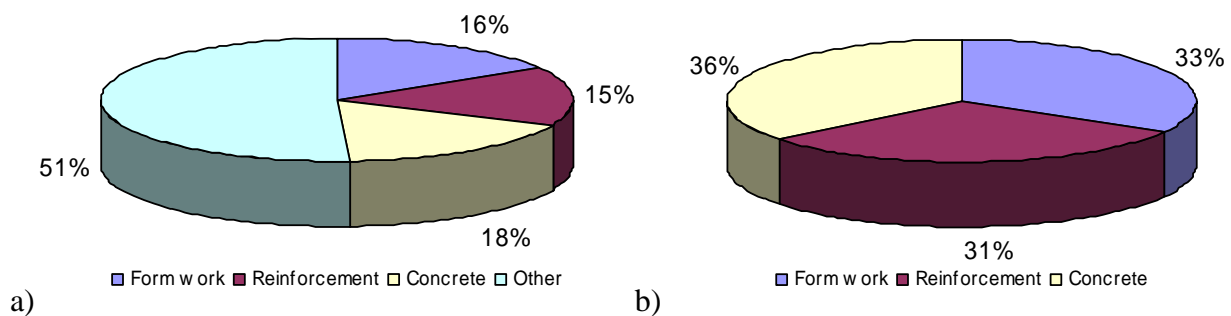


Figure 7. a) Distribution of total construction costs for concrete highway bridges. b) Distribution of costs for formwork, reinforcement and concrete, both figures according to follow up from ten medium sized bridges.

From a purely theoretical viewpoint, the implementation of industrialized construction methods (self compacting concrete, prefabricated reinforcement and left formwork) can reduce the manpower substantially for these bridges. For instance, if prefabricated reinforcement is used in the foundations and superstructure, the on-site construction time can be reduced with up to 80 %, Figure 8. A corresponding time reduction would also be achieved theoretically if permanent

formwork solutions are adopted. It should be emphasized that full benefit of course calls for detailed design and planning of logistics before construction can commence.

Main advantages of applying self compacting concrete, SCC, are that casting rates are increased and that the number of workers needed for concreting can be reduced. Today, only one person at site is needed for casting the concrete, but in the future, SCC opens for a form filling solely performed by the concrete pump operator.

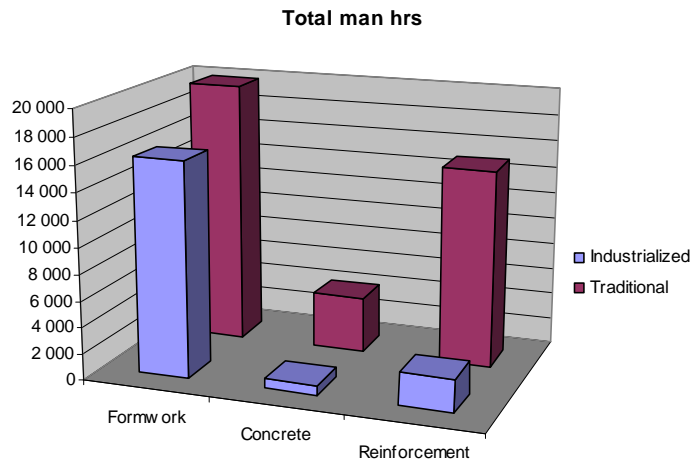


Figure 8. Theoretical reduction of on-site man hours during construction for an industrial process compared with traditional methods.

6 FULL SCALE PROJECTS

The general opinion among researchers and practitioners worldwide is that the construction industry to some extent suffers from having a lack of skilled personnel and having problems recruiting new people to the workforce. Therefore, the need to change production methods to less personnel and time consuming at the production site has increased. Thus, the research project has focused on how to implement “new” production methods to increase productivity and minimize waste and to decrease the number of workers needed at the production site. Another important parameter in the research is to try to improve the safety at construction sites.

The first full scale project was a bridge provided by the Swedish National Road Administration, north region, that was dedicated to research and development only. The bridge was located in Kalix in the northern part of Sweden and was a slab bridge with a span of 10 m and a width of 15 m, Figure 9. Here, SCC and prefabricated reinforcement in different shapes were tested.

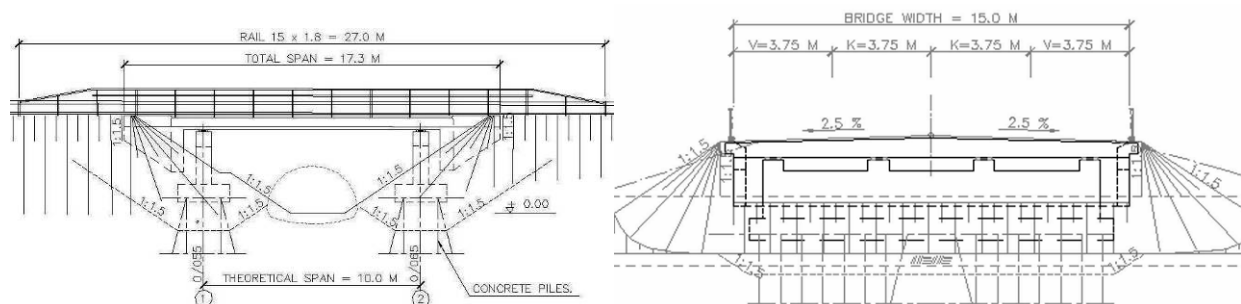


Figure 9. First full scale project with a bridge span of 10 m and a width of 15 m.

The second project was the erection of a bridge in connection to a hydro power plant in Boden, also in the northern parts of Sweden. The width of the bridge is 7,3 meters and the length is 60,2 meters. At that specific project solely the carpet reinforcement was tested.

The third full scale project within civil engineering consisted of two similar bridges as a part of a highway project at Nynäsvägen south of Stockholm. The bridges were somewhat larger than the first full scale project, with a span of 18 meters and a width of 9 meters. Primary, focus of the third case was on the SCC but the carpet reinforcement was also tested to some extent.

Moreover, a house construction site has also been followed up regarding the carpet reinforcement; this to study possible differences with the use in civil engineering projects.

6.1 Production methods

As known, SCC is not a new production method - it has been used in Sweden and the rest of Europe for the past ten years and for an even longer period of time in Japan. A central point for the successful realization of SCC is to define the performance of the product, which can, according to the Growth project Testing-SCC, be discerned into three main parameters: 1) *Filling ability* i. e. the ability to flow and to completely fill the formwork 2) *Passing ability* i. e. the ability to flow around reinforcement without blocking and 3) *Segregation proneness* i. e. the tendency of coarse aggregate to sink downwards. For these parameters, criteria can be established to be met by a proper mix design. These criteria depend on geometry of structure to be cast, reinforcement, form type and method and local tradition on how to pour the concrete [12].

The production benefits of SCC are that the need for workers during casting decreases; concrete workers can perform other activities during casting that should have been done at a later moment and the construction site becomes less congested, Figure 10.

There is also a considerable increase in health and safety of SCC when compared to traditional vibrated concrete, due to less noise level (no compacting work needed) and less heavy lifting of material and equipment.



Figure 10: a) Casting SCC on the Nynäsvägen project. b) Casting of normal vibrated concrete.

Considering the reinforcement, a very unhealthy and stressful operating position for the craftsmen is the assembly of reinforcement piece by piece, Figure 11a. It requires long working time and is therefore often a bottleneck in production [13]. Prefabricated reinforcement often consists of ready to use traditional mesh reinforcement or reinforcement welded together to

cages varying in size. Thus, prefabricated reinforcement is a most interesting alternative for Lean Construction.

For the foundation, the reinforcement was placed in two different prefabricated cages, one for each foundation, Figure 11b.



a)

b)

Figure 11: a) Normal working position for traditional placing of reinforcement. b) Cages of reinforcement placed directly in the form at the Kalix project.

Another option available in the last decade is the *carpet reinforcement* system, which are loose bars welded up on thin steel bands and then rolled together [14]. The roll of reinforcement is then fixed on the specific starting place for the reinforcement and rolled out into a finished product. The first full scale project was designed for using three different methods for placing the reinforcement.

The reinforcement for the plate structures was of a traditional type and the longitudinal reinforcement of the bridge deck was of the carpet reinforcement type, Figure 12. The shear reinforcement of the deck was pre-manufactured in sections and lifted on place.



Figure 12: Rebar carpets, rolled out on the superstructure at the Kalix project.

6.2 Designing of the full scale bridges

To be able to introduce changes in production methods at the first full scale project, it was important to utilize Lean Construction philosophies. Hence, it was essential for the different actors to understand each other and work together as a Lean Design Team. As a result the actors, that normally only are involved when construction starts, were involved in the design stage and production planning of the bridge. The main designer, the prefabricated reinforcement designer/supplier and the concrete supplier worked together in cooperation with the contractor and client using the techniques of Concurrent Engineering to solve problems and to find possibilities in their different areas simultaneously. This thinking was settled at the first meeting of the Lean Design Team which led to a redesign of the bridge to find alternative solutions for improving the constructability.

To be able to utilize the full potential of the SCC, the designer and the concrete material supplier decided together with the contractor and client to increase the strength of the concrete from a traditional concrete strength class C35/45 to class C55/60. In this way some of the very dense shear reinforcement could be left out.

Concerning the superstructure, carpet reinforcement has not been used in bridges in Sweden earlier, since rules and regulations do not allow welding of the reinforcement if it is exposed to stress variations larger than 60 MPa. It was however possible to analyze where those conditions were valid and redesign the bridge allowing for partly welded, and partly clenched carpet reinforcement.

Regarding the bridge in connection to the hydro power plant at Boden there was no need for any large redesign as the rebar carpet was only decided to be used in one layer on the superstructure.

For the third project, the bridges were redesigned partially to facilitate rebar carpets in the top and bottom layer of the superstructures. The main test on these bridges was, as mentioned earlier, the SCC which replaced the traditional concrete. No additional design was performed for enabling the use SCC.

The house construction site was only studied regarding the placing of the rebar carpets and no other insight of the project was possible. Hence, no information on how the buildings were designed has been available.

6.3 Organization

Using the traditional method of constructing, most often trades are subdivided into activities dedicated for formwork, reinforcement and concrete. At an optimized industrial process using different segments prefabricated and SCC, a new approach when composing the working teams must be introduced. The working team on site needs to be cross functional in knowledge and experience. Hence, in the optimized production, a worker needs to be able to handle formwork and reinforcement as well as casting the concrete. This of course depends on the size of the project and for these rather small bridges studied here, the prerequisites for the workers are that they simply have to be multi skilled.

6.4 Research activities at sites

To be able to follow up the activities at the different sites, various measurements and observations were conducted. Regarding the concrete, air content and slump flows were measured on the majority of the concrete deliveries to the bridges of the first and third projects. Concerning the rebar carpet, measurements were performed on productivity. Also, economical studies comparing traditional reinforcement with rebar carpets.

Interviews with the workers were also carried out to see if the attitude towards the different working moments changed during the project.

6.5 Working environment

To have the right working environment is an important factor of a fully operating construction site. It is therefore important that production methods are developed continuously and adapted to today's construction sites and workers. The Swedish construction work environment is regarded as the safest in the world on the subject of physical health, working conditions, illnesses and accidents [15]. Nevertheless, there are still work environment related health problems to be tackled.

At on of the building sites, ergonomic analysis through ErgoSAM was carried out. ErgoSAM is based on SAM (a sequence-based activity method), and a higher-level method-time-measurement (MTM) system. The SAM system is the result of work carried out in Sweden to shorten the time needed for analyses made with MTM systems [16]. The ErgoSAM method considers two pieces of information: the work zone relative to the worker's body in which the activity is carried out or ends; and the weight of the objects handled or the force exerted in the activity [17]. The output of ErgoSAM is the product of three types of variables namely, work posture, force and repetition (frequency), according to a scientific model, the Cube model [18].

The Cube Model, Figure 14 a, is used on site observations to acquire the risk of work-related musculoskeletal disorders, WMSDs, on combinations of the variables mentioned (work posture, force and repetition). For a specific working task, and for each variable separately, demand levels may be defined as low, medium, or high, where the demand criteria are chosen so as to discriminate between good or poor work ergonomics, and assigned weight factors 1, 2, and 3 respectively. Combinations of demands are evaluated by multiplication of the three weight factors, and this product determines the acceptability of the task [18].

ErgoSAM has been used by different Swedish companies within the manufacturing industry. For instance, studies have been carried out at Volvo Cars in Gothenburg [19].

At all the full scale projects, the observations were done in a form of walking through the site, video filming of identified steel reinforcement and/or concrete casting activity work cycles and interviews with the workers. These observations were the basis for a further risk assessment; the ErgoSAM analysis, see Section 7.5.

7 RESULT AND EXPERIENCE

7.1 Kalix

In Kalix the most comprehensive studies were carried out. The bridge was designed for the “new” production methods, i.e. SCC, prefabricated reinforcement and rebar carpets. Some 13 tons out of the total of 16 tons reinforcement on the superstructure were able to be rolled out using rebar carpets. The on-site construction time for this reinforcement went from predicted 80 hrs to 15 hrs, see Table 2a. This meant that the theoretical estimation of an 80 % reduction (Chapter 5, Figure 8) of on-site construction time when using prefabricated reinforcement was fulfilled at the first full scale test.

Table 2. Using rebar carpets for the different full scale projects as compared to traditional reinforcement (left). Casting of SCC as compared with traditional vibrated concrete (right).

Kalix	Traditional	Craft hrs/ton	Industrialized	Craft hrs/ton						
	Prd time at site	2,5 days	80 hrs	5 hrs			15 hrs			
	Craftsmen	4 persons	13,2 ton	3 persons			13,2 ton			
	Total	80 hrs	6 hrs 4 min	15 hrs			1hr 8 min			
Boden	Traditional	Craft hrs/ton	Industrialized	Craft hrs/ton						
	Prd time at site	4 hrs	8 hrs	27 min			1,5 hrs			
	Craftsmen	2 persons	1,48 ton	3 persons			1,48 ton			
	Total	8 hrs	5 hrs 24 min	1,5 hrs			1 hrs			
Nynäsvägen	Traditional	Craft hrs/ton	Industrialized	Craft hrs/ton	Kalix	Traditional Optimum SCC				
	Prd time at site	12 hrs	24 hrs	1 hr			3 hrs	10 hrs	7 hrs	
	Craftsmen	2 persons	3,6 ton	3 persons			3,6 ton	4 persons	2 persons	
	Total	24 hrs	6 hrs 40 min	3 hrs			50 min	Total	40 hrs	14 hrs
House	Traditional	Craft hrs/ton	Industrialized	Craft hrs/ton	Nynäsvägen	Traditional Optimum SCC				
	Prd time at site	12,5 hrs	25 hrs	64 min			3 hrs 15 min	Prd time superstr	20	14
	Craftsmen	2 persons	1,91 ton	3 persons			1,91 ton	Craftsmen	9	7
	Total	25 hrs	13 hrs 5 min	3 hrs 15 min			1 hr 42 min	Total	180	97

When studying the prefabricated reinforcement cages for the foundation, the time spent on the construction site went down from 2,5 days using two construction workers for each foundation to 1 hour in total, resulting in an on-site reduction with almost 40 man hours. Even though the prefabrication manufacturing time is added, there is still reduction in total production time. The main importance is though that the actual on-site production time can be vastly decreased and hence the total construction time for the project was reduced.

The production times given in Table 2 for the traditional placing of reinforcement and casting of concrete were estimated from both the experience of the local site manager and from the sum given in the calculation at the bidding stage.

Regarding the concrete in the Kalix project, the total man hours were reduced from predicted 70 hrs of casting to 19 hrs a reduction of approximately 70 % in on-site man hours, Table 2b. The concrete was cast at four different occasions, varying in volume and casting time.

7.2 Boden (hydro power station bridge)

At the hydro power station in Boden the research considered only the placing of rebar carpets. The bridge was not redesigned for optimizing the use of rebar carpets, and did not have the best conditions for using rebar carpets. However, as can be seen in Table 2 a, the implementation paid off in reduction of on-site construction time. Since it was only three rebar carpets used in total, the reduction was not large in hours but approximately 80 % of the predicted placing time for the reinforcement was reduced. This also meets the theoretical estimations of Chapter 5. The traditional production time given in Table 2 a was obtained from the local site manager.

7.3 Nynäsvägen

At Nynäsvägen, the most comprehensive concrete research was performed. All concrete used on this bridge was SCC. On the construction site the slump flow and air content were measured and at the concrete plant, in addition to the slump flow and air content, also the moisture of the aggregate was documented. The target value of the slump flow at the construction site was 720 mm \pm 20 mm. That outline was kept most of the time, i.e. the concrete was robust and had little variation in consistency, Figure 13. Some variations were however detected regarding the air content in the concrete during the beginning of a casting, but it was rapidly adjusted. The main experience of the concrete was that it was robust, easy to use and reliable.



Figure 13: Slump flow of tested SCC, measuring approximately 700 mm.

The only prefabricated reinforcement used in this project was the rebar carpets for the top and bottom layer of the reinforcement in the superstructure. The bridge was not redesigned for optimizing the use of rebar carpets, hence the amount used was sparse. However, even though the bridge was not optimized for rebar carpets and the amount used was only approximately 1,8 tons out of a possible 22,2 tons, which gives 8 % of the total amount, the results show the same as in the two previous cases. There is approximately an 80 % savings of on-site placing time possible when using rebar carpets in comparison to the traditional single piece placing of reinforcement. This is the third full scale test giving the same result!

The production time for traditional handling of reinforcement and casting of concrete was obtained by the experience of the local site manager and the bidding calculation.

7.4 House project

The results when using the carpet reinforcement in the housing project is the same as when compared with the civil engineering projects, there is, again, approximately an 80 % reduction in on-site production time.

It is difficult to compare the reinforcement design and construction within civil engineering with the design and construction of houses or dwellings because there are e. g. much tougher terms when considering the rules and. In fact, it is easier to introduce for instance rebar carpets into the design of houses than it is into the design of civil engineering structures.

7.5 Ergonomic analysis, ErgoSAM results

After several weeks of observing concrete workers performing their jobs on the construction site and after informal interviews with them, classic work cycles for different methods of reinforcement and concrete casting became obvious. Based on this information, video films were taken and analyses of representative short work cycles were performed to identify any risks for WMSDs (see Section 6.5) for concrete workers performing their tasks using different construction methods, namely conventional and industrialized methods.

Results of the analyses for representative work cycles are presented in Figures 14 and 15, where different loads on concrete workers are represented by Cube values. The Cube value or the load level falls within three levels; below 6 is acceptable (green colour), 6 to below 9 is conditionally acceptable (yellow) and 9 and above is unacceptable (red). For example, the work cycle mean value of 7.4 obtained in ErgoSAM analysis in Figure 14 falls into the conditionally acceptable area. The situations which still fall short of being acceptable are attributable to those tasks that have high degree of repetition and bending, such as fixing the steel structure and cutting metal rings off the rolled out carpet reinforcement.

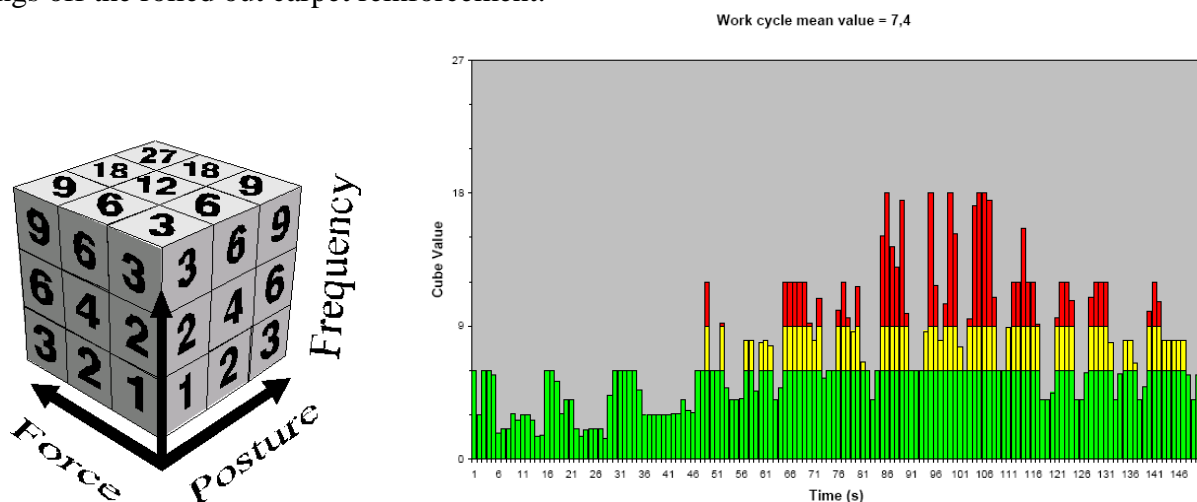


Figure 14: a) Using the Cube model [18] for a specific working task, force, posture and frequency are given weight factors 1, 2 or 3 and then multiplied to be able to discriminate between good and poor work ergonomics. b) ErgoSAM analysis of a short work cycle of a concrete personell working with prefabricated steel reinforcement, mean value 7,4.

If the worker performed tasks with the manual steel rebar work, the worker is exceedingly exposed to WMSD risk factors contributing to very high cube values and a mean value of 21, Figure 15. This number denotes almost three times higher risk exposure to WMSDs when working with the traditional rebar reinforcement than when working with the off-site manufactured steel reinforcement. The very high values represent manual lifting and carrying of heavy reinforcement bars, it also represents awkward working positions and the high repetitiveness when clenching single reinforcement bars.

In the case of using SCC, a work cycle mean value of 5.7 was obtained in the ErgoSAM analysis, Figure 16, thus making these work tasks acceptable as far as the workers work-related musculoskeletal health is concerned.

When the traditional concrete casting work cycle was examined, the ErgoSAM analysis showed a mean value of 18.2. Thus, the risk factor for WMSD is very high.

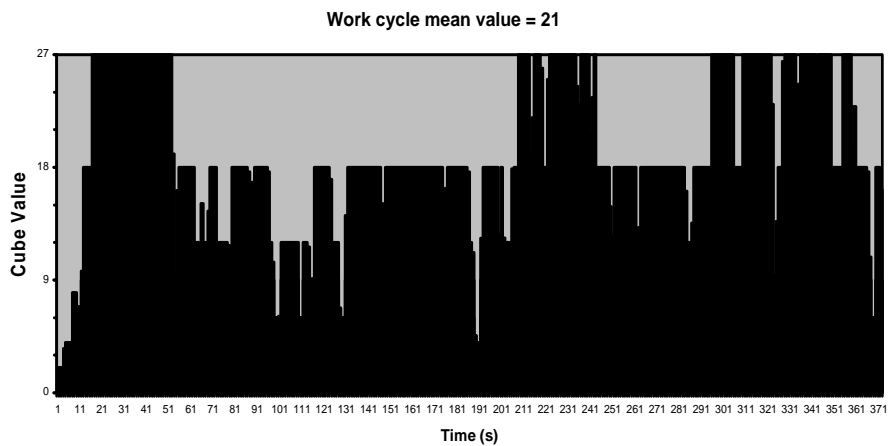


Figure 15: ErgoSAM analysis of a short work cycle of traditional reinforcement placing, mean value 21. Below 6 is acceptable, 6 to below 9 is conditionally acceptable and 9 and above is unacceptable.

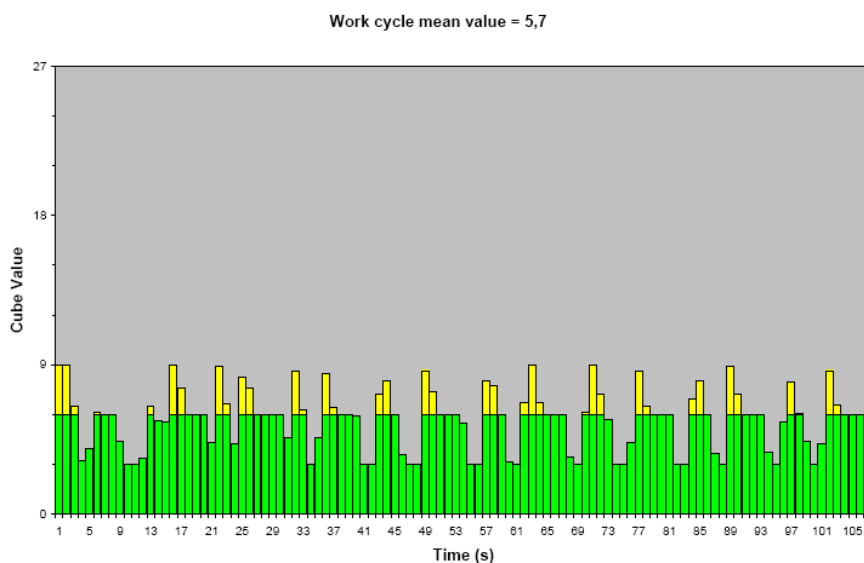


Figure 16: ErgoSAM analysis of concrete worker's short work cycle during SCC casting. Below 6 is acceptable, 6 to below 9 is conditionally acceptable and 9 and above is unacceptable.

8 CONCLUSIONS

It can be concluded that, applying Lean Construction principles is possible on bridge construction with ready mixed concrete. In fact, Lean Construction is an important prerequisite and tool for the development of a more industrial process.

The full scale projects performed were successful, although in different ways and to different extent. The first project, the bridge in Kalix, was thoroughly designed and planned for the “new” approach on production methods and therefore all involved actors were prepared, when production started. This has been proved to be a key factor to the success. For instance the introduction of SCC with higher strength could decrease the amount of the very dense shear force reinforcement in the superstructure.

At the bridges of Nynäsvägen the design for the new approach i.e. rebar carpets and SCC started late in the project and therefore, the possibilities for changes were limited. Consequently, there were only a few roles of rebar carpets used and the higher strength of the concrete was not considered in design.

To be able to utilize the “new” and improved production methods in a broader approach, for example when it comes to constructing, a larger part of a highway with a dozen bridges or so, it is of importance to standardize work tasks, material and different parts of the bridges or structures.

The reinforcement in a typical bridge superstructure of today most often consists of approximately 80 % longitudinal reinforcement and 20 % shear force reinforcement. If, as in the Kalix bridge project, all the longitudinal reinforcement, some 13 tons out of a total of 16 tons (i.e. 80 %), can be designed for placing through rebar carpets there is an immense opportunity to reduce the on-site production time and also to cut down production costs. Consequently, the on-site production time can be reduced with virtually 80 % of the traditional placing time. The total production cost for placing reinforcement will also decrease with roughly 30 % depending on the productivity at site, planning and management.

The risk analysis on steel reinforcement and concrete casting work tasks by the ErgoSAM method, has indicated that working with the prefabricated steel reinforcement and SCC reduced a great deal of physical loading on the musculoskeletal system of the worker. The prefabrication of steel reinforcement structures allowed a much safer working environment without risk factors such as heavy lifting and working in bent, awkward and repetitive postures. The casting of SCC, without the need for mechanical vibration usually associated with concrete placing, has led to the improvement of the construction work environment. Also, when working with these industrialized methods it does give significant benefits both in terms of a healthy and safe work environment for the workers, reduced staff-related costs for the company as well as the client and the society as a whole, both in short term and long term perspectives.

Considering the prefabricated sections, i.e. steel reinforcement cages, the on-site production time was reduced with more than 2 days or approximately 3 % of total construction time. The costs were only cut marginally for the studied bridge in Kalix, but if there had been another two foundations on the bridge were cages could have been prefabricated the cost would probably have been cut by 30 % due to scale effects.

SCC has the potential to decrease the total on-site production time, i.e. less man hours will be consumed during production, as can be seen in Table 2b. This is however in great deal a responsibility of management at site. The management needs to have a good knowledge on the benefits with SCC in comparison to traditional concrete.

The cost for purchasing SCC is greater than the cost for traditional concrete, consequently in order not to increase the total costs all the benefits of SCC needs to be implemented.

The plate structures are the part of a bridge that has the largest potential of improving when considering the working environment. When constructing these plate structures there can be a considerable tough working environment. For instance it is not exceptional that the plate structures are several meters high and the workers need to climb down on the reinforcement inside the formwork to be able to vibrate the concrete properly. Using SCC, there is no need for vibrating the concrete and hence no need to climb down inside the formwork either.

REFERENCES

1. Byfors, J and Jäderholm, B (2006), Presentation FIA-day 2007, http://www.fiasverige.se/templates/Fia/Page_____350.aspx?epslanguage=SV
2. Olofsson, T, Stehn, L and Lagerqvist, O (2004), Industriellt byggande - Byggbranschens nya patentrösning? (In Swedish), Väg- och vattenbyggaren no 8, 2004 pp 19-24.
3. Byfors, J. (1999), SCC is an important step towards industrialisation of the building industry, *Proceedings of the First International RILEM Symposium on Self-compacting Concrete*, Stockholm: RILEM Publications S.A.R.L, pp.15-21.
4. Liker, J (2004), *The Toyota Way*, ISBN 0-07-139231-9
5. Womack, J P, Jones, D T and Roos, D (1990), "The Machine that Changed the World" 1990. Harper Collins Publishers, New York, NY, USA. ISBN 0-89256-350-8.
6. Womack, J P and Jones, D T (2003), *Lean Thinking-Banish waste and create wealth in your organisation*, ISBN 0-7432-3164-3.
7. <http://www.iglc.net/>
8. Jongeling, R, Emborg, M, Asp M and Olofsson T (2005), Modelling and simulation of cast in place concrete constructions using N-dimensions. Research Report 2005:18 Luleå Technical University. ISSN: 1402-1528. ISRN: LTU – FR – 05/18--SE
9. Emborg, M (2005): Industrial site casting by combining innovative constructions methods with robust SCC, Proc Nordic Concr. Conf, Sandefjord, 13 -15 June. (Keynote lect)
10. Koskela, L (2000): An exploration towards a production theory and its application to construction. VTT Technical research center of Finland publications 408, Espoo 2000 ISBN 951-38-5566-X ([URL:http://www.inf.vtt.fi/pdf/](http://www.inf.vtt.fi/pdf/)).
11. Simonsson, P and Emborg, M (2005), Rationellt anläggnings byggande med platsgjuten betong, (in Swedish) Bygg & Teknik no7 2005.
12. Emborg, M, Jonasson, J-E, Nilsson, M, Utsi, S, Simonsson, P (2005): Designing robust SCC for industrial construction with cast in place concrete, SCC2005, Proc 4th Int RILEM-Symposium, Oct 30 – Nov 2, Chicago 2005, pp 1251-1259.
13. Sandberg, J and Hjort, B, "Rationell armering, ergonomi-ekonomi-miljö", (in Swedish) 1998. ISBN 91-630-7432-X.
14. Ålander, C, (2004), Advanced systems for rational slab reinforcement, the European Ready Mixed concrete Association, ERMCO, proceedings from the conference "Heading for concrete solutions", Helsinki 2004. ISBN 952-5075-64-8.

15. Simonsson, P and Rwamamara, R, (2007): Consequences of industrialized construction methods on the working environment, IGLC 2007.
16. Flanagan, F, Jewell, C, Larsson, B, and Sfeir, C, (2001) "Vision 2020: Building Sweden's Future", Department of Building Economics and Management, Chalmers University of Technology, Sweden.
17. Swedish Productivity Center, Sveriges Produktivitets Center AB (1995) SAM-Sekvensbaserad aktivitets- och metodanalys (in Swedish).
18. Laring, J, Christmansson, M, Kadefors, R, and Örtengren, R (2005) ErgoSAM: A preproduction Risk Identification Tool. Human Factors and Ergonomics in Manufacturing, Vol. 15 (3), pp. 309-325.
19. Sperling, L, Dahlman, S, Kilbom, Å, and Kadefors, R, (1993) A Cube Model for the classification of work with hand tools and the formulation of functional requirements. Applied Ergonomics, 24, 212-220.
20. Wikström, B-O, and Hägg, G M, (1999) "International seminar on Corporate Initiatives in Ergonomics" 1999:10. ISBN 91-7045-521-X.

Non-linear Finite Element Analysis for Practical Application



Hendrik Schlune
Ph.D. student
hendrik.schlune@chalmers.se

Mario Plos
Associate Professor
mario.plos@chalmers.se

Kent Gylltoft
Professor
kent.gylltoft@chalmers.se



Department of Civil and Environmental Engineering
Structural Engineering, Concrete Structures
Chalmers University of Technology
Gothenburg, Sweden



ABSTRACT

Despite the availability of sophisticated non-linear finite element (FE) analysis software, linear-elastic analysis is still the standard tool to model the response of reinforced concrete structures in practice. To allow for more frequent applications of non-linear FE analysis in practice, computationally fast, simple and reliable methods are needed. For non-linear FE analysis this article gives an overview and evaluation of ideals, approaches and methods, which are especially suited to application in practice. This includes simplified element formulations, non-linear constitutive formulations on the sectional and element level, and ways to treat numerous load combinations with non-linear FE analysis.

Key words: Non-linear analysis, Finite Element Method, Practical Application, Concrete Structure, Simplified Finite Element Analysis

1. INTRODUCTION

1.1 General

Linear-elastic finite element (FE) analyses are commonly used for the design of concrete structures. They reflect the response of the structure when the material responds linear elastically, i.e. no cracking and no yielding; they can also be used for the design in the ultimate limit state (ULS) with the assumption that plastic redistribution can lead to a given state of equilibrium. However, they yield limited information about the response in the most common

intermediate load levels which cause cracking but no plastic redistribution. This is problematic, as the focus in design is shifting more and more towards the requirements for these intermediate load levels in the serviceability limit state (SLS). Furthermore, linear elastic analysis cannot account for redistribution of forces and moments when stiffness changes because of development of cracks and yielding of the reinforcement; this is needed to utilize the full capacity available when analysing existing concrete structures. Consequently, this type of analysis leads to over-conservative results when the structural model used for the assessment differs from the model used for the original design.

On the other hand, non-linear FE analysis, which can realistically model the non-linear response of concrete structures, is commonly used in research to analyse and gain understanding of complex structures, see [1, 2]. As non-linear effects such as cracking and yielding are included, it is possible to follow the complete response of concrete structures. However, to be able to make a general non-linear FE analysis using three dimensional (3-D) material models, a much specialised knowledge, specialised software and computationally demanding calculations are usually needed. Hence, until now, non-linear FE analysis has only occasionally been applied in practice, see [3].

To study how the practical application of non-linear FE analysis can be simplified, the work presented here was carried out. A short description of general non-linear FE analysis is followed by an overview of approaches to simplify it. Finally, some different ways to treat the many load combination, for example for bridges, when doing non-linear analysis are discussed.

2. GENERAL NON-LINEAR FE ANALYSIS

There are many ways to make a non-linear FE analysis. Nevertheless, in this article the term ‘general non-linear FE analysis’ is used to denote that which is based on 3-D element formulations and 3-D non-linear material models.

2.1 Flow chart for general non-linear FE analysis

General non-linear FE analyses usually follow the three-step procedure which is shown in Figure 1. Starting from a state of equilibrium of external nodal forces, $F(t)$, and internal nodal forces, $P(t)$, on the system level, a time increment, Δt , is taken, which leads to new external nodal forces $F(t+\Delta t)$ and, hence, to a residual, R , between the external and internal nodal forces. The stiffness matrix, K , is then used to calculate the change of global nodal deformations, u . The nodal deformations, u , are used on the element level to calculate a new strain state, ϵ , for all integration points. On the material level, the constitutive model is used to calculate new stresses, σ , and to update the material stiffness matrix, D . This information is used on the element level to update the element force vectors, p , and the element stiffness matrixes, k . Finally, the element stiffness matrixes, k , and the element force vectors, p , are assembled on the system level to form a new global stiffness matrix and a new internal nodal force vector $P(t+\Delta t)$. If the internal force vector is in acceptable agreement with the external nodal forces, $F(t+\Delta t)$, a new time step with a new external force vector can be taken. If this is not the case, the residual nodal forces have to be reapplied on the structure and the complete procedure is repeated until sufficient agreement between external and internal forces is obtained.

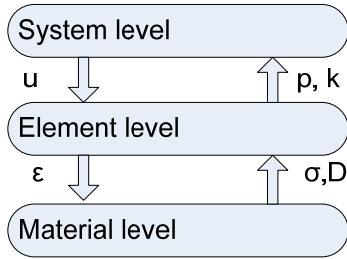


Figure 1 – Flow chart for general non-linear FE analysis

2.2 Simplifying element formulations

Real structures are 3-D and subjected to 3-D loading. However, in many instances the geometry and loading of the structure allows for introducing certain assumptions concerning the stress and strain field, which in turn, allows for using a model with reduced dimensions. This can simplify the formulation of the material model and reduce the computational cost significantly.

Commonly used simplifying assumptions are plane stress and plane strain. Plane stress is defined as a stress state for which the stresses associated with one direction are zero and the stress matrix reduces to:

$$\boldsymbol{\sigma} = \begin{bmatrix} \sigma_{xx} & \sigma_{xy} & 0 \\ \sigma_{yx} & \sigma_{yy} & 0 \\ 0 & 0 & 0 \end{bmatrix}. \quad (1)$$

This is a good approximation for thin shells that are loaded in the plane. Plane strain exists when the strains associated with one direction are zero, which reduces the strain vector to:

$$\boldsymbol{\varepsilon} = \begin{bmatrix} \varepsilon_{xx} \\ \varepsilon_{yy} \\ \gamma_{xy} \end{bmatrix}. \quad (2)$$

This often yields a good approximation for long bodies, such as tunnels or dams, which only deform perpendicular to the longitudinal axis.

Another way to simplify the structural model is to use a special class of elements, namely structural elements, to represent a structural member. Among them are truss -, beam - and shell elements, all of which are commonly implemented in commercial FE software packages; these allow reducing the dimensions of the FE model.

Beams

The most outstanding example of these simplifications is the Navier-Bernoulli hypothesis for beams, which states that plane sections normal to the beam axis remain plane and normal to the beam axis. Beams are structural elements in which extension dominates in the axial direction and can generally be subjected to a combination of six stress resultants, see Figure 2. However, the Navier-Bernoulli hypothesis does not include shear deformations and is valid only when the shear deformations can be disregarded. As a consequence, the response depends only on the normal force, N , and the two bending moments, M_y and M_z , which are associated with stresses in the axial direction. By disregarding shear deformations, and as a consequence shear stresses, it is

possible to reduce the general 3-D stress and strain state to 1-D stresses and strains in the axial direction.

As direct integration of the sectional response is usually not possible when the material response is non-linear, it is necessary to discretise the sections into small areas, represented what are known as integration points, for which a constant strain can be assumed. For mono-axial bending, possibly in combination with a normal force, the section has to be discretised into layers, while in general cases of biaxial bending, and possibly also a normal force, the section has to be discretised into fibres. The plane section hypothesis is used to calculate axial strains at each integration point; the application of an appropriate 1-D material model yields the corresponding stresses. The stress resultants are then determined by numerical integration of the stresses over the cross-section.

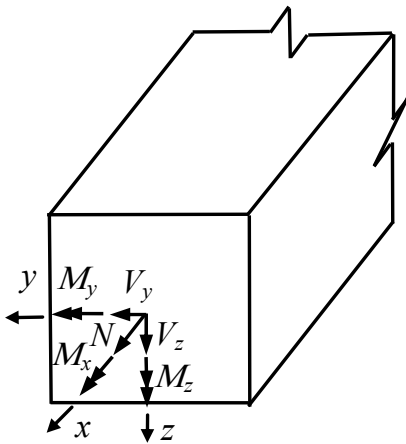


Figure 2 – Sectional forces and element coordinate system of a beam element

Due to the practical advantages of beam elements, in comparison with more demanding and more difficult to interpret solid analysis, efforts have been made to include shear deformations in beam elements. Bairan Garcia and Mari Bernat [4] classify the taken approaches into fixed pattern approaches, which either assume a fixed shear strain pattern, or a fixed shear stress one, over the section, or approaches which account for inter-fibre equilibrium. The commonly implemented Timoshenko beam element assumes a constant shear strain over the cross-section; hence it belongs to the class of fixed pattern approaches. It assumes that plane sections remain plane but, in contrast to the Navier-Bernoulli hypothesis, not necessarily normal to the beam axis.

For simplified analysis of beams that are subjected to normal and shear stresses due to axial and transverse loading, it is possible to assume that the axial and transverse directions are uncoupled. In this instance, the response in the axial direction can be described, using the plane section hypothesis, by a 1-D material model. For the response due to shear forces and torsional moments, a linear-elastic response can be assumed or a generalized force-generalized deformation curve can be used, see also Section 3. However, the assumption that normal and shear stresses are uncoupled does not hold for reinforced concrete, when inclined cracking introduces anisotropy which, as a consequence, can lead to unacceptably inaccurate results.

A more accurate approach which facilitates capturing the 3-D response of beams under a combination of all six possible stress resultants has been proposed [5] and refined [6]. In this

approach, the beam section is idealized as two systems. The first one assumes a linear strain distribution across the section and is used to describe the response in the normal direction, i.e. stresses and strains associated with normal forces and bending moments. In this system 1-D material response is assumed. The second system is used to describe the response in the transverse direction, i.e. shear stresses and strains associated with shear forces and the torsional moments. This system consists of a solid rectangular section of four shear walls which form a rectangular tube. For each shear wall, 2-D material response is used. Information about the interaction of the two systems and a comparison of the approach with test results have been published [5, 6].

Shells

Shell elements are a class of finite elements used to describe the response of structures with extension that dominates in two directions. Shells can generally be loaded perpendicular to the plane, in the plane or both, and can have up to six degrees of freedom and sectional forces in each node. Subclasses of shells are plate bending elements which can only be used when the structure is loaded perpendicular to the plane, and plane stress elements which can only be used when the structure is loaded in the plane.

An often used, kinematic simplification of shells loaded only perpendicular to the plane is the Kirchhoff plate theory. In contrast to the Mindlin-Reissner plate theory which also allows for shear deformation and thereby better suited for thicker plates, the Kirchhoff theory assumes that plane sections normal to the mid plane remain plane and normal to the mid plane. Hence, shear deformations are disregarded which makes the Kirchhoff plate element only applicable for thin plates. To include in-plane deformations, the Kirchhoff plate theory can be combined with the formulation of plane stresses. Finite elements based on this combination are also referred to as thin shell elements. Regardless of whether in-plane forces are included or not, the general 3-D stress and strain state is reduced to a 2-D problem, which allows for a simpler material model.

A further simplification for the simulation of the response of slabs (loaded only perpendicular to the plane) is a grid of beam element. This allows for using a 1-D material model or the sectional force-generalized strain relations which have been established for beams, see also Section 3. This simplification can be justified when the element grid can be aligned along distinct main directions in which the load is carried but introduces a gross simplification in general cases. Grids of elements to represent plates have for example been applied by Morrison [7], Tharmabala [8], Reitman and Ynakelevsky [9] and Noakowski et al. [10].

Discussion

All previously described approaches allow for the reduction of the general 3-D structural representation, which could facilitate the use of a simpler material model. However, in general FE programs the material models are general, and hence 3-D. This makes them unnecessarily complex for these approaches. For practical applications it would be desirable to be able to characterise the material response simply by a stress-strain relation. To achieve this, either special 1-D material models need to be implemented or an interface is needed where the user specifies the 1-D material response, and complementing default values for the 3-D material model are calculated automatically. For 2-D and 3-D material models, tools which allow assessment of the material and sectional response graphically would also be desirable and would facilitate an easier verification of the results.

3. SECTIONAL FORCE DEPENDENT STIFFNESSES AND SECTIONAL FORCE-GENERALIZED STRAIN RELATIONS

A way to avoid explicit material modelling in the form of stress-strain relations is to express the non-linear behaviour in the form of sectional-force dependent stiffnesses. Another very similar approach is to use phenomenological sectional force-generalized strain relations which directly relate the stress resultants (e.g. bending moment or normal force) to their associated strain resultant (e.g. curvature or mean axial strain). These approaches have been developed mainly for beams but have also been applied to shells.

3.1 Beams

The simplest approach to including the stiffness decrease due to cracking, when the sectional forces lead to tensile stresses which exceed the tensile capacity of concrete is to switch from the stiffnesses of an uncracked section, EA_I , $EI_{y,I}$, $EI_{z,I}$ to the stiffnesses of a cracked section EA_{II} , $EI_{y,II}$, $EI_{z,II}$. Although this is especially simple when the beam is subjected to only a single action, it can also be applied when a combination of normal forces and bending moments acts on the beam. This approach corresponds to a brittle drop of all stresses in the concrete tensile zone when the crack initiates. However, in reality, concrete shows a gradual, more ductile decrease of the tensile stresses after cracking [11]. In addition, the stiffnesses are calculated inside a cracked section where the reinforcement carries all tensile stresses. However, in reality cracks form at certain distances. Due to bond action between concrete and reinforcement, the concrete between adjacent cracks transfers tensile stresses. This effect, called tension stiffening, leads to a stiffer global behaviour than the local stiffness calculations inside a cracked section. By disregarding tension stiffening and assuming a brittle concrete behaviour, this approach underestimates the stiffness of a concrete beam after cracking. For a more accurate description of the response of concrete structures, sectional force-dependent stiffnesses or sectional force-generalized strain relations can be used: these implicitly include tension stiffening and the gradual decrease of the tensile stresses after cracking.

Moment-curvature relation

The moment-curvature diagram is probably the best studied type of sectional force-generalized strain relation. In the past, there have been different proposals like, e.g. an empirical effective stiffness approach by Branson [12] and the moment-curvature diagram of CEB-FIB Model Code 1990 [13]. While the first approach yields the bending stiffness directly for an applied moment, the second approach yields the curvature for an applied moment and vice versa. The diagram according to CEB-FIB Model Code 1990 [13] assumes the stiffness of the uncracked section, EI_I , up to the moment, $\sqrt{\beta_b}M_{cr}$, where $\sqrt{\beta_b}$ is a factor to include the effect of bond quality of the reinforcing bars and the load duration and M_{cr} is the cracking moment. For higher moments, curvature corresponding to the stiffness of the cracked section, EI_{II} , is assumed to be reduced by a coefficient, κ_{ts} , in order to account for the concrete contribution in between the cracks. For moments higher than the yielding moment, M_y , the stiffness, $2K_{III}$, is assumed, calculated as.

$$K_{III} = \frac{M_u - M_y}{\kappa_u - \kappa_y} \quad (3)$$

where M_u is the ultimate moment, M_y is the yielding moment, and κ_y and κ_u are the corresponding curvatures calculated for the fully cracked cross-section, see Figure 3.

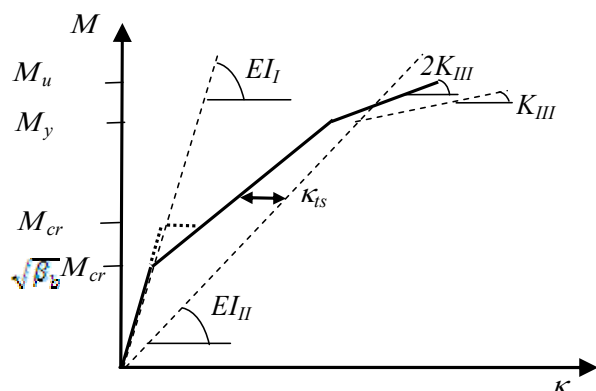


Figure 3 – Moment-curvature diagram according to CEB-FIP Model Code 1990 [13]

In Figure 4, the load-deflection curve for a four point bending test was calculated by applying the previously described moment-curvature diagram. The curve is compared with the experimental load-deflection curve and the load-deflection curve obtained by the commercial FE software DIANA which is based on 3-D material modelling. The test was reported by Ashour [14] who also gives detailed information about the test arrangement. For the analysis using the commercial FE software, 11 integration points over the height were used. The loading was displacement controlled and for the concrete a total strain rotating crack model was used. The post-cracking behaviour of concrete was modelled according to Hordijk [15]. Embedded reinforcement was used and strain hardening of the reinforcement was included. It can be seen that the non-linear FE analysis based on the moment-curvature diagram yields as accurate results as the computationally more demanding analysis based on 3-D material modelling.

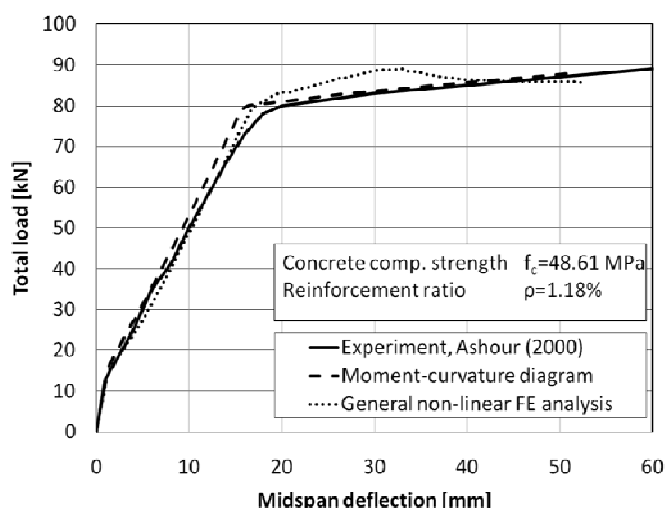


Figure 4 – Comparison of load-deflection curves

Normal force-mean strain relation

Analogously to moment-curvature diagrams in bending, normal force-mean strain diagrams can be used to describe the non-linear behaviour in the axial direction. For example, the stress-strain relationship of a section with embedded reinforcement [13] can be modified into a normal force-strain diagram, see Figure 5. The approach distinguishes four stages of the beam: the uncracked

stage, the crack formation stage, the stabilised cracking phase, and the post-yielding phase; this results in a quadruple-linear diagram. Up to the cracking normal force, N_{cr} , the stiffness of the uncracked section, EA_I , is assumed to determine the mean strain, $\varepsilon_{m,m}$. The strain in the crack formation stage is calculated by reducing the strain of the reinforcement inside a crack, $\varepsilon_{m,s2}$ by means of a linear decreasing value which accounts for the concrete contribution. In the stabilised cracking phase, when no further new cracks develop, a constant concrete contribution, $\beta_t \Delta \varepsilon_{sr}$, is assumed, to reduce the strain of the reinforcement inside a crack. To calculate the mean strain in the post-yielding phase, the equation for the stabilised cracking phase is extended by a linear function to account for the further increasing strains up to failure.

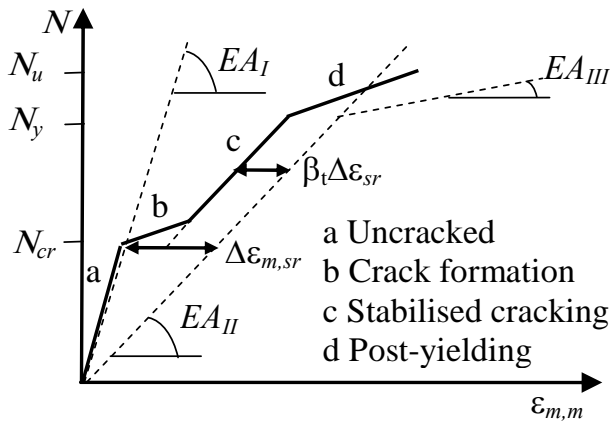


Figure 5 – Normal force-strain diagram, (modified stress-strain relationship of embedded reinforcing steel, CEB-FIP Model Code 1990 [13])

To describe the non-linear response of beams that are subjected to a combination of normal forces and bending moments, it is also possible to combine the moment-curvature and normal force-strain diagrams. For this, the neutral axis depends not only on the geometry and the material properties but also on the relation between the normal force and bending moment. A way of accounting for a constant normal force on the curvature is given in CEB-FIB Model Code 1990 [13] and further information is also available in CEB Manual Cracking and Deformations [16]. In this instance, the moment-curvature relation is based on the same principles as for pure bending. However, in order to account for the normal force, the cracking moment, M_{cr} , and the corresponding curvatures of the uncracked and cracked sections, κ_{Icr} , κ_{IIcr} are different. In addition, guidance on how to treat the effects of creep and shrinkage on the moment-curvature relations is available [16].

In comparison to CEB-FIB Model Code 1990 [13], simpler moment-curvature and normal force-strain relations are described by Noakowski and Schäfer [17]. As both relations are established on exactly the same principles, they are easier to combine in describing the response of beams subjected to a combined moment and normal force.

Shear force-shear strain relation

A way to formulate the non-linear response of beams due to shear loading is to use shear force-shear strain diagrams. A proposal for such a diagram is available in [16]; it is shown in Figure 6. For shear forces lower than the shear cracking force, the stiffness of the uncracked section, GA_w , is assumed. For higher shear forces ($V_{cr} < V < 4V_{cr}$), a function is given which

interpolates between the shear stiffness of the uncracked and the shear cracked beam, GA_{wII} . In addition, an expression is formulated which facilitates estimation of the shear cracking force, V_{cr} , depending on the effective shear strength of concrete, a size factor, the reinforcement amount, the concrete area, and the normal force in the beam. Hence, the effect of the normal stresses is implicitly included in the shear stiffness calculations.

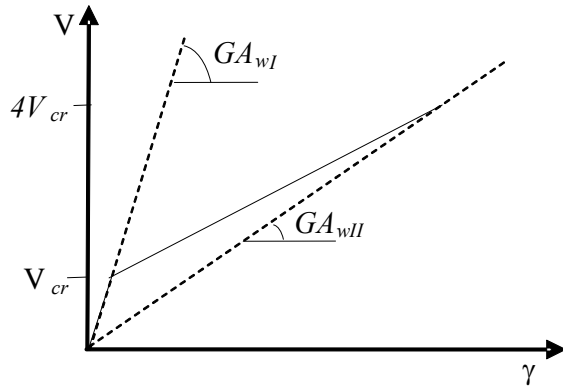


Figure 6 – Shear force-shear strain diagram [16]

Torque-twist relation

As with the shear force-shear strain diagrams, torque-twist diagrams can be used to describe the non-linear response of a beam subjected to a torsional moment. Tavio and Teng [18] proposed a method to construct a torque-twist diagram which showed good agreement with test results. However, the proposed method did not include the effect of the other sectional forces on the torsional stiffness calculations, which makes it applicable only for special cases. A more general, but at the same time very simplified method to calculate the torsional stiffness is available in the CEB-FIP Model Code 1990 [13]. In the proposed method the torsional stiffness is calculated according to the cracking state of the beam, see Figure 7; this means it depends on the principle stresses which are a result of all sectional forces.

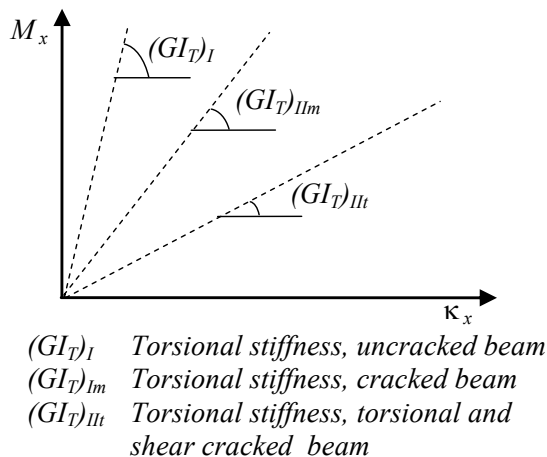


Figure 7 – Torque-twist relation, according to [13]

3.2 Plate bending

Due to the good results when using sectional force dependent bending stiffnesses or moment-curvature relations to describe the bending behaviour of beams, attempts were also made to extend this approach to plate bending. The approaches made by Jofriet and McNeice [19] and Bell and Elms [20] and more recently by Polak [21], focused mainly on deflection calculations for slabs. Quite good agreement with test results under serviceability conditions could be shown, but there were difficulties in capturing the final failure.

3.3 Discussion

In contrast to 3-D material modelling, formulating the constitutive relations by means of sectional force-generalised strain relations is descriptive and can be considered common knowledge for structural engineers. To utilise this type of strain relations for non-linear FE analysis, special purpose programs could be developed. In addition, some general FE programs allow for user-specified sectional force-generalised strains as input data for non-linear FE analysis. A disadvantage of these strain relations is that they need to be established separately for each cross sectional geometry. Furthermore, it must be possible to model the response for combinations of several sectional forces, if the method is to be general. A possible solution could be to develop a pre-processor that establishes the necessary sectional force-generalised strain relations based on material modelling.

In Figure 8, examples of moment and normal force over curvature and mean strain diagrams are shown. They were computed by numerical integration of the sectional response of a quadratic concrete beam ($f_c = 38\text{MPa}$) of 0.30 m width and height, reinforced with 8 reinforcement bars ($f_y = 500\text{MPa}$), diameter of 12 mm, 4 on the top and 4 on bottom. For the height, 20 integration points were used. The concrete compressive behaviour was modelled according to the stress-strain diagram in CEN [22]. In tension, a linear-elastic response up to the cracking strain, followed by the post cracking behaviour according to Hordijk [15], was assumed. The reinforcement steel response was modelled according to an idealised stress-strain diagram for reinforcement steel which includes hardening [22].

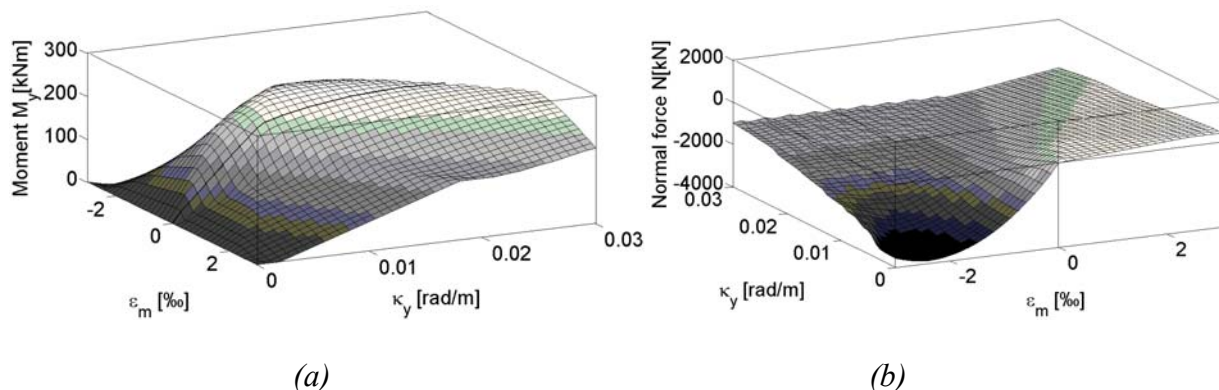


Figure 8 – (a) Example of a moment over curvature and mean strain diagram;
(b) Example of a normal force over curvature and mean strain diagram.

4. CONSTITUTIVE MODELLING IN THE NODAL FORCE-NODAL DEFORMATION SPACE

A constitutive model for plates and shells was developed by Glanzer [23] and Anderheggen et al. [24]. It was formulated on the element level to relate nodal forces to nodal deformations. The aim of the work was to develop a method suitable for practical and economical reinforcement design or capacity checking, in the ultimate limit state. Hence, a computationally fast method to facilitate utilising the full capacity by including plastic redistribution was the goal.

The formulation of the constitutive model as a nodal force-nodal deformation relation, instead of as a material model which relates stresses to strains, has the advantage that the computationally expensive numerical integration of the material response for the elements can be omitted. In addition, it has the advantage that the nodal forces are in perfect equilibrium with the external forces; in general FE analysis, an error is introduced when the equilibrium in the integration points is used to assure the equilibrium on the structural level. Furthermore, convergence problems which typically occur in general FE analysis, due to the brittle material response of concrete, may be reduced when formulating the constitutive model on the element level.

To allow for plastic redistribution, an elastic-plastic constitutive law has been used. To define the yield conditions, both the material response and the element geometry are needed, which complicates the analytical formulation of the yield surfaces. Hence, simplified, linearised yield surfaces in the nodal force space have been used.

The basic idea of this approach is to relate generalised stresses to generalised strains in common with the approaches described in Section 3. A major difference is that the relations presented in Section 3 have been mainly developed for hand calculations in sections, while in the approach just given they have been developed to be implemented as constitutive models for elements in non-linear FE analysis. Since beam elements are commonly used in structural FE analysis, an extension of the work, by Glanzer [23] and Anderheggen [24], to beams that are subjected to a more complex loading than just bending is desirable. To fit into the framework of commercial FE software, a reformulation of the constitutive model, as a sectional force-generalised strain relation in integration points, rather than on the complete element, would be needed.

5. NUMEROUS LOAD CASES IN NON-LINEAR FE ANALYSIS

A structure is designed for a large number of different loads that are combined to obtain the most critical load effect in each point or cross-section. How the loads should be combined is specified by load combinations given in design codes. For bridges and many other structures this results in a large number of different load cases including all possible positions, extensions and directions of the loads.

Using linear-elastic structural analysis, it is common practice to determine the most critical load case with respect to each load effect by superimposing the load effects of the different loads. However, superposition of loads is not valid for non-linear analysis. Consequently, the load effect of each load case has to be analysed separately. This leads to repeated, computationally demanding, non-linear FE analyses when complex structures with many loads have to be analysed. For bridges, with moving traffic loads, this leads to a huge number of non-linear analyses.

In the design of new concrete structures, linear-elastic FE analysis and superposition of loads can normally be used to design the structure in the ULS. This is based on the assumption that the final distribution of internal forces is determined by the plastic capacities after plastic redistributions. According to the lower bound theorem of the theory of plasticity, the structure will obtain sufficient load carrying capacity for any distribution of internal forces that fulfils equilibrium, provided it has sufficient plastic deformation capacity. The moment distribution obtained from a linear-elastic analysis of a concrete structure can usually be assumed to fulfil these requirements. On the other hand, the response in SLS is usually not very well reflected by a linear analysis. Here, a few governing load cases could be checked using non-linear FE analysis. This would combine the strength of linear-elastic FE analysis for the design in ultimate limit state with the accuracy of non-linear FE analysis in the serviceability limit state. A simple way to limit the number of non-linear FE analyses is to determine the governing load cases in advance by linear-elastic FE analysis.

When assessing an existing concrete structure, linear-elastic FE analysis can often not be used for ULS without underestimating the load carrying capacity substantially. Here, one possibility is to determine the governing load cases by linear-elastic FE analysis first, and then evaluating the load carrying capacity through non-linear analysis. However, the linear-elastic stiffness distribution can differ substantially from the real stiffness distribution in ULS, and there is a risk that the actually critical load cases are not included in the non-linear analyses.

One approach to improve this situation is proposed. This approach can be used when the self-weight, g , is the dominant action, which is typical for concrete bridges. In this situation, a reference load case consisting of the self-weight, g , and a mean distributed variable load, q_{mean} , is analysed non-linearly to obtain the secant stiffness of the structure for that load level. To analyse all other load combinations, this secant stiffness is used in linear-elastic analysis which allows for superposition, see Figure 9. This simplification is based on the assumption that the variation of the secant stiffness due to the variable loads does not significantly change the load distribution in the structure. This approach allows for superposition of loads, while at the same time more realistic stiffnesses are used than in purely linear-elastic FE analysis. Furthermore, the assumed linear elastic response allows for an easy comparison of load effects of different loads, which can be used for an automated determination of the governing load cases. The approach can be used for more realistic determination of governing load cases for both ULS and SLS, using different load levels for the secant stiffness evaluation.

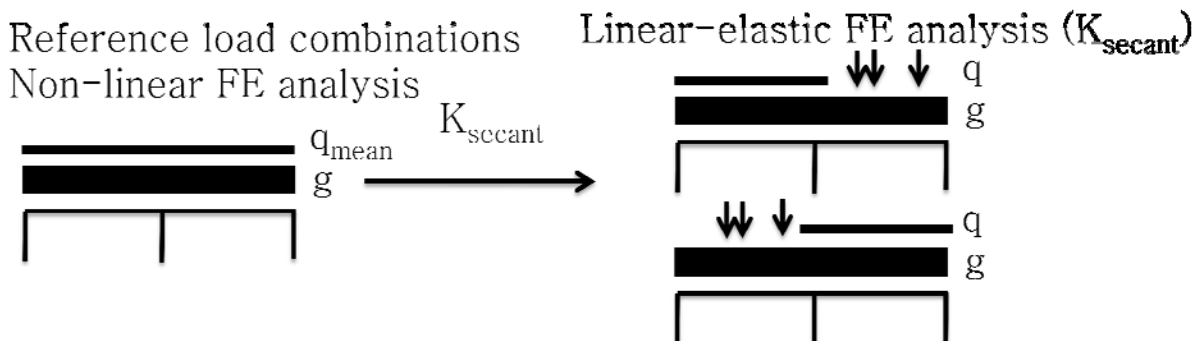


Figure 9 – Procedure to use one reference load combination to calculate K_{secant} , which can then be used to analyse the response under other loads

6. CONCLUSIONS

During the past four decades, tools have been developed which facilitate the realistic modelling of reinforced concrete structures by non-linear FE analysis. However, regardless of these advancements, non-linear FE analysis is still seldom used in practice. The practical obstacles are manifold and extend from the non-availability of user-friendly software, to the computational demands and convergence problems, to the lack of building code specification and difficulty in verifying results.

To encourage more frequent applications of non-linear analysis, this paper gives an overview of simplifying methods, approaches and ideas that can be useful in practice. Even though most of these methods and approaches might be less accurate and general than general non-linear FE analysis based on 3-D material modelling, they are nevertheless more accurate than linear-elastic analysis, they are applicable in many practical situations. Hence, both general FE analysis and simpler approaches can be seen to complement each other. While general FE analysis can serve as a more general tool to analyse details and parts of a structure for example, the simpler approaches might be more useful for the analysis of complete structures. To facilitate more frequent use of the simplifying approaches, they have to be generalised to be applicable for more complex combinations of sectional forces and structural elements of various types. In addition, they have to be provided in a user-friendly way, either as a pre-processor which can be coupled to commercial FE software or directly implemented in FE programs.

ACKNOWLEDGEMENTS

The authors thank the Swedish Road Administration, Vägverket, for their financial support.

REFERENCES

1. Plos, M. and Gylltoft, K. "Nonlinear FE analyses of RC bridge frame corners, based on fracture mechanics." *Journal of Bridge Engineering*, Vol. 3, No. 4, 1998, pp. 204-210.
2. Broo, H., Lundgren, K., and Engström, B. "Shear and torsion interaction in prestressed hollow core units." *Magazine of Concrete Research*, Vol. 57, No. 9, 2005, pp. 521-533.
3. Plos, M. Improved Bridge Assessment using Non-linear Finite Element Analyses. *First International Conference on Bridge Maintenance, Safety and Management, IABMAS'02*, Barcelona, 2002. International Center for Numerical Methods in Engineering (CIMNE), pp. 8.
4. Bairan Garcia, J. M. and Mari Bernat, A. R. "Shear-bending-torsion interaction in structural concrete members: A nonlinear coupled sectional approach." *Archives of Computational Methods in Engineering*, Vol. 14, No. 3, 2007, pp. 249-278.
5. Rahal, K. N. and Collins, M. P. "Analysis of sections subjected to combined shear and torsion - a theoretical model." *ACI Structural Journal*, Vol. 92, No. 4, 1995, pp. 459-469.
6. Rahal, K. N. and Collins, M. P. "Combined torsion and bending in reinforced and prestressed concrete beams." *ACI Structural Journal*, Vol. 100, No. 2, 2003, pp. 157-165.
7. Morrison, D. G. "Nonlinear Response of Reinforced Concrete Slabs Represented by Beam Grids." *Journal of Energy Resources Technology, Transactions of the ASME*, Vol. 105, No. 1, 1983, pp. 90-96.
8. Tharmabala, T. "Nonlinear analysis of grid systems." *Canadian Journal of Civil Engineering*, Vol. 16, No. 3, 1989, pp. 300-307.
9. Reitman, M. A. and Yankelevsky, D. Z. "A new simplified model for nonlinear RC slabs analysis." *ACI Structural Journal*, Vol. 94, No. 4, 1997, pp. 399-408.

10. Noakowski, P., Leszinski, H., Breddermann, M., and Rost, M. "Slender building floors, clarification of extreme deflections." *Schlanke Hochbaudecken Steifigkeitsorientierte Analyse zur Klärung extremer Durchbiegungen*, Vol. 103, No. 1, 2008, pp. 28-37.
11. Hillerborg, A., Modéer, M., and Petersson, P. E. "Analysis of crack formation and crack growth in concrete by means of fracture mechanics and finite elements." *Cement and Concrete Research*, Vol. 5, No., 1976, pp. 773-782.
12. Branson, D. E. "Instantaneous and Time-Dependent Deflections of Simple and Continuous Reinforced Concrete Beams." Alabama Highway Department, Bureau of Public Roads, 1965.
13. CEB. "CEB-FIP Model Code 1990". Bulletin d'Information 213/214, Lausanne, Switzerland, 1993.
14. Ashour, S. A. "Effect of compressive strength and tensile reinforcement ratio on flexural behavior of high-strength concrete beams." *Engineering Structures*, Vol. 22, No. 5, 2000, pp. 413-423.
15. Hordijk, D. A. *Local Approach to Fatigue of Concrete*. PhD Thesis, University of Technology, Delft, 1991.
16. CEB. "Cracking and Deformations." Comité Euro-international du Béton, Bulletin d'information N° 158, Lausanne, 1985.
17. Noakowski, P. and Schäfer, H. G. "Steifigkeitsorientierte Statik im Stahlbetonbau : Stahlbetontragwerke einfach richtig berechnen", vol. 1. Ernst & Sohn, Berlin, 2003.
18. Tavio and Teng, S. "Effective Torsional Rigidity of Reinforced Concrete Members." *ACI Structural Journal*, Vol. 101, No. 2, 2004, pp. 252-260.
19. Jofriet, J. C. and McNeice, G. M. "Finite element analysis of reinforced concrete slabs." *ASCE J Struct Div*, Vol. 97, No. ST3, 1971, pp. p 785-806.
20. Bell, J. C. and Elms, D. G. "Non-linear analysis of reinforced concrete slabs." *Magazine of Concrete Research*, Vol. 24, No. 79, 1972, pp. 63-70.
21. Polak, M. A. "Effective stiffness model for reinforced concrete slabs." *Journal of Structural Engineering*, Vol. 122, No. 9, 1996, pp. 1025-1030.
22. CEN. "Eurocode 2: Design of concrete structures - Part 1-1:General rules and rules for buildings." CEN, European Committee for Standardization, European standard EN 1992-1-1, Brussels, Belgium, 2004.
23. Glanzer, G. *Nichtlineare FE-Analyse von Stahlbetonplatten und -schalen mittels linearisierter Fliessbedingungen im Knotenkraftraum*. Institut für Baustatik und Konstruktion, ETH, Zürich, 2000.
24. Anderheggen, E., Glanzer, G., and Steffen, P. "Polyhedral yield surfaces in the element nodal force space." *Computers and Structures*, Vol. 78, No. 1, 2000, pp. 111-121.

Laboratory test and finite element analyses of a prototype bridge beam



Peter Harryson, Research Assistant.

Department of Civil and Environmental Engineering,
Structural Engineering – Concrete Structures,
Chalmers University of Technology, SE-412 96 Göteborg

Abstract

A laboratory load test and finite element analyses of a prototype bridge beam have been conducted at Chalmers University of Technology as a part of the feasibility study of a novel bridge concept, the *i-bridge*. The beam consisted of v-shaped glass-fibre reinforced polymer (GFRP) webs reinforced by a carbon-fibre reinforced polymer (CFRP) profile, with a deck plate made of GFRP in composite action with ultra-high-performance steel-fibre reinforced concrete (UHPSFRC). The FRP parts are jointed by means of epoxy adhesive, while the concrete is simply cast upon the specially roughened GFRP surface. The load test was done in four point bending and it confirmed the predicted structural behaviour from the finite element (FE) analyses. However, it was concluded that more testing will be needed in the forthcoming work before decisive recommendations about the design can be made.

In addition, materials tests of the UHPSFRC have been conducted, both in tension and compression.

Key words: Prototype beam, Four point bending, FE analysis, UHPSFRC, GFRP, CFRP, epoxy.

1. INTRODUCTION

The laboratory test and finite element (FE) analysis of a prototype bridge beam conducted at Chalmers University of Technology that are presented in this article form a part of the feasibility study of the *i-bridge* concept. The study in turn is part of a research project concerning industrial bridge engineering [1]. The aim of the study is to illuminate the possibilities given by new technology, new materials and other advancements when developing concepts of industrial construction (i-construction), and particularly industrial construction of bridges. In an overall perspective, the incentive of the research project is to encourage development in design and construction of bridges, with a more direct view towards i-construction.

The feasibility study is divided into three parts and each part is presented in an article. This article is the third and last part. The first part [2] is dedicated to a general description of the concept as well as the initial investigations and numerical analyses that have been undertaken. The second part [3] concerns an experimental study of bond in the bimaterial interfaces in the bridge deck, including laboratory tests.

2. BACKGROUND

The feasibility study, of which the third and last part is presented in this paper, is an effort to show how structural engineering can promote enhancement of efficiency in the overall process and support development. The study outlines a branch in the *product development* part of the industrial construction process; compare Figure 1. Still, the input to the overall process can be

considerable even though this is not the focus of the study. Hence, the main focus of the present study lies in the technical domain of the process, concerning mainly technical assessment of structural elements.

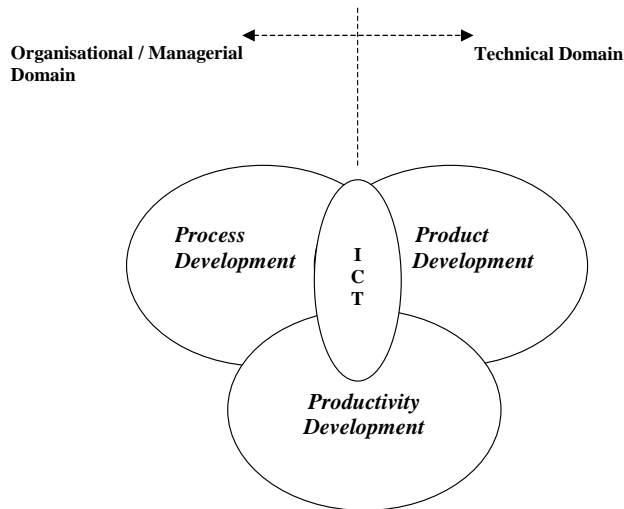


Figure 1. The cornerstones of Industrial Bridge Construction – the three P's, from [4].

The aim of the laboratory load test and FE analyses presented in this article is to assess a prototype bridge beam of the *i-bridge* concept. The *i-bridge* concept consists of v-shaped glass-fibre reinforced polymer (GFRP) beams. The beams are reinforced by carbon-fibre reinforced polymer (CFRP) profiles. The deck consists of GFRP plates in composite action with ultra-high-performance steel-fibre reinforced concrete (UHPSFRC), CRC concrete. CRC stands for compact reinforced composite, which is a commercially available product. More information about the concrete can be found in [5] and [6]. The results from the load test are presented more in depth in [7].

The performance of the *i-bridge* concept is more thoroughly described in [2]. On first sight the design of the shear connection for composite action in the deck can seem potentially dangerous; since it has a brittle behaviour and low ductility. But since the issue governing the design is the deflection criteria in the serviceability limit state, the capacity in the ultimate limit state is significant. Hence, the design approach in the ultimate limit state will therefore be to ensure that the load capacity when the composite action is lost is higher than the load capacity of the FRP structure alone. In turn, the FRP structure is designed to solely carry the entire load in the ultimate limit state without contribution from the deck plate. However, fatigue and cyclic load tests of the interface need to be carried out to ensure that the interaction not is gradually lost.

3. TEST OBJECTIVES AND LIMITATIONS

In developing a novel bridge concept, there is a range of tests that are essential and valuable to validate the performance. Thus, both materials tests and tests of structural details are needed, but also tests of the whole structure or large parts thereof. There is, however, a need to limit the areas of interest to the most essential issues in feasibility studies. In addition, it is important not to forget that the tests performed in feasibility studies are initial, and that improvements may be needed at a later stage.

The main focus of the load test is to demonstrate the structural performance with special attention to the composite action in the deck, to follow and infer the failure mode, and to validate the correctness of the numerical tools used. Some similarities in the approach to testing and analysis can be found in e.g. [8] and [9].

Of course, since this is a unique test the results cannot be statistically verified. Additionally, the test does not tell us anything about the behaviour in the transverse direction, i.e. how the deck

performs in that direction. Moreover, since the test beam is scaled down relative to the real structure, there might be a discrepancy in behaviour between the two. However, this is checked to some extent by comparing the numerical analyses of the two structures.

4. THE PROTOTYPE TEST BEAM

The beam prototype was composed similarly to the beams in the *i-bridge* concept (compare [2]); only its dimensions had been scaled down in some aspects. The span of the test beam was 5.0 m, whereas the span in the concept is 25 m. The total height was lowered from 1580 mm to 820 mm and the thickness of the CRC concrete was decreased from 70 mm to 20 mm. The width of the deck and the distance between the webs were decreased correspondingly, while it was decided to keep the thicknesses of the GFRP and the capacity of the CFRP intact as in the concept. This was mainly because an aim of the test was to validate the composite action between concrete and GFRP. Hence the FRP parts would not be critical, and testing the phenomenon of composite action could more easily be achieved in the test. In addition, the tolerances of the FRP components justified a certain margin. But a further practical reason was to be able to handle the structure and to perform the test with a reasonable magnitude of load. A cross-section and a picture of the prototype beam are shown in Figure 2.

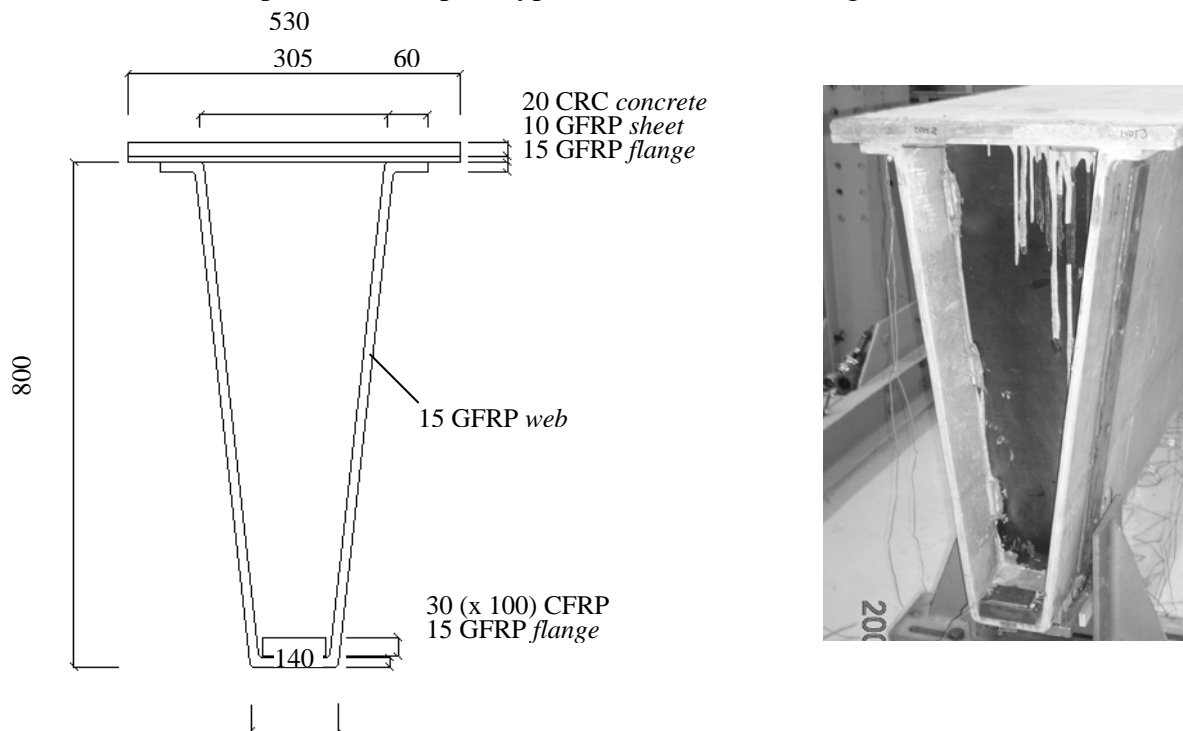


Figure 2. The cross-section of the prototype beam (to the left, dimensions in mm) and a picture showing the beam after casting of the concrete in the deck (to the right).

The GFRP consisted of E-glass in polyester matrix. Material properties for the GFRP were evaluated by assuming a fibre volume fraction of 50%. All laminates used were essentially bi-directional with only a small portion of the fibres (about 20%) in the diagonal directions. In addition, the volume fraction of fibres was differentiated across the thickness of the laminate, so that the amount of longitudinal fibres was increased in the middle half while the amount of transverse fibres was increased correspondingly in the two outer fourths close to the skin. The CFRP was made from prepreg of unidirectional high strength PAN carbon fibres embedded in epoxy resin. The volume fraction of carbon fibres was 60%. The FRP parts were joined by means of epoxy adhesive. The amount of steel fibres used in the CRC concrete was 6% by volume.

The surface of the GFRP deck sheet consisted of a special surface with a "peel-ply" on top which was removed prior to casting, resulting in a rough sandpaper-like surface. This was the surface with one of the best performances in the shear and tension bond tests; see [3]. The FRP beam was manufactured in a shop while the CRC concrete was cast in the laboratory. The GFRP components were made by hand lay-up and vacuum bagging using polyester resin, and the CFRP were made from epoxy prepreg as mentioned.

Crossbeams were cast at beam-ends above supports when casting the deck. For the reason of load transfer between the crossbeam and the GFRP web, double steel plates (placed on opposite sides of the web) with welded steel studs on the inner plate – to be cast into the crossbeams – were bolted and glued by means of epoxy adhesive to the webs. In addition, bearing plates of steel were epoxy-glued to the bottom flange at supports.

A few small shrinkage cracks in the transverse direction of the CRC surface were observed some weeks after casting. These were probably induced already in the early stage after casting (autogenous shrinkage), since it had been concluded that stresses from shrinkage would be much lower than the cracking stress of the hardened CRC. The beam was load-tested 49 days after casting.

5. FINITE ELEMENT ANALYSIS

5.1 Modelling

Numerical analysis has been carried out to simulate both the test beam and a full-size beam spanning 25 m. This has been done in order to ensure that the test beam behaves correspondingly when loaded to failure, and that the phenomena observed in the test also are those that can be expected in the full-scale structure.

The analysis was carried out with the general finite element program Diana; see [10]. Both FE models were done in 3D using curved shell elements, while all material interfaces and epoxy joints were modelled with interface elements. The different shells and interfaces of the models were connected with eccentric tyings, i.e. stiff connections. The materials models used allowed for nonlinear behaviour, although the FRP acts linear elastic until failure. The FRP was modelled with the Hoffman failure criteria, while the concrete was modelled based on smeared cracking and total strain, and the stress-strain model of Thorenfeldt accounted for the non-linearity of concrete in compression. In some analyses the concrete was modelled with isotropic plasticity and von Mises failure criteria. Additionally, the interface elements were modelled with multi-linear relationships; compare [10]. The modelling of the FRP could have been enhanced for example by the use of fracture mechanics, compare e.g. [11], but this did not seem necessary since the strains and stresses in the FRP were expected to be fairly modest due to the down-scaling of the beam. For the same reason the chosen failure criteria seems appropriate for the present study, while there are many failure criteria that can be adopted for FRP, compare e.g. [12].

Material properties for FRP were calculated on the basis of the properties of the fibres and the matrix from the manufacturers. Materials data for the joint epoxy were received from [13] and from the manufacturer. In addition, evaluation of the bond tests, see [3], gave supplementary information. Input data for the CRC were fetched from previous material tests as well as from [5]. For the interfaces between CRC and GFRP, parameters were evaluated from information about the response in shear and tension from the bond tests.

Since no materials testing could be conducted for the FRP parts, there was a certain level of uncertainty for the calculated material properties. However, due to the chosen scaling of the beam, this was not believed to be critical except for the shear resistance in the GFRP webs. In addition, it was not possible to assess information about the shear capacity of the matrix in the GFRP, so estimation was necessary.

The assumed material parameters used in the FE simulations are presented in Table 1. The element mesh of the test beam model is shown in Figure 3.

Table 1. Material properties used in the FE analyses.

CFRP	GFRP	CRC	Epoxy (interface) ¹	CRC - GFRP interface ¹
$E_x = 135 \text{ GPa}$	$E_x = 21,1 \text{ GPa}$	$E_c = 54,8 \text{ GPa}$		
$E_y = 10 \text{ GPa}$	$E_y = 21,1 \text{ GPa}$	$\nu = 0,24$	<i>normal direction</i>	<i>normal direction</i>
$E_z = 10 \text{ GPa}$	$E_z = 10,7 \text{ GPa}$	$f_{cc} = 150 \text{ MPa}$	$D_{11} = 53 \text{ GPa/m}$	$D_{11} = 100 \text{ GPa/m}$
$G_{xy} = 5,0 \text{ GPa}$	$G_{xy} = 5,1 \text{ GPa}$	$f_{ct} = 14 \text{ MPa}$	$\sigma_{nt} = 8 \text{ MPa}$	$\sigma_{nt} = 2 \text{ MPa}$
$G_{yz} = 3,0 \text{ GPa}$	$G_{yz} = 5,1 \text{ GPa}$	$f_{ct,cr} = 7 \text{ MPa}$	$\delta_{nt} = 0,15 \text{ mm}$	$\delta_{nt} = 0,02 \text{ mm}$
$G_{xz} = 5,0 \text{ GPa}$	$G_{xz} = 5,3 \text{ GPa}$	$g_f = 18 \text{ kN/m}$	$\sigma_{nc} = -60 \text{ MPa}$	$\sigma_{nc} = -70 \text{ MPa}$
$\nu_{xy} = 0,30$	$\nu_{xy} = 0,22$		$\delta_{nc} = 1,125 \text{ mm}$	$\delta_{nc} = 0,065 \text{ mm}$
$\nu_{yz} = 0,52$	$\nu_{yz} = 0,22$			
$\nu_{xz} = 0,30$	$\nu_{xz} = 0,21$		<i>shear direction</i>	<i>shear direction</i>
$\sigma_{xt} = 2200 \text{ MPa}$	$\sigma_{xt} = 340 \text{ MPa}$		$D_{22} = 53 \text{ GPa/m}$	$D_{22} = 89 \text{ GPa/m}$
$\sigma_{xc} = -1500 \text{ MPa}$	$\sigma_{xc} = -163 \text{ MPa}$		$\tau_{xy} = +/- 12 \text{ MPa}$	$\tau_{xy} = +/- 5 \text{ MPa}$
$\sigma_{yt} = 54 \text{ MPa}$	$\sigma_{yt} = 340 \text{ MPa}$		$\delta_{xt} = +/- 0,225 \text{ mm}$	$\delta_{xt} = +/- 0,056 \text{ mm}$
$\sigma_{yc} = -186 \text{ MPa}$	$\sigma_{yc} = -163 \text{ MPa}$			
$\sigma_{zt} = 54 \text{ MPa}$	$\sigma_{zt} = 76 \text{ MPa}$			
$\sigma_{zc} = -186 \text{ MPa}$	$\sigma_{zc} = -76 \text{ MPa}$			
$\tau_{xy} = 85 \text{ MPa}$	$\tau_{xy} = 25 \text{ MPa}$			
$\tau_{yz} = 90 \text{ MPa}$	$\tau_{yz} = 25 \text{ MPa}$			
$\tau_{xz} = 120 \text{ MPa}$	$\tau_{xz} = 25 \text{ MPa}$			

¹ interface properties

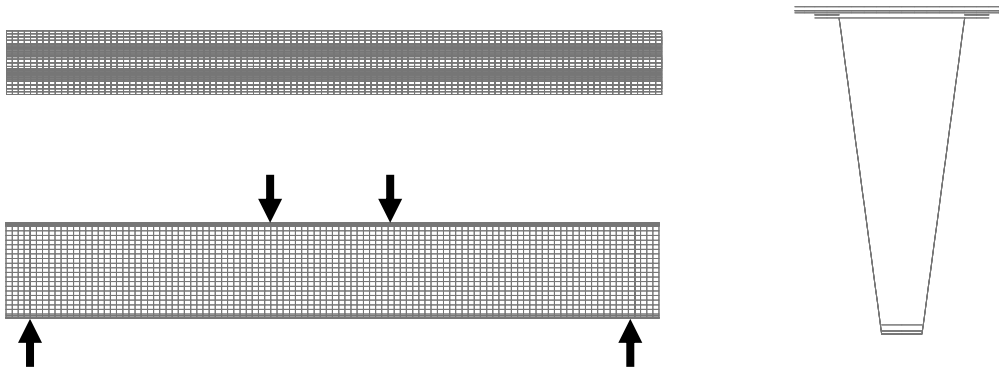


Figure 3. The mesh of the 3D FE model of the prototype beam, from above, a side view and the cross section. The span is 5.0 m and the distance from the loading points to the centre of the beam is 0.5 m.

5.2 Analyses

Non-linear FE analyses were conducted for both models. Comparison of the results from FE analyses of the two models reveals a reasonable conformity of behaviour between the models, especially concerning the composite parts of concrete and GFRP. The envisaged failure mode for the full-size beam was a local bond failure in shear within the bimaterial deck interface in the vicinity of the load, while for the test beam the expected failure was a combination of compression failure in the CRC concrete and a local bond failure close to the loading points. There was a possibility that the shear stresses in the webs also could become critical due to the decreased cross-sectional area of the webs, resulting from the down-scaling of the beam and the uncertainties in the material properties. However, there should be no risk of shear failure in the web if the adopted material properties were of the right magnitude.

Furthermore, the result from the analysis of the test beam showed acceptable agreement with the test results, thus demonstrating that the prototype beam behaved as expected. This is further

discussed in section 7, where also some of the FE results are compared with the test results. Contour plots from the two beams' models where concrete were modelled with isotropic plasticity are presented in Figure 4 and Figure 5.

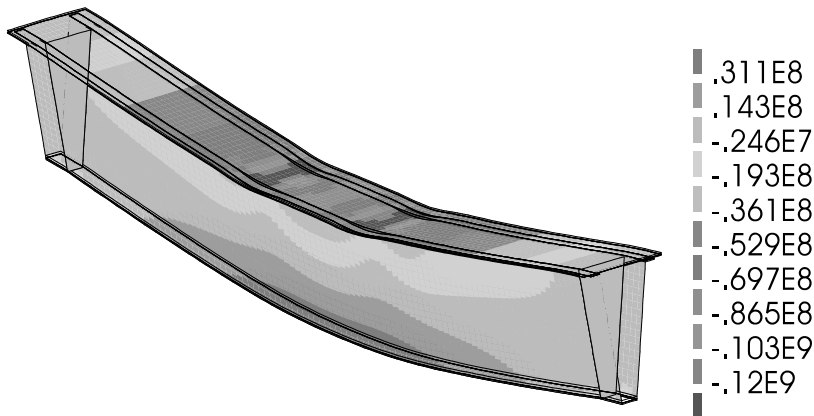


Figure 4. Contour plot of the deformed shape from FE analysis of the 5 m span prototype beam. Normal stresses [Pa] in longitudinal (x) direction at a load of 2×430 kN.

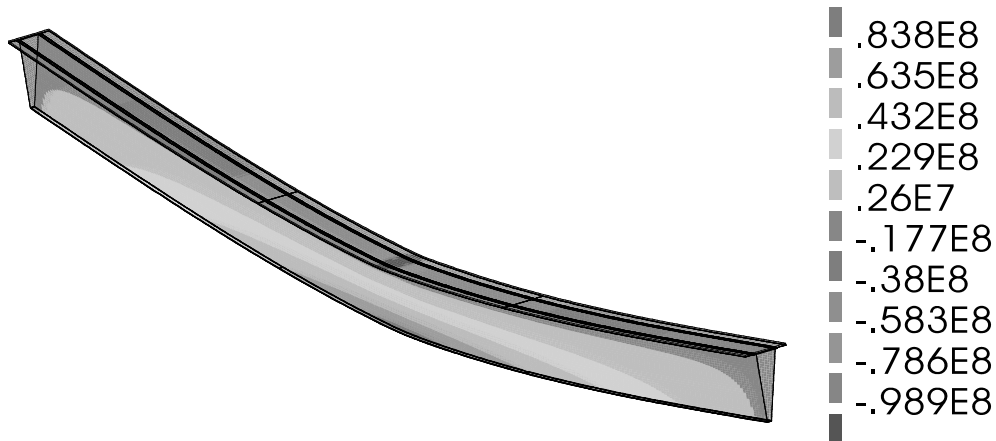


Figure 5. Contour plot of the deformed shape from FE analysis of the 25 m span full-scale bridge beam. Normal stresses [Pa] in longitudinal (x) direction at a central load of 900 kN.

Additionally, an analysis for control of Eigen values for buckling was conducted, stating that there would be no risk of buckling during the test. This was further verified by calculations according to Eurocomp [14]. Furthermore, from the FE analyses it was concluded that shrinkage would not constitute a problem since the maximum stress from shrinkage would be about 1 MPa. In addition, the shear stress from shrinkage in the bimaterial interface in the deck would act favourably, i.e. in the opposite direction, compared to the shear stresses from loading.

6. LABORATORY TEST

6.1 Test performance

The beam was loaded in four-point bending. The set-up can be seen in Figure 6 and Figure 7. Strain transducers were mounted on both sides of the interface between the GFRP plate and the CRC, i.e. on the surface of the GFRP plate and on short reinforcing bars cast into the CRC concrete, facing down towards the interface. These strain gauges were mounted in pairs in corresponding points before casting the concrete. In addition, strain was also measured by

means of strain transducers on the surface of the FRP and the CRC. Horizontal deflections and vertical relative displacements were measured with LVDT's. Two load cells accounted for the load measurement. The loading was deflection-controlled with a mid-span deflection rate of 0.5 mm per minute. This was decreased to 0.25 mm per minute when the load reached about 250 kN per jacking unit. In addition, the loading was interrupted continuously at predetermined loads to examine the beam. More information can be found in [7].

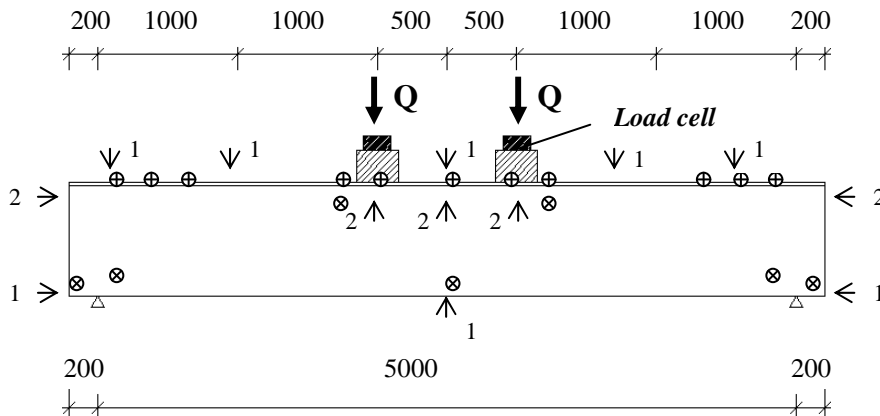


Figure 6. Set-up for the load test. Arrows denote LVDT's (number 1 stands for one transducer in centre of beam and number 2 stands for two transducers on corresponding sides of the beam). Vertical arrows downwards represent transducers that monitor deflection on top of the CRC concrete and vertical arrows upwards symbolize transducers that measure deflection on the bottom of the GFRP sheet flanges and the bottom of the GFRP beam. The upper horizontal arrows denote transducers that measure relative slip between the bottom of the GFRP deck sheet and the centre of the CRC overlay. The lower horizontal arrows stand for transducers that monitor relative slip between the bottom of the GFRP beam and the centre of the CFRP. Crosses denote schematic placement of strain gauges (vertical cross for gauges measuring strain in the deck interface and diagonal cross for gauges on the surface of the FRP beam).

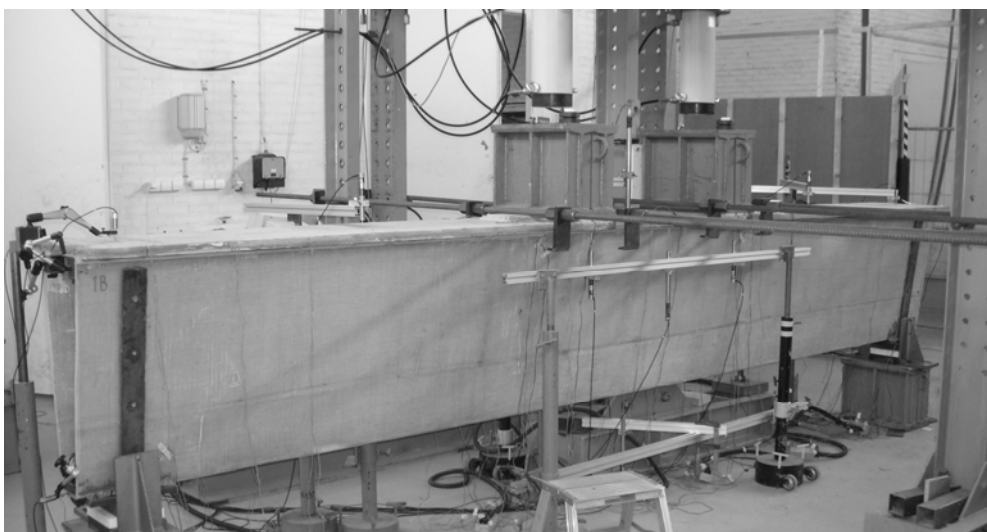


Figure 7. The prototype beam before loading.

6.2 Test results

The load test showed satisfactory agreement with the FE analyses. Thus, the structural performance predicted from the analyses could be verified. A comparison of the test results and the FE analyses is made in section 7, as noted earlier. Some of the results from the test are presented in Figure 8 and Figures 10–15. The results presented in the diagrams do not include effects of dead weight, etc., since the measurements are set to zero at the beginning of the loading in the evaluation.

The failure load reached was 2×429 kN and the failure was due to delamination in the GFRP plate in the deck, which was an unexpected failure mode. The failure was unfortunately induced by a transportation damage causing delamination of the plate, which was repaired prior to testing the beam. The defect can be noticed from Figure 8, showing the differential displacement between the bottom of the GFRP deck sheet and the centre of the CRC overlay at support 2. A significant displacement takes place on side A of the beam, which was the side that was damaged in the proximity of support 2 during transportation (the centre of the damage was approximately 1 m from support 2), while the displacement is practically zero on the undamaged side B. In addition, no noteworthy differential displacements were measured at support 1. The beam after loading to failure is shown in Figure 9.

However, the expected failure, a combination of compression failure in the CRC and local bond failure in the bimaterial interface at the loading points in the deck, was just about to be reached when the beam failed, and the beam behaved in accordance with what was foreseen during the loading. For example, calculating the compressive stress in the top of the CRC concrete at mid-span from the measured strain at failure (compare Figure 10), one obtains about 120 MPa in compression, hence demonstrating the vicinity of the ultimate compression stress. But in some respects, such as uneven distribution of strain and stresses over the cross-section, the damage is likely to have influenced the results, although it is not possible to judge how large this influence was. Nevertheless, in all essentials, apart from not reaching the expected failure mode, it is believed that the load test was successful and that the objectives of the test were achieved.

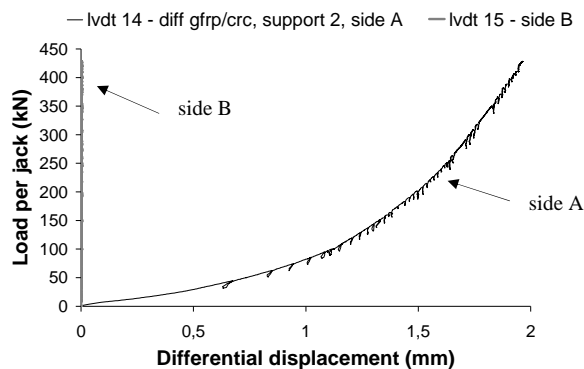


Figure 8. Differential displacement between the bottom of the GFRP deck sheet and the centre of the CRC overlay at support 2. Notice the significant displacement taking place on side A of the beam (the side which was damaged during transportation), while the displacement is practically zero on side B (the graph is almost parallel to the load axle).



Figure 9. The test beam after loading to failure.

After the failure the load dropped instantaneously to 2×258 kN (compare e.g. Figure 11), while the load was carried solely by the FRP beam without composite contribution from the deck. The thin part of the GFRP deck sheet, still connected to the beam (below the delamination), exhibited severe buckling.

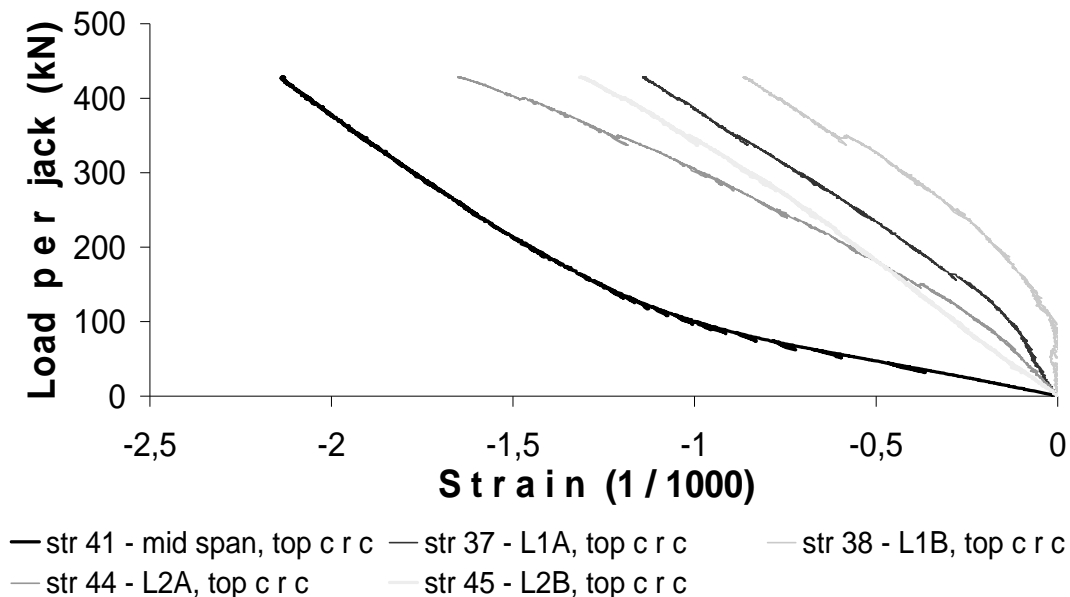


Figure 10. Strain measurements at mid-span and at the loading points for the top surface of the CRC (negative values means compression). The mid-span strain was measured in the centre of the beam, while strains at the loading points were measured above the centre of the beam flanges on both sides just outside the load distribution device (towards the supports).

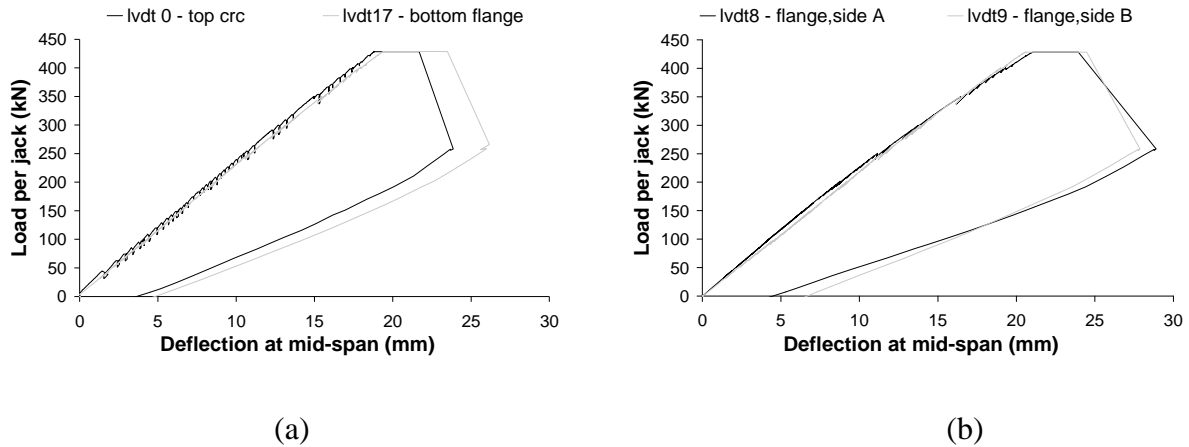


Figure 11. Load–deflection curves for mid-span: (a) for the top and bottom in the centre of the beam and (b) for the underside of the GFRP deck sheet at the edges.

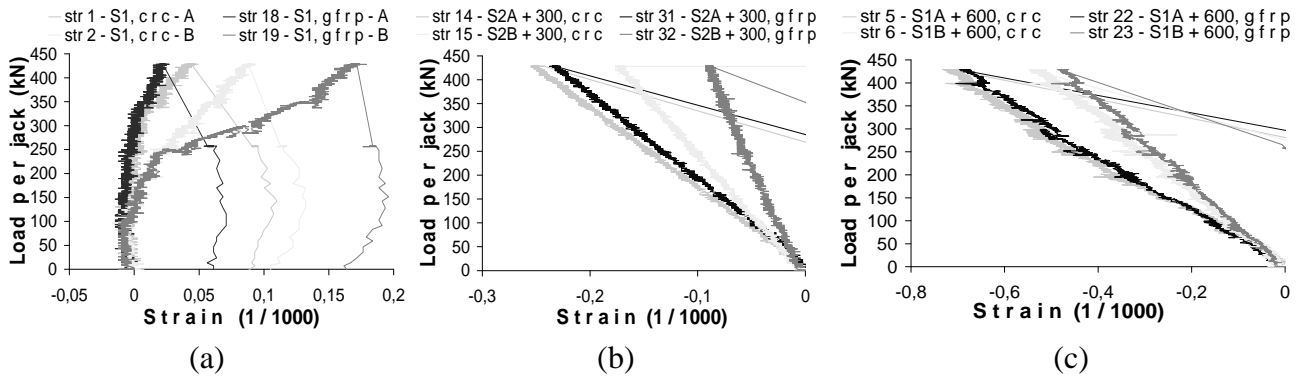


Figure 12. Strain measurements at opposite sides of the bimaterial interface in the deck for side A and side B of the beam (measured above the centre of the beam flanges) at various distances from the supports: (a) at support 1, (b) 300 mm from support 2 and (c) 600 mm from support 1.

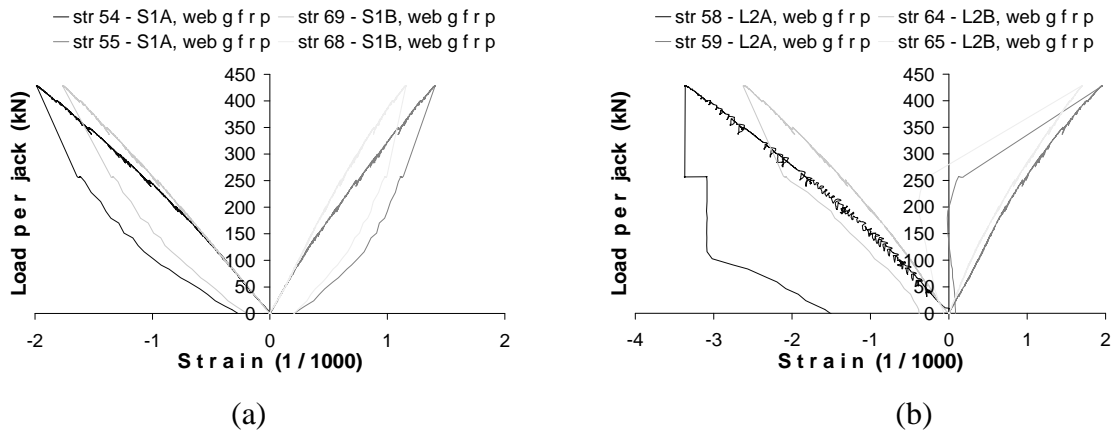


Figure 13. Strain measurements on the outer sides of the web surfaces in the two diagonal directions, at locations of maximum shear force: (a) at support 1 close to the bottom of the webs just outside the crossbeam, (b) at loading point 2 close to the top of the webs just outside the load distribution device.

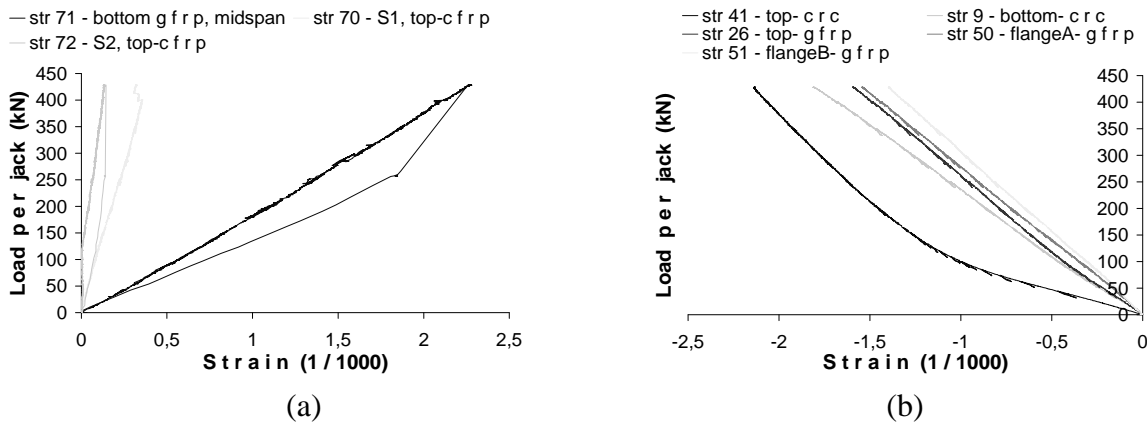


Figure 14. Strain measurements: (a) for bottom flange of GFRP at mid-span and top of CFRP on the protruding part just outside the crossbeam, and (b) at mid-span for top and bottom of CRC and top of GFRP deck sheet in the centre of the beam along with undersides of the GFRP deck sheet close to the edges.

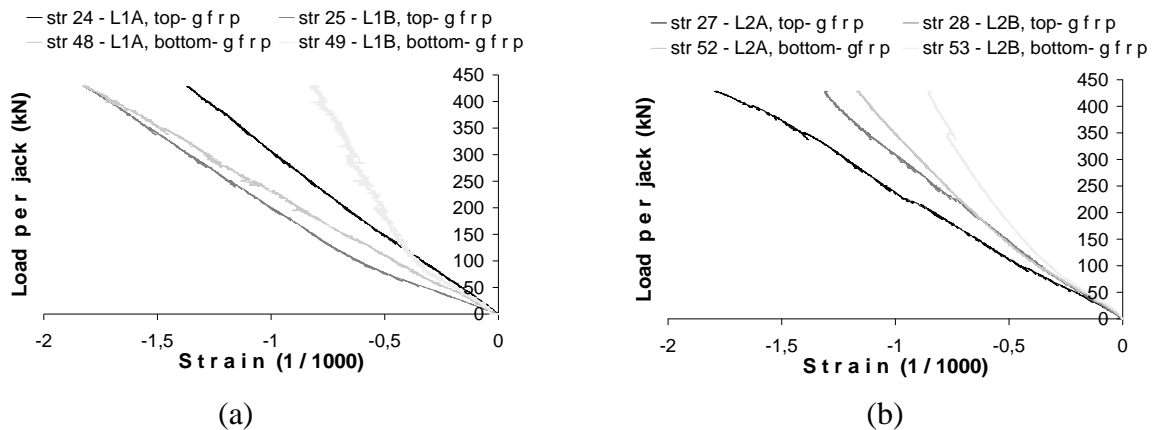


Figure 15. Strain measurements from the top (above centre of upper beam flanges) and bottom (just outside the edges of the beam flanges) of the GFRP deck sheet at loading points just outside the loading device (towards the supports) for beam sides A and B: (a) at loading point 1, (b) at loading point 2.

6.3 Materials testing of CRC

Tension tests

A series of six dog-bone-shaped specimens were cast for tension testing of the CRC concrete. The tests were done similarly to the experimental study; see [3]. The load, strain and displacement were measured with a load cell and through two strain gauges and two LVDT's mounted on the specimen.

A summary of the test results in terms of crack load and the corresponding calculated average tension stress, along with the failure load and the corresponding average calculated tension stress, is shown in Table 2. The crack load has been estimated from the test diagrams.

The failure loads were lower than expected, because the specimens did not show the strain hardening response that was supposed. The reason for this is probably the uneven distribution of steel fibres which was observed in the failure surfaces, which seems to be the result of too much vibration when casting the specimens. However, no uneven distribution of steel fibres was

noticed when checking cut-out specimens from concrete in the beam deck, where the distribution was found to be satisfactory.

Table 2. Summary of results from tension test of CRC concrete.

Specimen	Crack load (kN)	Average Crack load (kN)	Calc. Tension stress (MPa)	Average calc. Tension stress (MPa)	Failure load (kN)	Average load at failure (kN)	Calc. Tension stress (MPa)	Average calc. Tension stress (MPa)
DB7	-		-		-		-	
DB8	12,2		8,1		12,2		8,1	
DB9	11,7	11,5	7,4	7,4	13,7	12,0	8,7	7,7
DB10	9,7		6,2		10,0		6,4	
DB11	12,2		7,8		12,2		7,8	
DB12	11,9		7,6		11,9		7,6	

Compression tests

One series from each of the three casting batches, containing three cylinders each, was cast for compression tests and evaluation of elasticity modulus (on one series). The dimensions of the cylinders were $\phi 100 \times 200 \text{ mm}^2$. A summary of the results from the compression testing of CRC concrete and from the evaluation of the modulus of elasticity is presented in Table 3.

Table 3. Summary of results from the compression tests of CRC concrete.

Cylinder	Stress at failure f_{cc} (MPa)	Average f_{cc} (MPa)	Modulus of Elasticity E_c (GPa)	Average E_c (GPa)	Age (days)
1:1	153,4		58,0		
1:2	153,1	152,7	58,4	56,9	50
1:3	151,6		54,4		
2:1	-				
2:2	155,9	156,5			50
2:3	157,2				
3:1	155,6				
3:2	157,3	156,7			50
3:3	157,2				

7. COMPARISON OF RESULTS AND DISCUSSION

The load test exhibited reasonable agreement with the FE analyses. Thus, the structural performance predicted from the analyses was verified as can be concluded from the comparison of the test results and the FE analyses with isotropic plasticity of concrete, shown in Table 4 and Table 5.

Table 4. Comparison of deflections at failure load from the load test and the FE analyses. The failure load was 2×429 kN and the load in the FE analyses was 2×430 kN.

Placement	Load Test Deflections (mm)	FE Analyses Deflections (mm)	Placement	Load Test Deflections (mm)	FE Analyses Deflections (mm)
<i>top-face CRC, centre of beam</i>			<i>bottom-face GFRP-sheet</i>		
mid-span (0)	18,8	18,7	mid-span-A (8)	21,1	18,8
1/5-point-S1 (5)	10,5	10,4	mid-span-B (9)	20,6	18,8
1/5-point-S2 (12)	10,6	10,4	L1A (6)	20,3	18,9
			L1B (7)	20,2	18,9
<i>bottom of beam</i>			L2A (10)	19,7	18,9
mid-sp.-gfrp (17)	20,2	18,6	L2B (11)	20,3	18,9

Notations: S – support, L – loading point, A –side A of beam, B – side B of beam, () – the number of the LVDT's. The presented deflections are compensated for by settlements in the supports.

As seen in the tables, the scatter between the test and the analyses is sufficiently low compared to the uncertainties in the material parameters, especially for the GFRP. Hence, it can be stated that the adopted parameters are in the realistic range, e.g. the real moduli of elasticity should not differ much from those used in the FE analyses.

In all essentials, the prototype beam behaved linear elastic till failure, as expected. Since the test had to be terminated, due to the sudden delamination in the GFRP deck sheet, it was not possible to continue and evaluate the residual strength of the FRP beam without composite action. From the analyses, this strength represents a load level of about 2×340 kN in pure bending, which is somewhat higher than the load 2×258 kN reached just after the failure.

It can be seen from the test results that the bimaterial interface in the deck is activated, but it is not possible to quantify the shear stresses in the interface from the measured difference in strain. However, for measurements at side A of support 1 a rough estimation from the differences in average strain between the measure points indicates a shear stress of 2 –3 MPa in the bimaterial interface, which seems reasonable. It can also be noticed that the distribution of stress seems to be uneven over the interface, probably resulting from the uneven response as a result of the deficiency in the GFRP deck sheet. Furthermore, no signs of failure in the interface can be found, either from the test result or from the examination of the beam after testing. Even the interface at support 2 were undamaged despite the high energy release rate at the sudden interlaminar failure, compare Figure 9. Hence, the composite action seems to be intact.

In the transverse direction, the top of the CRC cracked at a load of about 2×40 kN beneath the loading points, and about 2×140 kN just outside the load distribution devices (stiff steel beams on soft board), whereas the FE analyses predicted a crack load of about 2×130 kN. The proximity to the loading points is likely to have influenced the crack development severely, but the location of the cracks just inside the GFRP beam flanges was the same in both analyses and test.

Table 5. Comparison of stresses and strains at failure load in the global longitudinal direction from the load test and the FE analyses. Load test stresses are calculated from the strains using the average measured elastic modulus for CRC and the elastic modulus assumed in the FE analyses for FRP. The failure load was 2 x 429 kN and the load in the FE analyses was 2 x 430 kN.

Interface in the deck	Load Test		FE Analyses		Material faces	Load Test		FE Analyses	
	Strain	Stress	Strain	Stress		Strain	Stress	Strain	Stress
	ϵ_x (‰)	σ_x (MPa)	ϵ_x (‰)	σ_x (MPa)		ϵ_x (‰)	σ_x (MPa)	ϵ_x (‰)	σ_x (MPa)
<u>300 mm from support, CRC</u>					<u>top-face CRC</u>				
S1A-crc (3)	-0,220	-12,5			L1A-crc (37)	-1,432	-81,4		
S1B-crc (4)	-0,329	-18,7			L1B-crc (38)	-0,868	-49,4	-1,79	-98,7
S2A-crc (14)	-0,254	-14,5	-0,233	-12,8	L2A-crc (44)	-1,650	-93,3		
S2B-crc (15)	-0,174	-9,9			L2B-crc (45)	-1,322	-75,2		
<u>300 mm from support, GFRP</u>					<u>bottom-face GFRP-sheet</u>				
S1A-gfrp (20)	-0,232	-4,9			L1A-gfrp (48)	-1,833	-38,7		
S1B-gfrp (21)	-0,264	-5,6	-0,231	-4,9	L1B-gfrp (49)	-0,828	-17,5	-0,976	-19,2
S2A-gfrp (31)	-0,235	-5,0			L2A-gfrp (52)	-1,165	-24,6		
S2B-gfrp (32)	-0,090	-1,9			L2A-gfrp (53)	-0,838	-17,7		
<u>at load, CRC</u>					<u>bottom-face GFRP-flange</u>				
L1A-crc (7)	-0,056	-3,2			mid-span-A (50)	-1,541	-32,5	-1,45	-30,2
L1B-crc (8)	-1,541	-87,7	-1,08	-58,3	mid-span-B (51)	-1,397	-29,5		
L2A-crc (10)	-1,515	-86,2			<u>bottom of beam</u>				
L2B-crc (11)	-1,088	-61,9			mid-sp.-gfrp (71)	2,274	48,0	2,22	47,2
mid-span-crc(9)	-1,815	-103,3	-1,45	-79,7	S1-top-cfrp (70)	0,134	18,1	0,44	59,7
<u>at load, GFRP</u>					S2-top-cfrp (72)	0,320	43,2	0,44	59,7
L1A-gfrp (24)	-1,363	-28,8							
L1B-gfrp (25)	-1,823	-38,5	-1,29	-25,7					
L2A-gfrp (27)	-1,797	-37,9							
L2B-gfrp (28)	-1,302	-27,5							
mid-sp.-gfrp(26)	-1,593	-33,6	-1,46	-30,7					

Notations: S – support, L – loading point, A – side A of beam, B – side B of beam, () – the number of the strain transducers.

As for the compression strains and stresses in the CRC in the longitudinal direction, it seems likely that the results of the FE analyses in the mid-span section are somewhat influenced by unrealistic load transfer from the loading arrangement, while at the loading points this does not seem to be the case. Hence, the agreement between analyses and test is better at the loading points than in mid-span. It is also possible that the small shrinkage cracks observed prior to testing somehow affected the results. The highest compressive stress in the CRC from the FE analyses was 137 MPa (for the load 2 x 430 kN) while the highest measured (calculated from the strain) was 121.4 MPa, although not in coinciding points.

From the strain measurements in the diagonal directions in the web (see Figure 12), it can be seen that the stress levels are high, especially at the loading points. This demonstrates that the concern about the shear stress in the webs was justified, but also that the expected shear capacity was sufficient.

8. CONCLUSIONS

The prototype beam exhibited a satisfying structural behaviour during the test, and reasonable agreement with the predictions from the FE analyses. Despite the somewhat unexpected failure

mode – delamination of the GFRP plate in the deck induced by a repaired damage – the beam behaved in accordance with what was foreseen during the loading. Thus, in all essentials the load test is believed to have been successful and, apart from not reaching the expected failure mode, the aims of the test were achieved. Since the test is unique, the results cannot be statistically verified, and further testing will be necessary in the forthcoming work before decisive recommendations about the design of the beam can be made.

ACKNOWLEDGEMENT

This research has been financially supported by the Swedish Road Administration and the Swedish Agency for Innovation Systems (VINNOVA). The work has been supervised by professor Kent Gylltoft at Chalmers University of Technology.

9. REFERENCES

1. Harryson, P.: *Industrial Bridge Engineering – Structural developments for more efficient bridge construction*. Department of Civil and Environmental Engineering, Structural Engineering – Concrete Structures, Chalmers University of Technology, Doctoral Thesis, new series nr. 2810, Göteborg, 2008, 209 pp.
2. Harryson, P.: The *i-bridge*, a novel bridge concept, Feasibility studies embracing industrial bridge engineering. *To be published*, 2008, 19 pp.
3. Harryson, P.: Bond between Fibre Reinforced Concrete and Fibre Reinforced Polymers, Experimental Study. *To be published*, 2008, 17 pp.
4. Harryson, P.: *Industrial Bridge Construction – merging developments of process, productivity and products with technical solutions*. Department of Structural Engineering, Concrete Structures, Chalmers University of Technology, Licentiate Thesis, Publication 02:1, Göteborg, 2002, 104 pp.
5. Nielsen, C V.: *Ultra High-Strength Steel Fibre Reinforced Concrete, Part I, Basic Strength Properties of Composit Matrix*, Department of Structural Engineering, Technical University of Denmark, Report No. 323, Serie R, Copenhagen, 1995, 188 pp.
6. Nielsen, C V.: *Ultra High-Strength Steel Fibre Reinforced Concrete, Part II, Structural Applications of Composit*, Department of Structural Engineering, Technical University of Denmark, Report No. 324, Serie R, Copenhagen, 1995, 154 pp.
7. Harryson, P.: *Belastningsprov av brobalksprototyp i fyrapunkts böjning* (in Swedish "Laboratory load test of a bridge beam prototype in four point bending"). Department of Civil and Environmental Engineering, Structural Engineering, Concrete Structures, Chalmers University of Technology, Report 2008:3, Göteborg, 2008, 53 pp.
8. Fam, A.: Pedestrian bridges using rectangular FRP box sections acting compositely with concrete slabs. Proceedings of the *7th International Conference on Short and Medium Span Bridges*, Montreal, 2006, 10 pp.
9. Moussa, G., Zhao, L.: Steel-Free FRP composite deck system. Proceedings from *Metropolitan Habitats and Infrastructure*, IABSE Symposium, Shanghai, 2004, 6 pp.
10. TNO: *Diana Finite Element Analysis, User's Manual, release 9*. TNO Building and Construction Research, 2005.

11. Moore, D.: *The application of fracture mechanics to polymers, adhesives and composites*. Edited by D. R. Moore, Elsevier, Oxford, 2004, 288 pp.
12. Hinton, M., Kaddour, A., Soden, P.: *Failure criteria in fibre reinforced polymer composites, The world-wide failure exercise*. Editors M.J. Hinton, A.S. Kaddour, P.D. Soden, Elsevier, Oxford, 2004, 1255 pp.
13. Ingles, N., Mendoza, C.: *Experimental Study of Steel-CFRP Composite Elements, Material Properties and Joint Behaviour*. Department of Structural Engineering, Steel and Timber Structures, Chalmers University of Technology, Master's Thesis 04:9, Göteborg, 2004, 68 pp.
14. Eurocomp: *Structural Design of Polymer Composites, EUROCOMP Design Code and Handbook*, The European Structural Polymeric Composites Group, edited by Clarke, E&FN Spon, Chapman & Hall, London, 1996, 751 pp.

Instructions for Authors Submitting Papers to Nordic Concrete Research {NCR}



Dirch H. Bager
M.Sc., Ph.D.
DHB-Consult
Lavendelparken 5, DK 9310 Vodskov
E-mail: dirch.bager@webspeed.dk

Siri Fause
Fagchef
Norwegian Concrete association / Tekna
Kronprinsensgate 17
Postboks 2312 Solli
N - 0201 Oslo
E-mail: siri.fause@tekna.no



ABSTRACT

The manuscript shall commence with a short abstract and at least four key words. The abstract ought to summarise problem, research method, and important results. It ought to be limited to 100 words.

Key words: Instructions, layout, headings, figures and tables, references.

1. INTRODUCTION

1.1 General

These instructions are written according to the rules for authors submitting papers to Nordic Concrete Research, NCR.

Papers for NCR shall deal with research and development within the Nordic countries related to concrete materials and structures.

The manuscript is to be written in English. Use the computer's spell check to avoid spelling errors. The manuscript should be limited to twenty (20) pages including illustrations and the reference list. The first draft of the paper shall be sent to the editor, Dirch H. Bager, who is responsible for reviewing of the paper before publishing. All papers are reviewed by three reviewers.

The manuscript shall preferably be typed in the word processing format MS Word and send either on a word processing disk or as an attached file to an e-mail. In both cases, the author has to provide a camera-ready paper version as well to be used for comparison. Automatic

numbering of paragraphs, tables, figures and references must not be used. Avoid footnotes if possible. If you must use them, please be sure that they are typed within the margins specified in section 2.

NCR is normally published in June and December. Deadline for submitting papers are respectively 15th of March and 15th of September.

1.2 Paper title, author presentation, abstract, and key words

The paper title should be of type size 14 and limited to two lines. Below the headline, there should be a photograph(s) of the author(s) and a short presentation of the author(s). The photograph should be about 40×50 mm and ranged left. If there is more than one author, the photographs should be arranged in a vertical row. The presentation of the author should include the following data: Name, degree (if any); title, affiliation, address, e-mail address. If there are any co-authors, they should be presented straight below the first presentation. An abstract and key words should be ranged below the author presentations. The spacing between paper title and photograph and author presentation should be one line. The spacing between author presentation and abstract should be two lines. The author presentation(s), abstract, and key words should be indented 50 mm from the left margin.

Since a requirement for receiving "The NCR Best Paper Award" is that the author is less than 35 year old, the editor of NCR need to know the age of the main author.

2. PREPARATION OF THE TEXT

To provide uniformity in the proceedings, the following rules of style are to be followed:

2.1 Paper size

The manuscript should be written on white paper, page size A4 (210×297 mm) or letter (216×279 mm). The typing area is limited to 164×244 mm. All text, figures, and tables must fit within this frame. Prior to printing, the pages are photographed and diminished to 81 % (170×240 mm), which should be borne in mind when deciding on illustration format.

2.2 Spacing, margins, and paragraphs

The manuscript should be singly spaced. Paragraphs should be separated by one line, a paragraph and a major heading or the first level of subheading by two lines. The text should be justified both left and right.

The top margin should be 30 mm and the left margin 23 mm.

2.3 Type font and size

The manuscript ought to be typed in the font Times New Roman 12, if that is possible, otherwise in some similar font. The paper title should be of type size 14 and in **Bold Lower Case Letters** with initial capitals on essential words. Text within tables might be of type size 10.

2.3 Headings and subheadings

General

Headings and subheadings should be limited to three levels. They should all be ranged left. Major headings should be numbered consecutively and in **BOLD UPPERCASE LETTERS**. It should be separated with two lines above and one line after to the adjacent paragraphs. The first level of subheading should be numbered with two digits. It should be in **bold lower case letters**. The spacing above and below should be two and one line, respectively.

Second level of subheading

If a second level of subheadings is used, it should be in *italics* with one line of spacing above and none below. The second level of subheading should not be numbered.

2.4 Pagination

Page number should be placed in the middle of the top margin, beginning with page 1 in each manuscript. The pages will be repaginated in the printing.

2.5 Nomenclature

The nomenclature used in relevant European standards as Eurocodes, EN 206-1 and EN 13670 should be used as far as possible. Only SI-units are allowed. All symbols should be explained where they first appear.

2.6 Equations

Equations should be indented 10 mm from the left margin. They should be numbered consecutively with a number in brackets indented 10 mm from the right according to the following example:

$$f_{ct} = 0.30 f_{cc}^{2/3} \quad (1)$$

2.7 Illustrations

Illustrations are to be placed fully inside the margins. The quality of the illustrations is essential. For best quality of the proceedings, we recommend authors to draw all figures on the computer. Only clear, original photographs in black and white may be used.

The illustrations should be placed in context, with accompanying explanatory legends or texts under these, but table legends should be placed on top of the tables. Illustrations and tables are to be numbered separately, starting with 1. Figure captions and table texts should be in *italics* and spaced one line from the adjacent paragraph.

Examples of a table and a figure are given on page 4.

Table 1 – Field tests on bond in zones with either positive or negative moment

Bridge	Failure stress in zones with positive moment (MPa)		Failure stress in zones with negative moment (MPa)	
	at time of repair	in 1995	at time of repair	in 1995
Bjurholm	1.66	1.66	2.06	2.43
Mälsund	-	1.84	1.63	1.44
Umeå	-	1.65	-	1.79
Vrena	1.50	1.58	1.36	1.97



Figure 1 – Capital from ancient Greece.

2.8 References

The references should be numbered consecutively in order of appearance. The number should be written in brackets, e.g., [1]. The references should be listed at the end of the paper under the major heading **REFERENCES**, see below.

REFERENCES

1. Silfwerbrand, J., "Improving Concrete Bond in Repaired Bridge Decks," *Concrete International*, Vol. 12, No. 9, September 1990, pp. 61-66.
2. Silfwerbrand, J., & Petersson, Ö., "Thin Concrete Inlays on Old Concrete Roads," Proceedings, 5th International Conference on Concrete Pavement Design & Rehabilitation, Purdue University, West Lafayette, Indiana, USA, April 1993, Vol. 2, pp. 255-260.
3. Swedish National Road Administration, "Regulations for Bridges," Part 7, "Bridge Maintenance," Borlänge, Sweden, 1994, 47 pp. (In Swedish).
4. Zhu, Y., "Evaluation of Bond Strength between New and Old Concrete by Means of Fracture Mechanics Method," Bulletin No. 157, Dept. of Structural Mechanics and Engineering, Royal Institute of Technology, Stockholm, 1991, 102 pp.

5. Bager, D.H., Geiker, M.R., Jensen, R.M, “Rheology of self-compacting mortars, influence of particle packing”, *Nordic Concrete Research* no. 26, 2001 pp. 1-16

